ISTINYE UNIVERSITY
GRADUATE EDUCATION
INSTITUTE
(MASTER'S THESIS)

CONDUCTIVE TISSUE ADHESIVES INSPIRED BY MUSSELS FOR USE IN CARDIOVASCULAR SURGERY

YAĞMUR KALENDER

SUPERVISOR
ASSOC. PROF. DR. AYÇA BAL ÖZTÜRK

STEM CELL AND TISSUE ENGINEERING

ISTANBUL – 2024

ISTINYE UNIVERSITY
GRADUATE EDUCATION INSTITUTE
(MASTER'S THESIS)

CONDUCTIVE TISSUE ADHESIVES INSPIRED BY MUSSELS FOR USE IN CARDIOVASCULAR SURGERY

YAĞMUR KALENDER

SUPERVISOR
ASSOC. PROF. DR. AYÇA BAL ÖZTÜRK

This study has been supported by the Health Institute of Turkey (TUSEB) with project number 13302.

ISTANBUL – 2024

ETHICS STATEMENT

I hereby affirm that, as I submit my Master's thesis titled “Conductive tissue adhesives inspired by mussels for use in cardiovascular surgery” I have conducted myself with full adherence to ethical standards in all stages from the planning to the writing of this thesis. I declare that all the information in this thesis has been acquired following academic and ethical guidelines. I have appropriately cited all sources for any information or interpretations that were not obtained through this thesis, and I have included them in the list of references. Furthermore, I confirm that I have not engaged in any actions that would violate patent or copyright rights during the research and writing of this thesis.

Yağmur Kalender

DEDICATION

I dedicate this thesis to all the researchers dedicated to advancing the scientific community. With profound respect and gratitude, I acknowledge the dedication and efforts of this vast community committed to pushing the boundaries of science and generating new knowledge.

ACKNOWLEDGEMENT

I wish to express my profound gratitude to all those who have contributed to the successful completion of this thesis. First of all, I want to convey my deepest appreciation to my family and my boyfriend for their continuous support and encouragement during my academic journey. Their unwavering faith in me has been my primary source of motivation.

I am deeply appreciative of my mentor, Assoc. Prof. Ayça BAL ÖZTÜRK, for her guidance throughout the course of this research.

I extend my heartfelt gratitude to Dr. Ece Özcan BÜLBÜL for her invaluable support in every aspect and for facilitating the acquisition of the H9C2 cell line from the Department of Technology at Istanbul University Faculty of Pharmacy which was essential for my research. Her assistance was instrumental in the successful execution of my study.

I am grateful to my colleagues, Şevval Melis ÖZYÜREK, Gülşah TORKAY, Burçin İZBUDAK, and Omid NEJATİ, who provided unwavering support and valuable insights in overcoming challenges and interpreting the findings. Their contributions and collaborative efforts were instrumental in bringing this work to fruition.

To all those who have been a part of this endeavor, I extend my sincere thanks. It is the combined dedication and efforts of each one of you that have transformed this thesis into a reality.

This study has been supported by the Turkish Health Institutes Presidency (TUSEB). Project No: 13302.

TABLE OF CONTENTS

LIST OF TABLES

LIST OF FIGURES

LIST OF SYMBOLS AND ABBREVIATIONS

3D	**:** Three-Dimensional
APTMS	**:** 3-(2-aminoethyl amino) propyltrimethoxysilane
AV	**:** Atrioventricular
Afib	**:** Atrial Fibrillation
Alg-MA	**:** Methacrylated Alginate
Alg-MA-Ox	**:** Methacrylated and Oxidized Alginate
AuNp	**:** Gold Nanoparticles
AuNp+Alg	**:** Gold Plus Sodium Alginate Nanoparticles
BCD	**:** Bovine Serum Albumin, Citrate Acid and Dopamine
BSA	**:** Bovine Serum Albumin
CA	**:** Citrate Acid
CFs	**:** Cardiac Fibroblasts
CMs	**:** Cardiomyocytes
Chi	**:** Chitosan
CS	**:** Chondroitin Sulfate
Cecm	**:** Cardiac Extracellular Matrix
DDW	**:** Deionized Water
DMSO	**:** Dimethyl Sulfoxide
DOPA	**:** 3,4-dihydroxyphenylalanine
ECHs	**:** Electroconductive Hydrogels
ECM	**:** Extracellular Matrix
FBS	**:** Fetal Bovine Serum
FDA	**:** Food and Drug Administration
FTIR	**:** Fourier-transform Infrared Spectroscopy
$FeCl_3$	**:** Iron (III) Chloride
GAG	**:** Glycosaminoglycan
GO	**:** Graphene Oxide
Gel-ADH	**:** Adipic Acid Dihydrazide Modified Gelatin
HA	**:** Hyaluronic Acid
IGF-1	**:** Insulin-like growth factor-1
IPSCs	**:** Induced Pluripotent Stem Cells
LAP	**:** Lithium phenyl-2,4,6-trimethylbezoylphosphinate

Lys	**:** Lysine
MI	**:** Myocardial Infarction
MSCs	**:** Mesenchymal Stem Cells
MTT	**:** (3-(4,5-Dimethylthiazol-2-yl)-2,5-Diphenyltetrazolium Bromide)
Mfps	**:** Mussel Foot Proteins
NMR	**:** Nuclear Magnetic Resonance
NaOH	**:** Sodium Hydroxide
OA	**:** Oxidized Alginate
OMA	**:** Oxidized Methacrylated Alginate
OMA-PPy	**:** PPy Conjugated OMA
OSA	**:** Oxidized Sodium Alginate
PBS	**:** Phosphate-buffered Saline
PCL	**:** Polycaprolactone
PDA	**:** Polydopamine
PDA-SA-PAM	**:** Polydopamine-Sodium Alginate-Polyacrylamide
PDMS	**:** Poly(dimethylsiloxane)
PEG	**:** Poly(ethylene glycol)
PES	**:** Polyethersulfone
PGS	**:** Polyglycerol Sebacate
PLA	**:** Polylactic Acid
PLGA	**:** Pol(lactic-co-glycolic acid)
PPy	**:** Polypyrrole
PPy/Alg	**:** Polypyrrole/alginate
PSF	**:** Penicillin-streptomycin-fungizone
PU	**:** Polyurethane
PVA	**:** Polyvinyl Alcohol
RGD	**:** Arginine-Glycine-Aspartate
SA	**:** Sinoatrial
SL	**:** Semilunar
UV	**:** Ultraviolet
VEGF	**:** Vascular Endothelial Growth Factor
XRD	**:** X-ray Diffraction

bFGF	**:** Basic Fibroblast Growth Factor
hMSCs	**:** Human Mesenchymal Stem Cells
rGO	**:** Reduced Graphene Oxide

ÖZET

Kalender, Y. (2024). Kalp Damar Cerrahisinde Kullanılmak Üzere Midyelerden İlham Alınarak Geliştirilen İletken Doku Yapıştırıcıları. İstinye Üniversitesi Lisansüstü Eğitim Enstitüsü, Kök Hücre ve Doku Mühendisliği. Yüksek Lisans Tezi. İstanbul.

Kardiyovasküler yaralanmaları tedavi etmek için yaygın olarak cerrahi dikişler ve zımbalar kullanılmaktadır. Ancak, kardiyovasküler defekt bölgesini tamamen kapatmak ve kanamayı kontrol etmede yeterli seviyede etkili değildirler. Bu nedenle klinik uygulamalarda genellikle sütürler ve zımbalar için bir takviye olarak doku yapıştırıcıları kullanılır. Bu tez çalışmasında, kardiyovasküler cerrahide kullanılmak üzere, deniz midyelerinin güçlü yapışma özelliklerinden esinlenerek doğal polimerlerden hareketle biyouyumlu ve ıslak yüzeylerde yapışabilen ve iletken özellikte, biyouyumlu doku yapıştırıcısı geliştirilmiştir. Deniz midyelerinin ayaklarında bulunan proteinler, su altında güçlü yapışmayı sağlamak için katekol bakımından zengin, yüksek performanslı yapışkan sistemler geliştirmek için ideal bir model sunmaktadır.

Tez çalışmasında, ilk olarak aljinat polimeri oksidize edilmiş ve ardından metakrilik anhidrit kullanılarak metakrile edilmiştir (OMA). Elektroiletken özellik kazandırmak için OMA polimerine polipirol takılmıştır (OMA-PPy). Geliştirilmesi planlanan doku yapıştırıcısının ıslak ortamda yapışma davranışlarını arttırmak için, OMA polimeri dopamin hidroklorür (DOPA) ile reaksiyona sokularak OMA-DOPA polimeri elde edilmiştir. Ek olarak doku yapıştırıcının hedef dokuyu daha iyi taklit etmesi, hücre dışı matrikse (ECM) benzer bir mimariye sahip olması için formulasyon içeriğinde metakrilik anhidrit ile modifiye edilen jelatin polimeri (GelMA) kullanılmıştır. Sentezlenen modifiye polimerler OSA, OMA, OMA-PPy, OMA-DOPA ve GelMA, Fourier-transform Infrared Spectroscopy (FTIR) ile karakterize edilmiştir. Doku yapıştırıcıları fotobaşlatıcı olarak Lithium phenyl-2,4,6-trimethylbenzoylphosphinate (LAP) varlığında, 60 sn boyunca ışık altında çapraz bağlanarak hazırlanmıştır. Geliştirilen doku yapıştırıcıları yapısal karakterizasyon, şişme, degradasyon, basma testi, iletkenlik, *in vitro* Lap-shear, *in vitro* t-soyulma, *in vitro* patlama basıncı, *ex vivo* patlama basıncı, *ex vivo* yara kapama testleri ile karakterize edilmiş olup; özellikle sıkıştırma dayanımı açısından doğal kalp dokusuna yakın özellikler sergilemiştir (GelMA/OMA-PPy/DOPA sıkıştırma dayanımı ~1007.35 kPa). Koyun miyokardiyum, perikardiyum ve arter dokularında gerçekleştirilen *ex vivo* patlama basıncı ve *ex vivo* doku adezyonu testleri, geliştirilen GelMA/OMA-PPy/DOPA doku yapıştırısının güçlü yapışma özelliği sergilediğini göstermiştir. Doku yapıştırıcılarının sitotoksisitesi, H9c2 kardiyak miyoblast hücre hattı üzerinde MTT testi ile değerlendirilmiştir. Elde edilen sonuçlar, geliştirilen GelMA/OMA-PPy/DOPA doku yapıştırıcılarının kalp damar cerrahisinde kullanılabilir olduğunu göstermiştir.

Anahtar Kelimeler: Doku Yapıştırıcı, İletken, DOPA, Polipirol, Kalp Damar Cerrahisi

Bu çalışma, Türkiye Sağlık Enstitüleri Başkanlığı (TÜSEB) tarafından desteklenmiştir. Proje No: 13302.

ABSTRACT

Kalender, Y. (2024). Conductive Tissue Adhesives Inspired by Mussels for Use In Cardiovascular Surgery. Istinye University Graduate Education Institute, Stem Cell and Tissue Engineering Department. Master's Thesis. Istanbul.

Cardiovascular injuries are commonly treated using surgical sutures and staples; however, these methods are often insufficient in completely closing the cardiovascular defect area and controlling bleeding effectively. Therefore, tissue adhesives are frequently used in clinical applications as a supplement to sutures and staples. In this thesis, inspired by the strong adhesive properties of marine mussels, a biocompatible and conductive tissue adhesive that can adhere to wet surfaces has been developed for use in cardiovascular surgery. Proteins found in the feet of marine mussels offer an ideal model for developing high-performance adhesive systems rich in catechol to achieve strong underwater adhesion.

In this thesis, alginate polymer was first oxidized and then methacrylated using methacrylic anhydride (OMA). To impart electroconductive properties, polypyrrole was attached to the OMA polymer (OMA-PPy). To enhance the adhesive behavior of the planned tissue adhesive in wet environments, the OMA polymer was reacted with dopamine hydrochloride (DOPA) to obtain the OMA-DOPA polymer. Additionally, to better mimic the target tissue and have a similar architecture to the extracellular matrix (ECM), gelatin polymer modified with methacrylic anhydride (GelMA) was used in the formulation. The synthesized modified polymers, OSA, OMA, OMA-PPy, OMA-DOPA, and GelMA, were characterized using Fourier-transform Infrared Spectroscopy (FTIR). Tissue adhesives were prepared by crosslinking under light for 60 seconds in the presence of the photoinitiator Lithium phenyl-2,4,6-trimethylbenzoylphosphinate (LAP). The developed tissue adhesives were characterized through structural characterization, swelling, degradation, compression testing, conductivity, *in vitro* Lap-shear, *in vitro* t-peel, *in vitro* burst pressure, *ex vivo* burst pressure, and *ex vivo* wound closure tests. They exhibited properties close to natural heart tissue, particularly in terms of compression strength (GelMA/OMA-PPy/DOPA compression strength ~1007.35 kPa). *Ex vivo* burst pressure and *ex vivo* tissue adhesion tests conducted on sheep myocardium, pericardium, and artery tissues demonstrated the strong adhesive properties of the developed GelMA/OMA-PPy/DOPA tissue adhesive. The cytotoxicity of the tissue adhesives was evaluated on H9c2 cardiac myoblast cell line using the MTT assay. The results indicate that the developed GelMA/OMA-PPy/DOPA tissue adhesives are suitable for use in cardiac vascular surgery.

Keywords: Tissue Adhesive, Conductive, DOPA, Polypyrrole, Cardiovascular Surgery

This study has been supported by the Turkish Health Institutes Presidency (TUSEB). Project No: 13302.

1. INTRODUCTION

Every year, tens of millions of people have different types of tissue wounds, from simple skin cuts to serious injuries caused by trauma, chronic wounds such as diabetic ulcers, and surgical cuts. Clinical treatments for such injuries mainly involve reattachment of the injured tissue and closure of the defect site in order to stop bleeding, prevent leakage, and ultimately restore tissue shape and function [1]. Historically, stitches and staples have been the main tools used to achieve these ends. While these gold standard techniques for wound closure are effective in most cases, they can leak up to 30% in some challenging situations. In addition, when sutures are present at the surgical site, the likelihood of bacterial infection increases. Suture placement can take time as healed tissue must be carefully adjusted before each pass of the suture needle and sutures can damage particularly delicate tissue. In addition, suturing in minimally invasive operations is difficult and undesirable in emergencies; for instance, incorrect suture placement necessitates its removal and replacement, which can damage delicate tissues. Also, when wounds are large, these materials face difficulties in achieving effective wound closure [2].

Tissue adhesives have developed rapidly over the past 30 years, becoming more and more essential components of modern medicine. It enables natural wound healing processes to take place by adhesion of tissue to nearby tissue or to non-tissue surfaces near tissue. As a result, it exhibits some clinically desirable features such as no post-operative stitching, easy application, less traumatic closure and suturing, targeted drug release, and excellent cosmetic results [3]. Tissue adhesives can seal the wound site and stop leaks while offering hemostatic properties and mechanical support. A good tissue adhesive (1) has the chemistry that promotes strong tissue adhesion, (2) is biocompatible and non-toxic, (3) has mechanical capacity in order to withstand repeated and repetitive dynamic forces exerted by the tissue, (4) is similar in terms of mechanics to the underlying tissue, (5) has tissue's capacity to degrade at a rate compatible with healing, and (6) has an acceptable swelling profile to minimize tissue compaction [1]. However, only a few of these needs are met by existing adhesives. The choice of adhesive suitable for a particular application is determined by the properties required for that application. The performance of the adhesive is primarily determined by its mechanical and chemical interactions with the tissue, its physicochemical properties,

the local environment, and the host's immune response, which requires interdisciplinary work involving biology, chemistry, and mechanical knowledge for successful tissue adhesive development [4].

Taking into consideration the limitations of existing tissue adhesives, the objective of this thesis is to develop a tissue adhesive specifically designed for application in cardiovascular surgery. In this context, mussels serve as an ideal model for developing high-performance adhesive systems due to the remarkable underwater adhesion facilitated by the byssal thread protein in mussel feet. The proteins, particularly those containing significant amounts of DOPA, a catecholic amino acid, play a crucial role in adherence.

Recently, hydrogels with electroconductive properties have been introduced. The adhesive is expected to exhibit conductive features, biocompatibility, and the ability to undergo biological degradation. Among the various conducting polymers, polypyrole (PPy) is preferred in this thesis due to its simple synthesis, stability in the oxidized state, strong electrical conductivity, advantageous redox characteristics and biocompatibility.

The primary focus is on establishing hydrogel systems based on modified sodium alginate and GelMA, exploring their potential applications in the field of cardiovascular tissue engineering.

2. GENERAL INFORMATION

2.1. Tissue Adhesives

The capacity to stop bleeding and wound closure extends back to the prehistoric era, when primitive man employed leaves and grass as a form of wound dressing. Sutures were used to close wounds as early as 1100 BC, together with grass and leaves, according to historical records [5]. Sutures have great tensile strength and minimal dehiscence, making them the method of choice for wound closure and hemorrhage control for many years. Suturing does have a number of drawbacks, though, including a high likelihood of infection, difficulty in handling, and potential for the spread of blood-borne illnesses. Furthermore, controlling bleeding during surgery has many benefits, including reducing the requirement for blood transfusions, avoiding unstable hemodynamics, reducing the probability of infection, reducing time for operation, decreasing the total death and morbidity rate, and cutting cost [5]. Other approaches have been developed to address these issues, including the use of various staples, clips, agents of hemostasis and tissue adhesives, to aid in faster and more efficient hemorrhage control and wound closure. In order to control bleeding and avoid leakage of body fluid, tissue adhesives are frequently used.

The use of tissue adhesives offers a quick, painless, and removal is not necessary in a subsequent visit strategy for wound closure. When exposed to a moist surface (such as the skin), tissue adhesives, which are liquid monomers, undergo an exothermic process, transforming into polymers that firmly bind tissues together [6]. To improve on current adhesives, a great deal of work has been put into creating a new type of tissue adhesives in recent years. It has been stated that several biologically inspired adhesives have improved mechanical characteristics and functioning over the past 20 years. The finding served as inspiration for the development of active adhesives, which show promise as potential alternatives to staples and sutures [7].

2.1.1. Structure and Properties of Tissue Adhesives

An in-depth knowledge of the tissue-adhesive contact is necessary to design a successful tissue adhesive. Two areas of the interface can be distinguished spatially: the adhesion layer, where the adhesive comes into close contact with the tissue, and the

adhesive matrix, which is made up of the bulk polymeric network that makes up the adhesive. The adhesion layer is structurally supported by the adhesive matrix, which also controls the properties of adhesive such as viscoelasticity, material stiffness, energy loss, resistance to fatique, swellability and degradability [1].

Material adhesion is determined by the physical and chemical properties of tissue surfaces because strong bonding at the material interface between tissue and glue can be accomplished through either chemical or physical contacts. The macro- and microenvironments of the tissue will alter the substance's performance with time. For instance, changes in pH, endogenous enzymes and reactive species might have a significant impact on the properties of materials by lowering the cohesive and adhesive strengths [2]. Figure 2.1 illustrates the primary functions of the tissue adhesive.

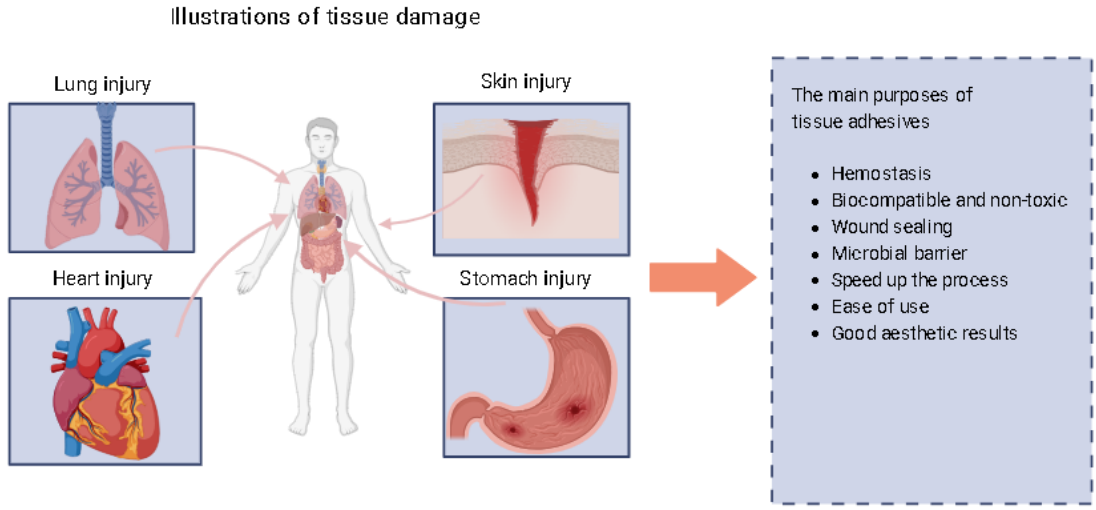

Figure 2.1: Illustration of tissue damage and the main purposes of tissue [1] (Made with Biorender).

Ideally, a tissue adhesive:

- needs to be easy to prepare, risk-free, non-toxic and sterile;
- must also have the necessary flow qualities to be administered precisely and easily to the specified region;
- decreases bleeding and surgical time by quickly solidifying in the physiological situation;

- displays effective tissue adhesion and bonding for the appropriate amount of time, as well as hemostatic properties, tissue regeneration and healing traits, and control of infection;
- retains necessary mechanical characteristics during the process of healing.
- has minimum or no toxicity and be able to degrade and absorb in a reasonable timeframe
- simply and quickly ready for usage in clinical settings;
- be cost-efficient and cheap to gain widespread clinical acceptability.

It is difficult to adress each of these topics in a single material. As a result, when designing a tissue adhesive, one may need to prioritize the desired properties based on clinical needs and the targeted tissue [5].

2.1.2. Classification of Tissue Adhesives

Obtaining appropriate adhesion to soft tissues is the key obstacle, particularly when such tissues are wet and being exposed to dynamic forces. Following is a description of the various classes of adhesive technologies that have been created to date. As depicted in Figure 2.2, three categories of tissue adhesives that are now being used in clinics can be identified: natural tissue adhesives, synthetic and semi-synthetic tissue adhesives, and biomimetic tissue adhesives according to their composition [8].

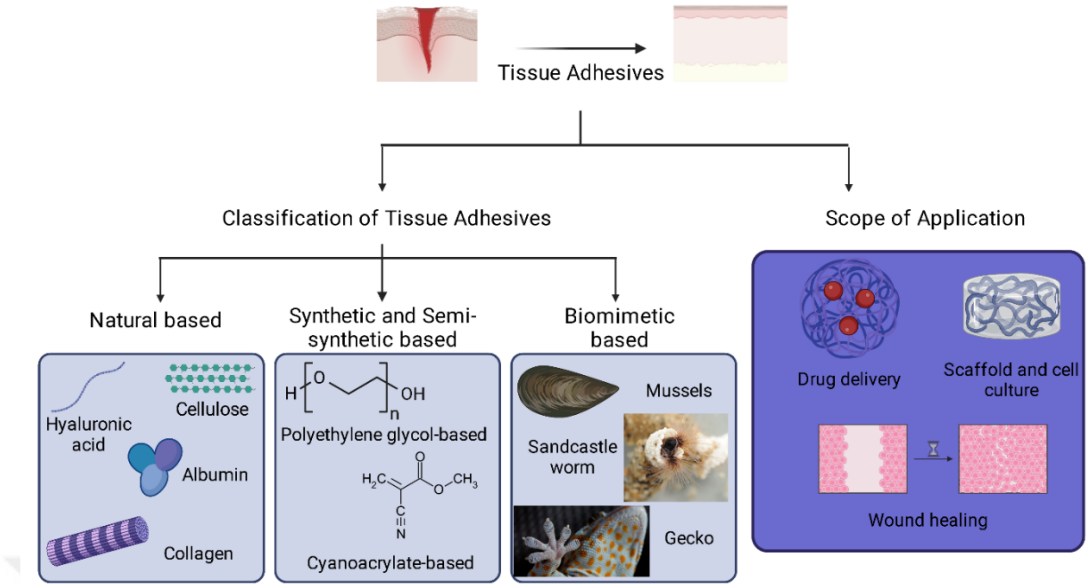

Figure 2.2: Scope of applications and classification of tissue adhesives for use in biomedical purposes (Made with Biorender).

2.1.2.1. Natural Tissue Adhesives

In general, natural polymer-based surgical adhesives and sealants that are cross-linked through biochemical reactions provide a more biocompatible option than synthetic glues [9]. Hydrogels made of natural polymers, in particular, exhibit self healing properties. In contrast to natural polymers, synthetic polymers have excellent mechanical qualities but low biodegradation and biocompatibility. Examples given in the literature include adhesives made of polysaccharide such as alginate, chitosan (Chi) and chondroitin sulfate (CS), hyaluronic acid (HA), dextran, cellulose and protein-based adhesives such as collagen, fibrin, gelatin and albumin. The primary biological adhesives will subsequently be explained in depth.

Tissue adhesives based on Fibrin: The term "Fibrin tissue adhesive" describes products that imitate the last phase of the physiological coagulation cascade, which results in a fibrin clot. Plasma proteins were originally used to create these products [10]. Combinations of thrombin and fibrinogen are the fundamental components of fibrin sealants and wound healing and hemostasis are aided by them. In general, fibrin sealants are composed of two major constituents: thrombin and fibrinogen (with or without factor XIII and fibronectin), along with trace amounts of calcium chloride and, in a few rare instances, antifibrinolytics such aprotinin [8]. A soluble mesh is created

when fibrinogen is broken down by thrombin into fibrin monomers. Since fibrin is generated from human or animal plasma, the danger of transmission of disease exists even when procedures like as detergent or solvent extraction and heat inactivation are used to decrease the likelihood of virus contamination [11]. The development of virus-inactivated fibrin sealants aided to solve the issue of potential contamination. While having a difficult preparation process, a weak bonding strength, and a slow curing time, these adhesives have great biocompatibility and minimal toxicity [9]. Additionally, adhesives based on fibrin, exhibit a decrease in mechanical strength when exposed to moisture (such as when there is substantial amount of blood present), which renders them unsuitable for maintaining tissue joints that will be subjected to significant tensile loads on wet surfaces. Therefore, in order to stop rapid bleeding during surgery, they are administered with a carrier sponge, along with staples or sutures [12]. Numerous commercial fibrin sealants are being produced globally, including Beriplast P (Aventis Behring, Marburg, Germany), Hemaseel APR (Haemacure Corporation, Sarasota, FL, USA), Bolheal (Fujisawa, Osaka, Japan), Quixil (Omrix, Brussels, Belgium), and Tisseel (Baxter Immuno, Vienna, Austria) [13].

Tissue adhesives based on Collagen: Collagen is a key component of the extracellular matrix (ECM) and a biological substance which generates granulation tissue following blood clotting in the initial stages of wound healing. Additionally, it has been demonstrated to play a variety of significant roles in the control of growth, attachment, division, motility and detachment of the cells as well as organ regeneration. Implanted collagen has gained popularity as a ideal biodegradable material because at the implantation site, host tissue replaces it [14]. In terms of adhesion, collagen sealants and fibrin-based sealants are similar. Collagen based adhesives have been utilized in variety of medical applications including, wound dressings, hemostatic glue and surgical suture materials. Since collagen is from a mammalian source, the risk of infection is low because it is biocompatible. The collagen-bound factor XII is activated by collagen type I, which results in a dose dependent reduction in the time that human plasma takes to coagulate. Through the activation of glycoprotein VI, it amplifies the effects of platelets and promotes the plasma production of thrombin. Furthermore, adhesion to the wound is achieved as a result of blood and coagulation products being absorbed into the collagen fibers and stuck in the interstices. Nevertheless, collagen based hemostats may enlarge when pressed on tissue. As a result, it can not be utilized for ophthalmologic or

urologic procedures [15]. After the introduction of collagen-based adhesives to the market, regulatory authorities from various parts of the world have approved several of these products. The CoStasis® surgical hemostat, functioning as a spray liquid applicable to open wounds, is actively employed in vascular surgery for sealing cerebrospinal fluid leaks. FloSeal®, initially developed by Fusion Technologies Inc., utilizes a mixture similar to CoStasis. Baxter's FloSeal® matrix incorporates human thrombin and bovine gelatin. Pahacel® Absorbable Hemostat is a wet-absorbable collagen sponge applicable to bleeding surfaces, particularly when standard techniques for controlling capillary, venous, and minor arterial bleeding are impractical or ineffective. It has been used in surgical interventions. Helistat® Absorbable Collagen Hemostatic Sponge is produced from the deep bovine flexor tendon, acknowledged as one of the purest collagen sources easily accessible in commercial quantities. Avitene®'s (Davol, Inc.) collagen-based hemostatic sponge is another commercial product, available in collagen hemostat microfibrillar sheets. Introduced in 1976, it has undergone continuous product development. Compared to their fibrin counterparts, collagen-based adhesives carry a lower risk of infection and are relatively more cost-effective [16].

Tissue adhesives based on Gelatin: Collagen, which makes up the majority of proteins in an animal's body, is partially hydrolyzed to produce gelatin. After hydration, it turns into a semi-solid colloidal gel. Gelatin has a chemical resemblance to connective tissue. Depending on the method of manufacture, gelatin is classified as Type A or Type B. Type A, if made via acid extration, Type B when conditioned with a base following acid extraction [15]. Gelatin has several beneficial features, including biocompatibility, biodegradability, commercial availability at low price and low immunogenicity. In order to stop bleeding until the body's natural clotting system comes in, gelatin is utilized as a mechanical hemostatic substance. These substances offer a mechanical barrier to which the platelets can bind and which promotes the coagulation process. As a result of the gelatin matrix's granular structure, the substance may adapt to any irregularity in the wound surface. Gelatin's biological and mechanical features can be considerably changed by crosslinking it or by adding additional substances [17]. Tissue adhesive made of photo-crosslinked gelatin has recently been created and with the use of Bolton-Hunter modification, created photo-crosslinked gelatin and added more phenolic side chains, resulting in photo-crosslinked polymers with outstanding

characteristics also, for the purpose of closing wounds, it was created photo-crosslinked gelatin with excellent elasticity and powerful adhesion [18]. Adipic acid dihydrazide modified gelatin (Gel-ADH) and oxidized sodium alginate (OSA) were used to create an injectable hydrogel tissue adhesive in a different investigation. This tissue adhesive was discovered to have a homogeneous structure, an adequate swelling ratio, outstanding injectability and great cytocompatibility and hemocompatibility [19]. Based on all of these findings, it appeared that the created hydrogel offered great potential as a soft tissue adhesive.

Tissue adhesives based on Albumin: In the past, animal blood was employed as glue, and serum albumin, a significant component, probably played a crucial part in its adhesive characteristics. BioGlue®, a commercially available surgical adhesive, is made of bovine serum albumin (BSA) that has been covalently crosslinked with the toxic coupling chemical glutaraldehyde [20]. Better formability, lack of need for prior preparation, and a lengthy shelf life without refrigeration are just a few of distinguishing benefits of Bioglue. Since no components of pooled human plasma are used, the risk of viral transmission is decreased; however, there is a chance of BSA will cause an alergic reaction. These characteristics have made Bioglue very effective at stopping bleeding at vulnerable cardiovascular anatomoses but, it is useless for the control of active bleeding since it needs a bloodless area to adhere [15]. Another commercially available adhesive derived from albumin is Progel (Davol), utilized as a pleural air leak sealant for postoperative complications [16]. In a recent study, citrate acid (CA), BSA and dopamine were combined to create a “BCD” tissue glue with inspiration from mussels. In comparison to commercially available fibrin glue in a moist environment, this newly designed BCD tissue glue can offer over ten times the adhesion stress in just 30 minutes [21]. Its excellent qualities as an internal tissue adhesive also include good cell compatibility *in vitro*, good biocompatibility *in vivo*, adequate degradation rate and excellent swelling behavior and gelation. In addition, the preclinical effectiveness of BCD tissue glue as a tissue adhesive for diverse internal medical purposes was ultimately proven by successful animal experiments in prevention of seroma and rapid hemostasis.

Tissue adhesives based on Chitosan: Chi, derived from the deacetylation of chitin, is a positively charged polysaccharide that holds significant value in biomedical

applications due to its excellent biodegradability, non-toxicity, antibacterial properties, and lack of antigenicity. In the 1980s, Chi powders were employed for hemostasis in open wounds by utilizing electrostatic interactions with erythrocytes and manual compression to expedite blood clotting. The FDA has granted approval for two hemostatic agents, CloSur PAD and Hemcon chitosan, which effectively control blood loss through platelet aggregation effects [22]. In a recent research, an injectable hyrdrogel with mussel-like characteristics was created using catechol and methacrylate modifications to gelatin and Chi, and it was found to be biocompatible, have antibacterial properties, and adhere well to moist tissues. It was determined that it was a potentially useful surgical sealant and wound dressing that might speed the healing of wounds, even those that were infected [23]. In another study, Chi modified with hydrocaffeic acid and with Chi lactate that has been hydrophobically modified hydrogel, which is biodegradable and biocompatible, effectively closed the wound and accelerated wound healing. The outcomes demonstrate the significant potential of this hydrogel for the smooth closure of surgical wounds [24].

Tissue adhesives based on Alginate: Alginate is a widely produced biosynthesized polymer, a hydrophilic and anionic polysaccharide found in nature. As depicted in Figure 2.3, it is primarily produced by bacteria and brown seaweed [25], and it has various applications in tissue engineering.

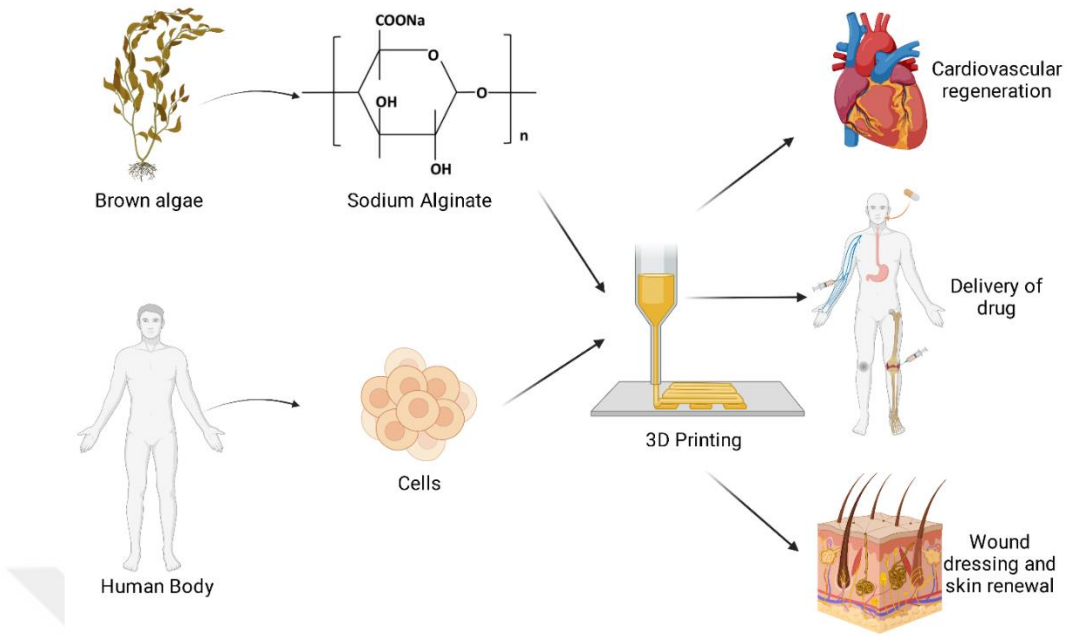

Figure 2.3: Various uses in tissue engineering of alginate structures created through 3D printing (Made with Biorender).

Alginate is a biomaterial that has received significant attention due to its wide range of potential uses, particularly as a supportive matrix or delivery system for drugs, tissue repair and regeneration, and wound dressing because of its outstanding properties such as chelating power, biodegradability and biocompatibility. Additionally, it was discovered that sodium alginate hydrogels had the strongest *in vitro* bioadhesive properties [26]. As depicted in Figure 2.4, 1,4-linked **β**-D-Mannuronic acid and ∝-L-guluronic acid are two monosaccharides and their repeating units connected with glycosidic linkages and form the alginate salt which is sodium alginate [27].

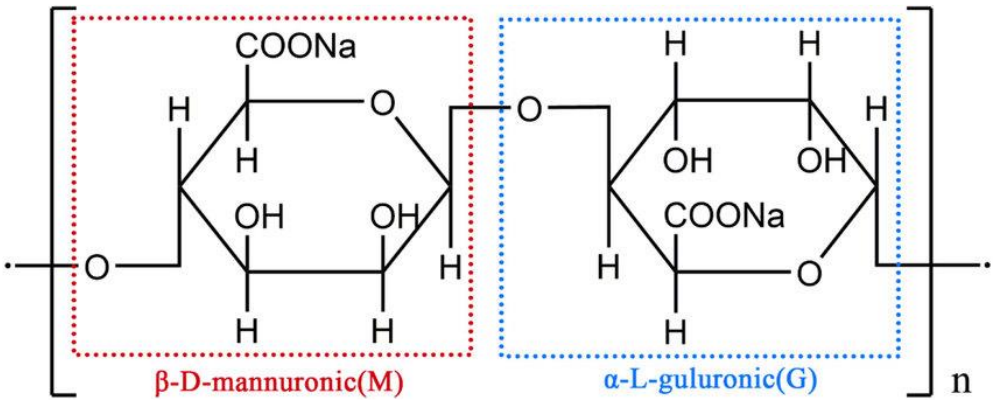

Figure 2.4: Chemical composition of sodium alginate [28].

The proportions of these monosaccharides vary depending on the type of seaweed from which the alginate is derived, and this causes the produced sodium alginate to have different chemical properties. Depending on the kind of alginate employed, alginate hydrogels can have varying degrees of resilience. The source and circumstances of the extraction technique might have an impact on the viscosity of aqueous alginate solutions, decreasing it under difficult circumstances. *Laminaria digitata* creates hydrogels with a softer to medium strength, but *Laminaria hyperborea* can yield robust hydrogels through meticulous extraction. Compared to alginate extracted from seaweed, alginate produced via bacterial biosynthesis may have distinct chemical compositions. Typically, stronger hydrogels are produced using alginate with a lower M/G ratio [29].

Sodium alginate is commonly a powdery substance that appears in hues varying from white to yellowish-brown, whithout any detectable scent or flavor, and has the ability to dissolve in water but not in organic solvents. The molecular weight of sodium alginate polymer, which has a linear structure, ranges between 32,000 to 400,000 g/mol. The mannuronic acid (M block) is in charge of the alginate's solubility in water, whereas the guluronic acid (G block) is in charge of the development calcium induced gelation. Sodium alginate is an anionic polymer capable of interacting with positively charged ions including calcium ions and metal cations because the M and G blocks of sodium alginate contain carboxyl groups. Level of polymerization, the molecular weight, and pH of the solution are some of the variables that affect sodium alginate's solubility. The solubility of alginate in water decreases with increasing molecular

weight and polymerization level. The solubility of the alginate is also affected by the pH of the solution. The alginate's carboxyl groups are protonated at low pH levels, causing it insoluble in water whereas, the carboxyl groups become deprotonated when the pH rises, making the alginate more soluble [30].

Applications for sodium alginate as a natural adhesive include textile printing, papermaking and wound dressings. Applications for sodium alginate in biomedical include tissue engineering, drug delivery systems, and wound healing. The capacity of sodium alginate to gel when in contact with calcium ions is what provides its adhesive qualities. By adding chelating chemicals like EDTA or citrate, which reverse the gelation process, the gel can be broken down [31].

The use of sodium alginate in adhesive compositions for diverse applications has been the subject of numerous investigations. For instance, a research produced a biodegradable adhesive for cartilage tissue engineering based on sodium alginate and Chi. The adhesive's capacity as a natural and biocompatible sealant for medical purposes was demonstrated by its ability to bind cartilage tissues and encourages their regeneration [32]. The adhesive qualities of sodium alginate in a composite film containing silver nanoparticles and polyvinyl alcohol (PVA) were assessed in a paper published in 2020. The findings demonstrated that the inclusion of sodium alginate enhanced the film's water resistance and adhesive strength [33]. In another research, dopamine was added to OSA in order to create a novel crosslinker (COA), which was then incorporated into the collagen/polyacrylamide double network to create a hydrogel which was inspired by the strong adherence of natural mussels. Scanning electron microscopy was used to characterize the hydrogel's morphology, and the results showed that COA caused the hydrogel to create a more tangled, disordered structure. PAM-Col-COA hydrogel demonstrated strong mechanical qualities, absorbed water, adhered to skin tissues well and maintained biological activity. Hydrogel has the potential to be used in wound dressings since *in vivo* wound healing investigations have shown that it speeds up the healing process [34].

The most widely used adhesive hydrogels in the biomedical industry are those based on polydopamine (PDA), although it is still difficult to combine various qualities on a single adhesive hydrogel. They created PDA-sodium alginate-polyacrylamide (PDA-SA-PAM) based hydrogels with a variety of biological and physiological

characteristics for use in skin tissue engineering applications, drawing inspiration from the chemistry of mussels. The hydrogels successfully adhere to a variety of substrates, and quick blood coagulation was also achieved by the PDA chains' strong hemostatic characteristics [35].

Natural tissue sealants have poor to moderate mechanical characteristics, which restricts their use in dynamic medical applications. Alginate-based hydrogels that utilize visible light for crosslinking have been developed to overcome these restrictions. The effectiveness of using visible light crosslinked methacrylated and oxidized alginate (Alg-MA-Ox) hydrogels as medical tissue adhesives in dynamic *in vivo* systems was examined in a research study. Alginate and related polysaccharides can be chemically altered to allow for controlled covalent crosslinking, which allows the physical and mechanical characteristics of engineered alginate hydrogels to be tailored. This method successfully overcomes the drawbacks frequently connected to ionically crosslinked alginate hydrogels.

Alginate is methacrylated to introduce an acrylate functional group, which can then polymerize by free radicals with the help of a photoinitiator to make covalent bonds with itself. Also, methacrylated alginate (Alg-MA) can undergo covalent crosslinking when exposed to visible light when a photosensitizer is present, making it a safer option than using ultraviolet (UV) light. Moreover, the addition of oxidation to alginate's backbone structure also produces functional aldehyde groups even though alginate is normally non-adhesive polymer. These amine groups on tissue can establish covalent connections with these aldehyde groups, enabling adhesive contacts [36].

Tissue adhesives based on Hyaluronic Acid: N-acetyl-d-glucosamine and d-glucuronic acid combine to form the polysaccharide that is naturally occuring known as HA which has numerous biomedical uses, including tissue engineering and wound healing [37]. As a naturally occurring element of ECM, HA possesses great degradation, compatibility and gelation characteristics. In addition, it can facilitate signaling of cells and mediate migration and proliferation of cells which enable tissue regeneration. HA has been regarded as a particularly attractive option for a tissue adhesive due to these factors [38]. Because of its weak mechanical characteristics, unaltered HA presents challanges when used in a variety of medical applications, as a

result, this weakness can be fixed by chemically altering the catechol, thiol and amine groups on the HA backbone [37].

Available clinical and commercial tissue adhesives are restricted by their poor biocompatibility, decelerate adhesion development and poor bond strength on tissue surface that are wet. Despite the development of catechol modified HA adhesives, they have some drawbacks: due to insufficient catechol group replacement, there is inadequate adhesiveness and too quick disintegration. Dopamine-conjugated dialdehyde-HA hydrogels have outstanding adhesion properties to tissue than HA hydrogels that can be photo-cross-linked and some of the commercial tissue adhesives [38].

Tissue adhesives based on Dextran: Consisting of an α-1,6-linked D-glucopyranose residue, dextran, similar to various polysaccharides, possesses numerous hydroxyl groups in its anhydroglucose unit, making it easily amenable to chemical modification. Furthermore, its notable water absorption provides dextran with hemostatic capabilities, rendering it suitable as a tissue adhesive agent [22]. Dextran, which has biocompatible, biodegradable, low cytotoxicity and inflammatory response properties, is a polysaccharide and is frequently used as a tissue adhesive. Due to lack of tissue reactive groups, aldehyde groups are frequently created by the oxidation of dextran in the polymer backbone. The degree of oxidation is a crucial factor in adhesion regulation. Dextran aldehyde will crosslink too quickly if its oxidation level exceeds 60%, leaving insufficient time for the substance to connect to the tissue. An ideal level of oxidation was discovered to be around 50% [3].

In order to create low-cost tissue adhesive hydrogel with hemostatic properties, Chi and oxidized dextran can be crosslinked, also poly(ethylene glycol) (PEG) can often be used in combination with dextran. For increased shelf life in commercial applications, dextran aldehyde can be swapped out for a synthetic counterpart [3].

Tissue adhesives based on Cellulose: Cellulose, which constitutes a primary element of the plant cell wall, is a homopolysaccharide composed of D-glucopyranose. Cellulose is a biological macromolecule that is common in nature and has strong biocompatibility, biodegradability, water absorbing capability, mechanical toughness and because of its cost-effectiveness and affordability its widely used as a tissue engineering material.

However, there are no reactive functional groups in cellulose, therefore chemical changes must be made in order to create tissue adhesives [39].

Many useful cellulose-based hydrogels have been created recently by cross-linking using carboxymethyl Chi with dynamic Schiff-base connections, metal ions and poly(acrylic acid) chains via numerous coordination connections. Nevertheless, anti-inflammation, haemostasis, remodelling and proliferation abilities of such cellulose based hydrogels demonstrated limited capacity. Double network adhesive hydrogels that are based on cellulose with 3,4-dihydroxyphenylalanine (DOPA) cation copolymer were developed for wound healing in order to control bleeding more effectively in incompressible and irregularly shaped wounds. The collaboration effect between catechol and cations increases the wet adherence of hydrogels to skin tissue surfaces [40]. In another research, the development of tissue adhesive, denoted as CDB-PAM, utilizing borate crosslinked pendant catechol groups derived from the carboxymethyl cellulose-dopamine conjugate (CMC-DA) within a crosslinked network of polyacrylamide (PAM). The hydrogel exhibited self-healing and recyclable characteristics, showcasing self-adhesive properties with prolonged reusability through the preservation of redox-active catechol groups within the hydrogel. *In vitro* biocompatibility tests conducted with skin fibroblasts and keratinocytes cells confirmed the favorable biocompatibility of the hydrogels [41].

Tissue adhesives based on Chondroitin Sulfate: Glucuronic acid and N-acetyl-galactosamine are alternately arranged in a chain to form the polysaccharide known as chondroitin [3]. The primary component of cartilage ECM is chondroitin sulfate (CS), is glycosaminoglycan (GAG) which is sulfated and it is typically found linked to proteins as part of a proteoglycan. It has gained interest as a biomaterial for the tissue engineering [42].

Nevertheless, due to their inadequate degradation kinetics, poor mechanical similarities, and absence of integration with the native cartilage tissue, existing CS hydrogel systems still have restrictions for use in effective cartilage tissue engineering. In order to get over these restrictions, researchers have also attempted to mix CS with supporting substances including carbon nanotubes, graphene and various natural or synthetic polymers such as CS, HA, PEG, polyacrylamide etc. [43]. Furthermore, a functional CS hydrogel with good tissue adherence for effective integration with natural

tissues was created in a recent work employing catechol chemistry that is inspired by the mussel adhesive. In this investigation, this hydrogel showcases adjustable physical and mechanical properties, along with outstanding tissue adhesion, enabling effective integration with native tissues. The catechol-functionalized CS (CS-CA) hydrogel, indeed, promoted the chondrogenesis of human adipose-derived mesenchymal stem cells (hADSCs) through its biocompatible and chondroinductive environment [44].

2.1.2.2. Synthetic and Semi-synthetic Tissue Adhesives

The adhesion of synthetic and semi-synthetic group of adhesives are superior compared to natural adhesion. Nevertheless, these adhesives have a number of drawbacks, include increased cytotoxicity, poor metabolism and bio-absorption and weaker adhesion to moist surfaces. Furthermore, it enhances chronic inflammation caused by the release of certain breakdown products [3]. Whereas, the mechanical characteristics of the hydrogel, like toughness, can be improved by synthetic polymers. Covalent bonds, which are frequently found in tough hydrogels and make them difficult to rebuild after deformation, reduce the hydrogel's capacity for heal itself. In addition, tissue adhesive hydrogel must have the capacity to self heal, particularly during cyclic loading [45]. The initial synthetic material for wound closure, CA (cyanoacrylate), was developed by a German chemist in 1949 and was first clinically employed by a British plastic surgeon in 1959. Subsequently, N-butyl-2-cyanoacrylate was utilized for skin incisions in Canada and Europe. In 1998, Octyl-2-cyanoacrylate (OCA), known as Dermabond, received FDA approval. Studies indicate that CA provides robust mechanical adhesion for sealing leaks. However, internal use may lead to issues such as inflammation, tissue necrosis, or infection.

While CAs gain popularity in dentistry and plastic surgery, their limitations, including exothermic polymerization, release of toxic monomers, low viscosity, and insufficient flexibility for strong mechanical properties, hinder their broad application. Scientists are exploring ways to enhance CA's biocompatibility, including modifying its forms, using hydrophilic isoforms like methoxypropyl CAs, incorporating different plasticizers, and adjusting viscosity to broaden their applicability in various tissue applications [16].

2.1.2.3. Tissue Adhesives Inspired by Mussel

Adhesion require the ability to adhere and endure in wet and submerged conditions for many general purpose and industrial adhesive applications. In addition to this, hydration film formation significantly affects the adhesion behavior in wet conditions, the hydration film forms on the substrate surface and therefore acts as a weak boundary layer, preventing direct contact of the adhesive with the substrate [46]. Furthermore, water molecules and the adhesive functional groups can interact with each other by hydrogen bonding, reducing the surface energy of the substrate, resulting in a decrease in the interactions that is necessary for adhesion [47]. Consequently, humidity has a tendency to reduce or even eliminate the effect of adhesion. The applications of adhesives are severely constrained by their limitations in wet environments.

Nature is a great source of inspiration. In tumultuous aquatic situations, sandcastle worms and mussels may firmly adhere to reefs, and octopuses can attach to surfaces and move dexterously in wet surroundings. Amphibians are also able to travel unrestrictedly in both dry and wet environments [47]. Researchers were initially interested in mussels and sandcastle worms due to their excellent adherence [48].

The underwater adherence of mussels and the characteristics of their adhesive proteins have drawn a lot of attention from researchers in recent years. Mussel-inspired adhesives have also become more attractive due to their, non-immunogenic, biodegradable and non-toxic qualities.

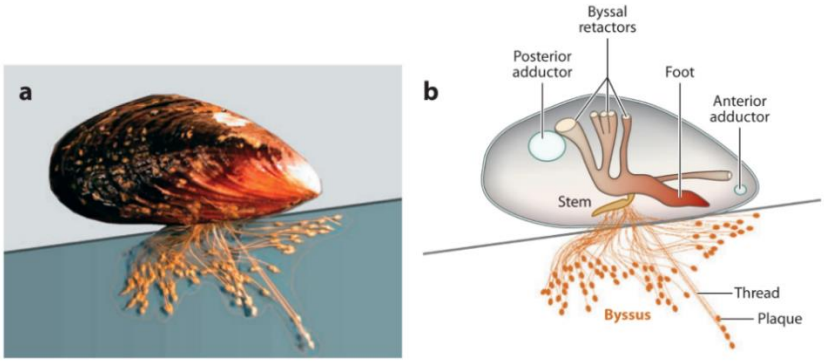

Figure 2.5: (A) A mature mussel staying attached to a mica surface and displaying a large byssus. (B) Schematic representation of mature mussel adhering to a mica surface [49].

As depicted in Figure 2.5, every single byssus is made up of a bundle of threads that are finished with adhesive plaques. The threads are linked at the stem, which is inserted into the foot's base. Twelve byssal retractor muscles, six per valve, control byssal tension. The valves are opened and closed by the two adductor muscles [50]. Because of the byssal thread protein produced by the mussel foot, mussels have remarkable underwater adhesion. Only five of the approximately 30 species of mussel foot proteins (mfps) have been found in the mussel plaques, and these are mfp-4, mfp-3, mfp-6, mfp-2 and mfp-5 [51]. As depicted in Figure 2.6, among these, mfp-5 and mfp-3, which are containing large amounts of DOPA that is, catecholic amino acid, and found at the plaque surface, are crucial for adherence [52].

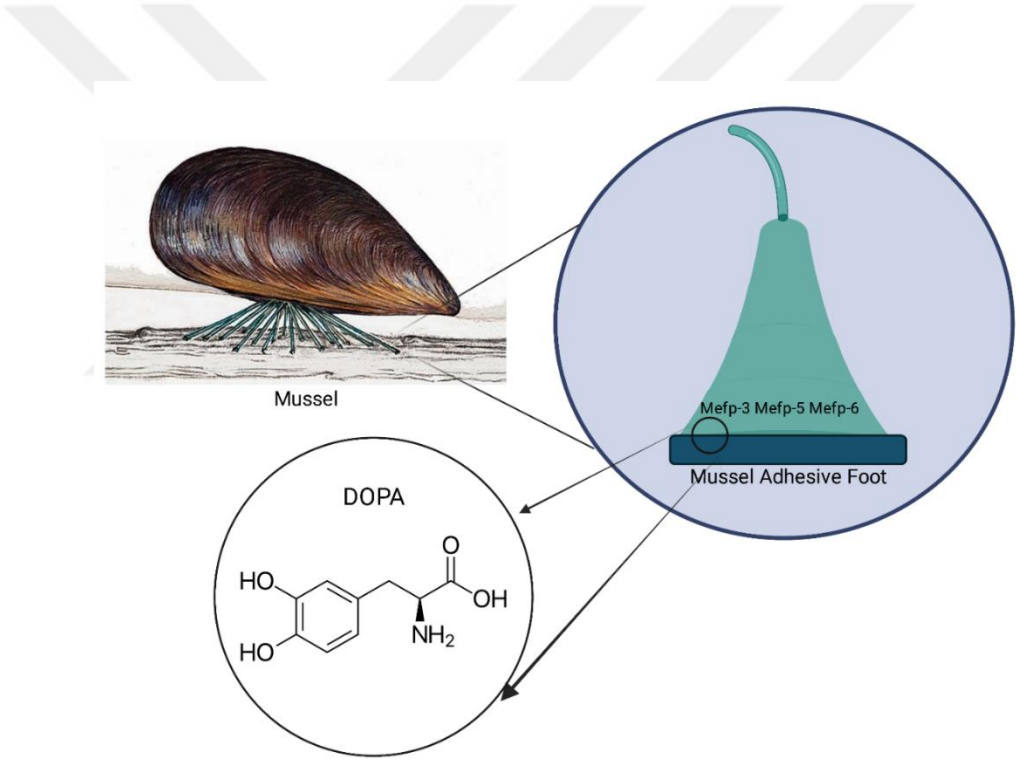

Figure 2.6: Illustration of the *Mytilus edulis* foot proteins (Mefp) in the byssal adhesive plaque of the mussel and molecular structure of DOPA from mussel *M. edulis* (Made with Biorender).

Also, DOPA is produced post-translationally from tyrosine by the hydroxylation process. The presence of high lysine (Lys) amino acid in the mussel adhesion proteins has caused it to be rich in positively charged components, and the hydrated membrane or cationic hydrated barrier layer is eliminated due to the positive charge's repelling

power. Thus, adhesives based on mussel-inspired in order to accomplish underwater adherence, the inclusion of organic cations and catechin groups are required [46].

Catechol oxidase's oxidation of DOPA, the alkalinity of the sea, and the complexation of ions all contribute to the adhesive's increase crosslinking density and cohesion strength [53]. In both sandcastle worms and mussels, DOPA is essential for the moist adherence of the adhesive protein glues [54].

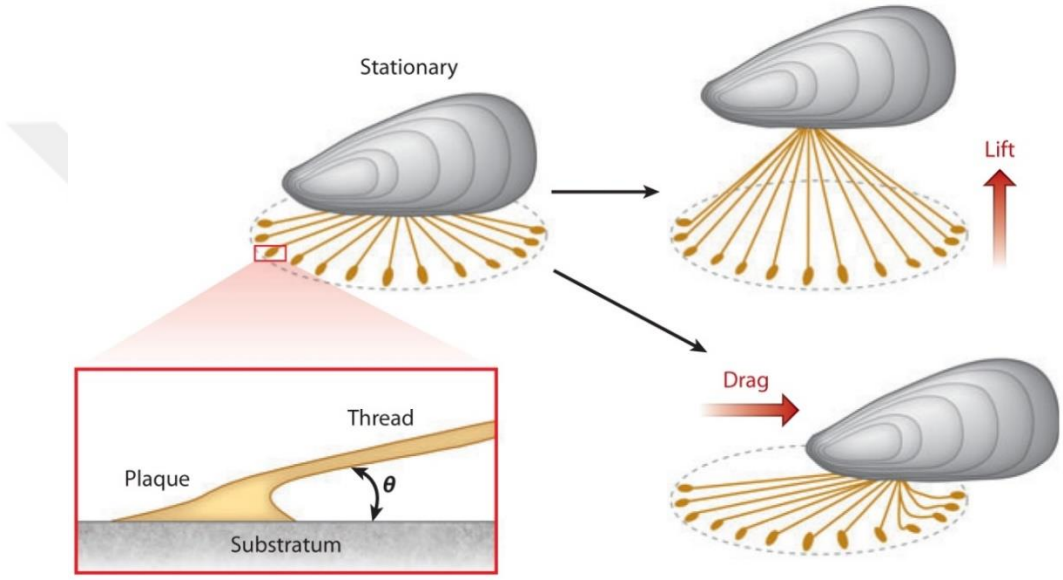

Figure 2.7: Mussels in a flow encounter both lift and drag. A mussel in a calm water is seen on the left with an idealized byssus, equally spaced threads of the equivalent length make a little angle with the surface [50].

Since DOPA is unstable, DOPA-quinone can be produced simply. The catechol of DOPA is changed to quinone upon oxidation by an oxidizing substance, higher pH value, or an enzyme and then it can take part in chemical cross-linking via number of different processes [1]. While the oxidation of DOPA enhances the adherence to organic surfaces by generating highly powerful irreversible covalent connections, it tends to significantly weaken interactions with inorganic surfaces therefore, it's crucial to regulate DOPA's level of oxidation in order to maintain a balance between adhesion and cohesiveness. The presence of many non-polar amino acids on DOPA groups, for example glycine, in adhesive protein glues of sandcastle worms and mussels, provides a balance between cohesion and adhesion by preventing excessive oxidation of DOPA by

electrostatic protection or hydrophobic interactions [47]. In addition the oxidation of DOPA after secretion depends on the pH value of the surrounding medium switches from weakly acidic to weakly alkaline and hydrolytic activation of latent catechol oxidase [55]. In a conducted study, the tyrosine residues present in human gelatin underwent enzymatic conversion into DOPA through a reaction involving tyrosinase. Upon introducing Fe^{3+} ions, the DOPA-modified gelatin rapidly formed an adhesive hydrogel within seconds, facilitated by the complexation between DOPA molecules and Fe^{3+} ions. The resulting DOPA-modified gelatin hydrogels, crosslinked by Fe^{3+} ions, demonstrated excellent stability as hydrogels at body temperature in an aqueous environment, exhibiting suitable mechanical properties [56]. In a different investigation, CS was modified with DOPA groups to facilitate crosslinking. Subsequently, the newly developed dopamine-conjugated chondroitin sulfate (CSD) adhesive hydrogel underwent characterization both *in vitro* and *in vivo*. Its potential for application as a bioadhesive in various internal medications was also assessed using animal models. *In vitro* tests verified the good elastic compliance of CSD to soft tissues, its promising adhesive strengths, and the favorable cytocompatibility of its degradation products with surrounding cells [57].

2.2. Properties of Hydrogels

Hydrogels are regarded as soft substances that are often made of crosslinked, 3D, networks of hydrophilic, natural or synthetic polymers that are rendered insoluble [58]. Hydrogels have been created and used in a number of medical procedures because of their high biocompatibility and high content of water. As depicted in Figure 2.8, because the characteristics of the hydrogel can be adjusted by using a number of chemical techniques, hydrogels are now being used as tissue engineering scaffolds for controlling the fate of the cell, stem cell growth and tissue regeneration, their engineering have made it possible to develop new methods for delivering cells, proteins and small molecules [59].

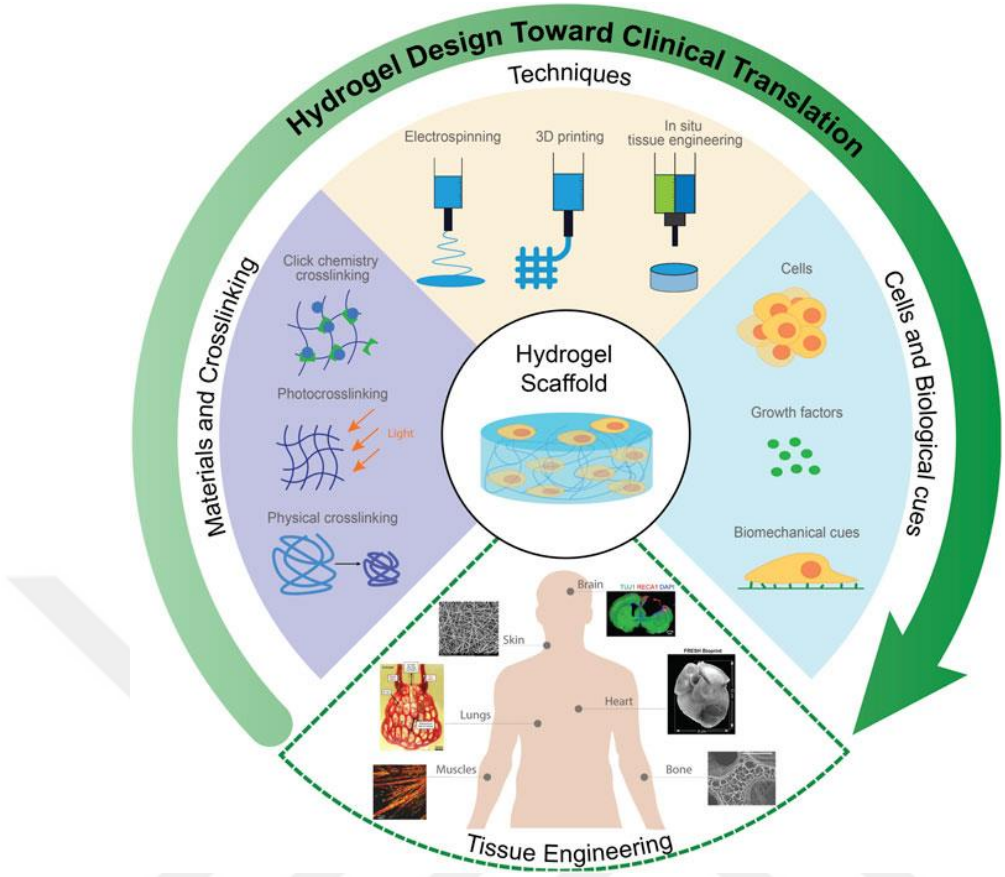

Figure 2.8: The design of hydrogels for biomedical applications [60].

The type of hydrogel affects how well it adheres to cells and surfaces, and thus, how well it is applied. As materials for hemostasis and wound dressings, tissue adhesive hydrogels are applied. The abundance of water molecules in conventional hydrogels makes it difficult for them to adhere surfaces. The strength of the adhesion is weakened when a thin layer of water builds up between surface and hydrogel. However, hydrogels with high adherence could be used for a variety of tissue types, hence different adhesion processes are needed. In order to achieve adhesion, mechanical interlocking, non-covalent interactions or covalent bonds can be used [45]. Those polymer networks usually interact physically or chemically to form cross-links. Several networks are frequently created due to the single chemically cross-linked network's low mechanical qualities, in order to create tough hydrogels, such as the double network hydrogel [61]. Permanent hydrogel is created using a chemical cross-linking technique that uses of covalent bonds among polymer chains. In comparison to those of hydrogels that are physically crosslinked, the majority of their bonds are robust and permanent.

Conjugation of polymers, small cross-linking compounds, photosensitive substances, or reactions that catalyzed with enzymes can all used to create the cross-links [62]. Hydrogels that are crosslinked chemically, typically display improved stability under physiological circumstances, superior mechanical qualities and tuneable degradation characteristics, as opposed to hydrogels that have been physically crosslinked [63].

Furthermore, the best materials for mimicking the mechanical, physical and chemical qualities of natural ECM are believed to be hydrogels. Hydrogels are a particular class of moist and soft materials that are frequently researched and produced as potential options for cell scaffolds and tissue organs [61].

However, since hydrogels are generally non-conductive, their uses as bioactive scaffolds for excitable tissues such as cardiac, neuronal and skeletal muscle tissues is limited [64]. Hydrogels with electroconductive properties have recently been developed, by adding various conductive polymers such as polypyrrole (PPy), polyaniline, polythiophene and various nanomaterials such as silver nanowires, gold nanoparticles (AuNp), graphene oxide (GO) and carbon nanotubes to their network [65]. These electroconductive hydrogels (ECHs) are an assortment of smart biomaterials that bring together biocompatible, highly hydrated hydrogel networks and inherently conductive component's electrical characteristics. Conductive hydrogel can have tunable physical and biochemical features that are tailored to diverse biomedical needs by using various conductivity techniques. With its high swelling and stimulus reactivity, the conductive hydrogel can be used as a scaffold to support cell growth *in vitro* and to promote tissue regeneration, medication administration, and wound healing *in vivo* [66]. The usage of ECHs and conductive polymers has been investigated for different biomedical applications, such as electrochemical biosensors [67] and electro-responsive drug delivery systems [68], because many tissues are susceptible to electrical stimulation. ECHs have also been widely used as tissue-engineered scaffolds to encourage cellular adhesion, differentiation, proliferation and growth, in addition to electroactive modulation of many different kinds of cells, such as cardiomyocytes (CMs), cardiac fibroblasts (CFs), neurons, endothelial cells, preosteoblasts, and mesenchymal stem cells (MSCs) [69]. In a study, when human mesenchymal stem cells (hMSCs) were seeded onto electrically conductive polypyrrole/alginate (PPy/Alg) composites, it was discovered that these materials encouraged hMSCs' adherence, proliferation, and

differentiation into neural cells [70]. PPy is a biomaterial that conducts electricity and can be used to modify the responses of many different cells, including electrically excitable cells like neurons [71]. Due to the material's outstanding electrical conductivity, lack of toxicological issues, and excellent environmental stability in ambient circumstances, PPy is an extensively investigated π-electron conjugated conducting polymer [72]. Because of its simple synthesis, stability in the oxidized state, strong conductivity to electricity, and advantageous redox characteristics, PPy is by far among the most well investigated of the several conducting polymers [73]. In its oxidized state, PPy is a positively charged conducting polymer; excessive oxidation causes it to lose both conductivity and charge. Also, in its neutral condition, it is insulating and mechanically weak. As an extremely smart biomaterial that can have its properties dynamically controlled by the application of an electric field, PPy has exceptional stimuli response abilities. In addition, the biocompatibility of it's both good *in vitro* and *in vivo* [74].

However, PPy, is difficult to process due to its brittleness, insoluble nature, and infusibility. Both academia and businesspeople have worked very hard to make PPy easier to process. There are several PPy composites that have been created, and their electrical, mechanical or electrochemical features have all been studied [74]. Nevertheless, the fragility of PPy as a conjugated conducting polymer restricts its useful applications. Either PPy can be blended with other polymers to increase the material's processability, or PPy can be formed into copolymers to improve the materials's mechanical qualities [75].

In order to give the fabrics or fibers electrical characterisics akin to those of semiconductors or metals, PPy-based composites may be used. It may be created with various porosities and a high surface area, both of which can be easily altered by adding bioactive compounds to make it more suited for biomedical purposes. Fuel cells, computer displays, protection of corrosion, biosensors, microsurgical instruments, systems for delivering drugs, and also, cardiac and neural tissue engineering are just a few of the modern uses for PPy [76].

2.3. Structure of the Heart

The cardiovascular system is made up of a web of arteries and veins and the heart. The heart is a vital organ that is critical to the body's ability to circulate blood. The heart's job is to provide metabolic substrates and oxygen to the body's peripheral tissues. Its role is crucial because the tissues require a constant flow of nutrients and oxygen, as well as the elimination of waste products from metabolism, in order to survive. When cells are devoid of these needs, they quickly experience fatal, permanent alterations. Throughout life, the typical adult heart pumps around 5 liters of blood each minute and the persons's life is at danger if it ceases to pump for even a little period of time. In order to control blood pressure and heart rate, it also collaborates with other systems in the body [77]. Among these, nervous and endocrine systems are primary systems. Heart rate is regulated by the neurological system. It provides messages instructing the heart to beat more quickly under stress and slower when at rest. Hormones are sent by the endocrine system. Blood vessels are instructed to tighten or relax by these hormones, which has an impact on blood pressure. Thyroid gland hormones can also instruct the heart to beat more quickly or more slowly [78]. It can work properly because of its specific structure and special qualities furthermore, its highly specialized structure is made up of various tissue types that cooperate to promote appropriate blood flow. Thus, the pathologic condition known as heart failure can be described as one in which the heart is unable to pump blood at the pace needed by the tissues that are metabolizing it or can only do so with a raised filling pressure. Adults who develop heart failure typically have issues with their left heart. Therefore, the left ventricle's function is primarily assessed clinically during the assessment of cardiac function [79].

The complex muscular organ with a hollow cone form known as the heart is located in the middle of the chest, just behind the sternum. It weighs about 250 and 350 grams and has a fist-size estimated size [80]. The heart is made up of walls, chambers, blood vessels, valves and an electrical conduction system. The muscles that contract and relax to pump blood throughout the body are found in the heart walls and these heart walls are divided into the left and right sides by a layer of muscle tissue known as the septum. As depicted in Figure 2.9, the inner layer, muscular middle layer, and protective outer layer of the heart are known as the endocardium, myocardium, and epicardium, respectively [81]. A layer of the pericardium is called the epicardium. The

whole heart is protected by a sac called the pericardium. The heart is lubricated by pericardium's fluid, which prevents the heart from friction against its neighboring organs.

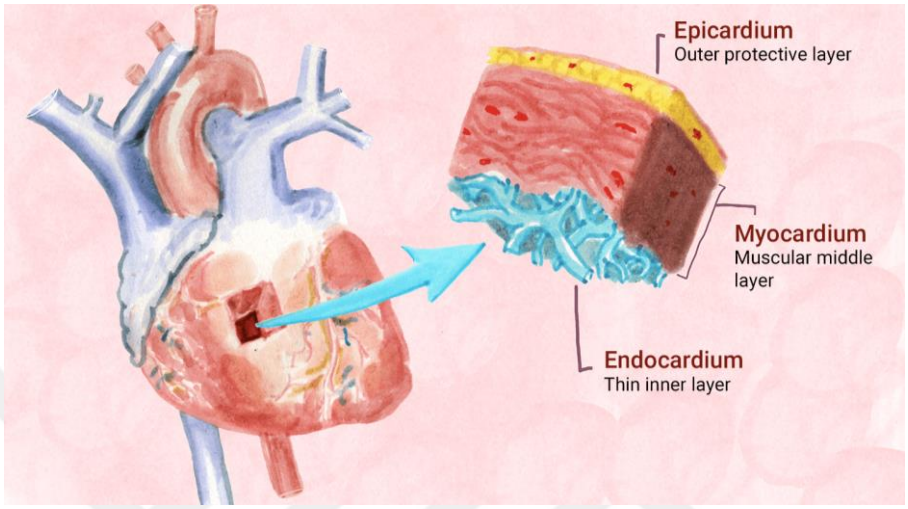

Figure 2.9: Three layers that comprise up the heart, respectively, from the outside to the inside [82].

As depicted in Figure 2.10, the heart's four chambers are divided into two upper and two lower chambers, which are referred to as the right and left atria and the right and left ventricles, respectively. The term "right heart" refers to the right atrium and ventricle as a unit, while, "left heart" refers to the left atrium and ventricle as a unit [83].

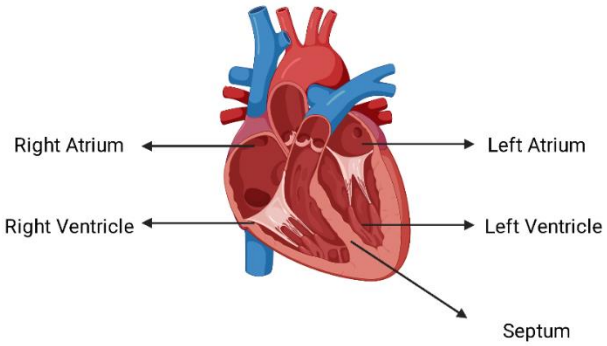

Figure 2.10: Four chambers of the heart (Made with Biorender).

As depicted in Figure 2.11, blood with less oxygen is transported to the right atrium by two major veins. Blood from the upper body is carried through the superior vena cava whereas blood from the lower part of the body is brought up by the inferior vena cava. The blood is then pumped to the right ventricle from the right atrium.

The pulmonary artery is used to move blood that is deficient in oxygen from the right ventricle, which is the lower right chamber, to the lungs, where the blood is then refilled with oxygen. The blood is transported to the left atrium by the pulmonary veins after the lungs have filled it with oxygen. Blood is pumped from this upper chamber to the left ventricle. In comparison to the right ventricle, the left is slightly bigger and from here, blood that is rich in oxygen is pumped to the remainder of the body [84].

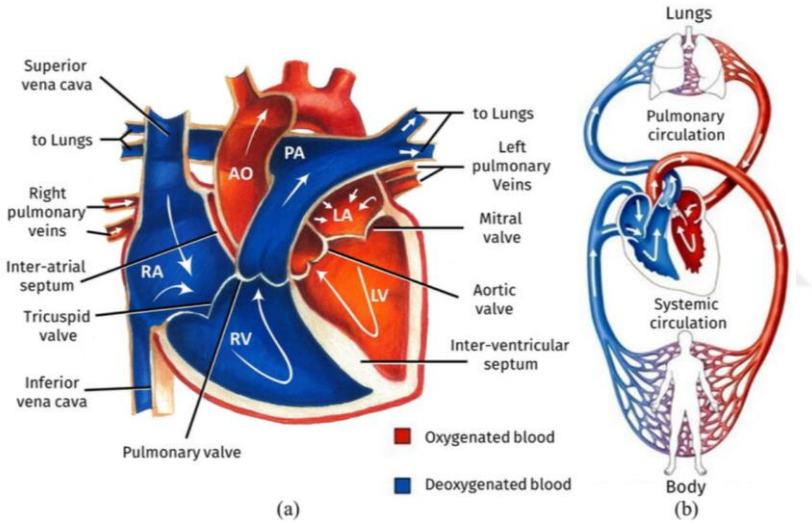

Figure 2.11: (A) The flow of blood through the heart (B) The heart is located within the entire circulatory system [85].

The valves that divide these chambers control the blood's flow through the heart and the septum of the heart which is muscular wall is made up of the ventricular and atrial septa, which divide the ventricles and the atria, respectively. Between the heart chambers, heart valves act as doors, to allow blood to pass through, they reopen and close. The upper and lower heart chambers are connected by the atrioventricular (AV) valves. They consist of tricuspid valve and mitral valve. The passageway connecting the right atrium and right ventricle is tricuspid valve whereas, in the left atrium and left ventricle is a door called the mitral valve. In order for blood to exit the ventricles,

semilunar (SL) valves must open. Aortic valve and pulmonary valve are parts of SL valve. When blood leaves the left ventricle and enters the aorta, which is the artery that supplies body with blood that is high in oxygen, the aortic valve opens, whereas, when blood travels from the right ventricle to the only arteries that deliver oxygen-deficient blood to lungs, the pulmonary valve, which opens as a result [86].

Blood vessels that pump blood throughout the body include arteries, veins and capillaries. The body's tissues receive blood that is full of oxygen from the heart through arteries. Pulmonary arteries, which supply blood to the lungs, are an exception. Poor in oxygen blood is returned to the heart by veins. In addition, the body exchanges rich in oxygen and oxygen-deprived blood in capillaries, which are tiny blood vessels. A network of coronary arteries carries nourishment to the heart and these arteries follow the surface of the heart. The two branches arising from the left coronary artery are the circumflex artery and the left anterior descending artery. The left atrium, as well as the side and rear of the left ventricle, receive blood from the circumflex artery. Additionally, blood is supplied to the bottom and front of the left ventricle as well as the front of the septum via the left anterior descending artery. However, blood is supplied by the right coronary artery to the right ventricle, right atrium, lower region of the left ventricle, and septum's back [87].

A fibrous sac around the heart known as the pericardium houses a little amount of fluid that lubricates the beating of the heart. The inferior and superior vena cava, pulmonary arteries, pulmonary veins, as well as aorta are all attached to the heart [88].

The conduction system is made up of various parts, as depicted in Figure 2.12. The sinoatrial (SA) node is the initial component that makes up the conduction system. SA node displays regular rhytmicity in the absence of neural stimulation by generating impulses at a frequency between 70 and 80 times per minute. It is known as the cardiac pacemaker because of its function in determining the basic heart rhythm. The atrioventricular bundle, atrioventricular node, bundle branches and conduction myofibers are additional parts of the cardiac conduction system. The contraction and relaxation of the heart chambers are synchronized by each of these elements [89].

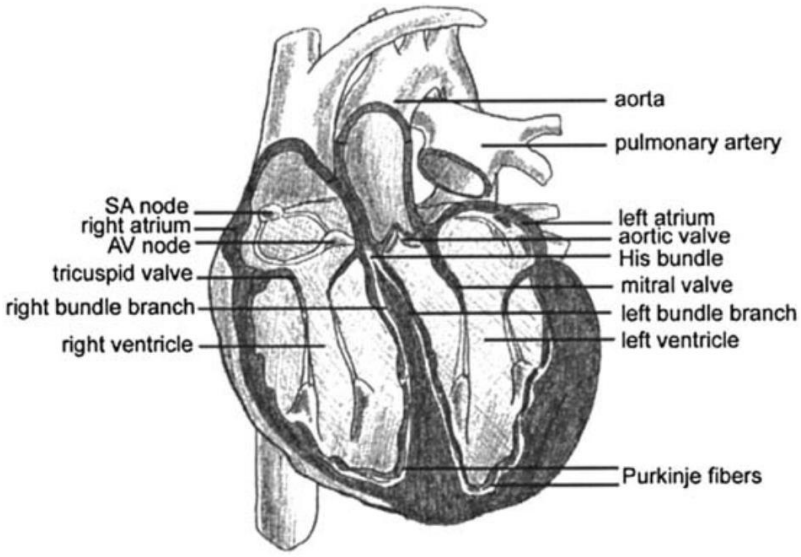

Figure 2.12: The electrical system of the heart and its anatomy [90].

Main function of the heart is to keep blood pumping throughout the body through the circulatory system. It accomplishes this through the cardiac cycle, which is the coordinated contraction and relaxation of the heart. In addition systole and diastole are the two phases the heart goes through within the cardiac cycle and systole is characterized by the contraction of the ventricles, which force blood into the arteries from the heart while the ventricles relax during diastole and enabling blood out of the veins into the heart [79]. The SA node, which is the beginning of the electrical conduction process and is situated in the right atrium, regulates the synchronized relaxation and contraction of the heart muscle. The heart has a number of characteristics that make it capable of carrying out its job well.

These qualities consist of:

1) Contractility: In order to circulate blood throughout the body, the heart muscle must be able to contract and relax consistently.

2) Automaticity: Electrical impulses can be produced by the pacemaker cells of the heart on their own, without help from outside factors.

3) Conductivity: The pacemaker cells, which are specialized cells found in the heart, produce electrical impulses that flow across the organ and regulate the heart's contractions.

4) Elasticity: Each time the heart beats, the heart muscle can stretch and contract, enabling the body to receive blood and push it out [91].

2.4. Cardiac Tissue Engineering and Applications

In developed nations, heart disease continues to be the primary reason for illness and mortality. In the United States, heart-related conditions are the leading cause of mortality for the majority of racial and ethnic groups as well as for all genders [92].

The following are common conditions that affect the heart:

1) Electrical impulses that are irregularly distributed across the atrium are known as atrial fibrillation (Afib).

2) Possessing a heart rate that is abnormally high, abnormally low, or irregularly rhythmic is known as an arrhythmia.

3) Cardiomyopathy is the term used to describe an abnormal thickness, enlargement, or rigidity of the myocardium, the heart's muscle tissue.

4) Congestive heart failure develops when the heart's ability to pump blood is compromised by excessive stiffness or weakness, which leads to insufficient blood flow throughout the body.

5) The buildup of plaque in the coronary arteries, which results in a narrowing of the arterial lumen, is what causes coronary artery disease.

6) The term "pericarditis" describes the pericardium's inflammation [92].

An abrupt blockage of a coronary artery causes a heart attack, depriving a section of the heart muscle of oxygen. Heart attack, scientifically known as myocardial infarction (MI), which ranks first among the causes of death in the world cardiovascular diseases ranking, causes the most common death with a rate of 40.5% [93]. Heart attack causes damage to cardiac cells, and since heart cells are fully differentiated cells, they do not have the ability to renew themselves, which causes permanent damage to heart functions. Although there are medical and surgical options for treating heart failure, the number of patients who are affected by it is increasing. Therefore, novel techniques are urgent necessity for repairing damaged heart tissues as well as more effective

medications for the treatment of heart disease. Tissue engineering has attempted to create biomimetic cardiac tissue since the 1990s with the goal of regenerating the heart. For scientific research and tissue restoration, tissue engineering provides the opportunity to produce functional tissue counterparts [94]. The purpose of the tissue engineering is to develop new tissue scaffolds that are tailored to the geometry of damaged or dysfunctional tissue/organ structures and to develop artificial tissue that is compatible with the body and carry out the function of the tissue/organ [95]. In a conventional tissue engineering procedure, a biopsy is used to extract patient's particular cells, and the extracted cells are then proliferated under controlled circumstances on a 3D scaffold. For new tissue development, a cell-scaffold structure is applied to the wounded area of the patient and the scaffold is expected to degrade over time with tissue formation [96]. There are 3 basic elements to be considered in this concept as depicted in Figure 2.13; first one is a scaffold that possesses strong mechanical and biological qualities that encourages development and differentiation of cell, the second element is creation of desired cell types by differentiation from progenitor cells and the third element is cellular activity and differentiation are regulated by chemicals or growth factors [97].

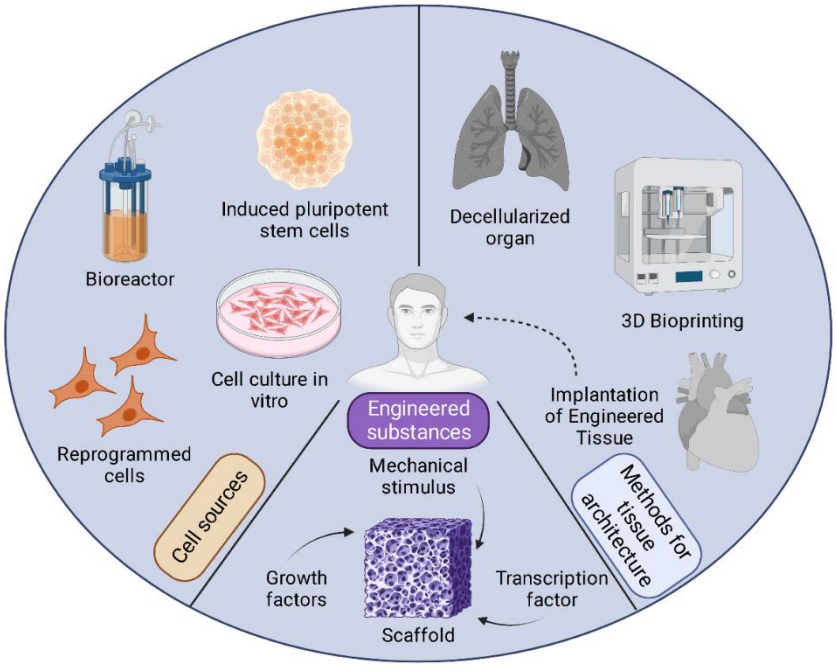

Figure 2.13: Techniques for tissue design, new cell sources, and engineered substances for tissue engineering (Made with Biorender).

Stem cell therapies are among the regenerative medicine methods and studies have been carried out in recent years because they are very promising. However, although clinical studies gave positive results in the early period for the improvement of heart functions, it was observed that this situation disappeared when examined in the long-term, and this led to the conclusion that its benefits are limited [98]. Apart from this, it has been determined that the cells cannot stay in the injured area after cell therapy application and they move away from the injured site or do not remain alive after short time [99]. Therefore, researchers focused on cardiac tissue engineering and created structures with regenerative effects in order to improve the limited benefits of cell therapy and clinical success. When creating these constructs, researchers used both natural and synthetic biomaterials, and they attempted to mimic the mechanical and structural characteristics of the cardiac extracellular matrix (cECM) by combining these biomaterials to create hybrid nanofiber or porous tissue scaffolds.

The heart, an organ with essential duties for survival and great structural and functional complexity, is a marvel of natural engineering. Fibroblasts and myocytes are closely packed together in the heart wall along with a intense supporting vasculature and ECM made of collagen. Due to the cells have a great metabolic demand and high density, the myocardium uses a lot of oxygen and can not endure hypoxia. The contractile cells of the heart which are known as myocytes, combine together to generate a three-dimensional (3D) syncytium which allows electrical signals to pass across particular intracellular junctions and cause blood to be pumped forward through mechanical contractions [100]. The most promising applications of tissue engineering may be in the repair of congenitally defective children's hearts and the renewal of failing adult hearts. A set of design criteria for cardiac tissue is based on the natural myocardium's three fundamental characteristics: first one is effective oxygen transfer among blood and cells; second one is high density of supporting cells and myocytes; and lastly synchronous contractions regulated by electrical signal transmission [101]. The goal of cardiac tissue engineering is to produce constructs of useful tissue that can restore the structure and functionality of damaged myocardium, and these engineered structures can be used as highly accurate models for heart development and disease studies. In most cases, highly regulated three dimensional surroundings that can promote functional assembyl and differentiation of cell are used to activate cell's biological potential. Some of the most important conditions that must be fulfilled for

cardiac regeneration are the choice of a human cell source, electromechanical cell connection, creation of the tissue matrix, strong and consistent contractile activity and vascularization that is functional [102]. For cardiac tissue engineering, choosing the ideal cell source is just as important as choosing the ideal materials. The choosen cell source must have the capacity to differentiate into every type of cardiac cell, be functionally integrated, nonimmunogenic, easy to harvest and be resistant to malignant transformation in order to regenerate cardiac tissue. MSCs, which can proliferate indefinitely, self-renew, and differentiate into any cell type, have been used alone or in combination with a tissue scaffold in several pre-clinical and clinical trials in addition, induced pluripotent stem cells (iPSCs) seem to be prominent in current investigations in cardiac tissue engineering applications. According to studies, these cells can be used to create contractable but immature cardiomyocytes [103]. Products made from cardiac tissue engineering need to blend in with the surrounding tissue in order to be successful and functional. Bioactive molecules are just as important as the scaffold and cell type used. Therefore, in order to enhance the healing and repair effects of these products, researchers use a variety of growth factors such vascular endothelial growth factor (VEGF), insulin-like growth factor-1 (IGF-1) and basic fibroblast growth factor (bFGF) [104]. The biophysical circumstances that cardiac muscle cells are subjected to under physiological conditions are equally important to the biological pathways and epigenetic profile that are crucial for the cardiomyogenic differentiation of stem cells. Since mechanical and electrical stimuli have an impact on natural heart tissue *in vivo*, function and differentiation of the cardiac muscle are significantly influenced by the mechanical characteristics of the cellular environment [105]. Cardiac tissue engineering techniques frequently support heart-specific morphogenesis and maintenance of cell viability. Cardiac patches are designed to substitute for a section of the heart that is no longer functional. It is crucial to choose the right cell population and substance for creating a patch that will deliver a therapeutic agent to the wound site [106]. Products of cardiac tissue engineering, which are heart patches, are anticipated to be biocompatible, biodegradable, physiologically compatible with the microstructure of the heart tissue, and to have flexibility and stiffness characteristics that are similar to the mechanical characteristics of heart tissue [107]. Other crucial properties sought-after include the capacity for powerful and steady contraction as well as vascularization [108].

Surgical sealants have produced important clinical advances in the cardiovascular system. These sealants are commonly utilized to stop bleeding or to reinforce sutures. Adhesive materials face several difficulties in the complex and fluid environment of the cardiovascular system, which is characterized by high pressure. A good sealant should be able to withstand strong pulsatile stresses, maintain adhesion in wet conditions, and work well when exposed to blood, which could potentially disrupt the material's reactive functional groups. Sealants must adhere to both biological and artificial substrates, including synthetic grafts, following multiple operations using medical equipment. The most difficult condition for attaining robust adhesion is that the material mimics the properties of vascular or cardiac tissue while retaining its mechanical characteristics over time. Sealants must be capable of enduring physiological pressure in a non-pathological state [2].

Synthetic polymeric tissue scaffolds play a crucial role in cardiac tissue engineering, offering simplicity in synthesis and processing to mimic natural tissue characteristics. Their customizable mechanical properties and degradation rates make them advantageous for specific requirements [109]. The ability to tailor microstructure, porosity, and durability allows synthetic polymers to precisely emulate cardiac tissue. Polycaprolactone (PCL), polyglycerol sebacate (PGS), pol(lactic-co-glycolic acid) (PLGA), biodegradable polyurethane (PU), and polylactic acid (PLA) are among the most often utilized synthetic polymers in cardiac tissue engineering applications [110]. PCL, favored for its availability, cost-effectiveness, and FDA approval, has been successfully used in electrospun mesh scaffolds supporting cardiomyocyte culture [111]. Hybrid scaffolds combining PCL with natural polymers like elastin and collagen aim to enhance mechanical properties and mimic heart tissue more effectively [112]. PPy and PCL interpenetrating networks promote electrophysiological development, contributing to myocardial-like structures with live and contracting cells [107]. Researchers have addressed PCL limitations through modifications, achieving improved mimicking success and enhanced electrical conduction in tissue scaffolds, this was done to assist with electrical conduction in cardiac tissue [113]. Another notable synthetic polymer, PGS, exhibits structural and mechanical similarity to myocardium, showcasing enhanced vascularization, reduced scar area, and excellent integration with native tissue in animal models of myocardial infarction [114]. PLGA, known for its biodegradability and biocompatibility, has been successfully utilized in electrospun

tissue scaffolds, leading to ventricular tissue regeneration and improved heart functioning in rat models of MI [115]. Overall, synthetic polymeric tissue scaffolds offer versatile solutions in cardiac tissue engineering, addressing various aspects of mimicry and functionality.

Despite their advantages, such as simplicity in processing, high biological compatibility, cheap cost, and fast biodegradation, synthetic polymers fall short of imitating the complex biochemical, physical, and mechanical features of the cECM. The cECM, as previously stated, is a highly complex framework including multiple proteins. Additionally, when synthetic materials are introduced into organisms, they cause a significant foreign body reaction and, as a result of the production of a fibrotic capsule, prevent integration between the surrounding tissue and the material [116]. Natural tissue-derived materials or acellular materials, on the other hand, produce a milder foreign body reaction than synthetic polymers. This is due to the presence of ECM components that can form a contact between the tissue and the substance.

Collagen, CS, fibrin, HA, matrigel, alginate and other biologically produced materials, as well as hybrid structures created by combining these materials, have been widely used in cardiac tissue engineering [117].

Alginate, a versatile biomaterial, finds application in various biomedical fields, including tissue engineering, drug delivery, and wound healing. Its use in cardiac regeneration and valve replacement has gained attention due to features like easy gelation and biocompatibility [118]. The biocompatibility of sodium alginate-based tissue adhesives is advantageous, as they are well-tolerated and do not trigger immune reactions. Additionally, sodium alginate is biodegradable, aiding in progressive breakdown and elimination, supporting tissue regeneration. Heart tissue adhesives made from sodium alginate show promise in cardiovascular procedures, addressing wound sealing, reinforcing weak heart tissues, and treating heart defects [119]. While further research is needed to enhance their formulation and performance for specific procedures and patient populations, sodium alginate-based adhesives have demonstrated potential in preclinical and clinical studies.

In a conducted study, alginate blends with other polymers, such as gelatin, which has been demonstrated the capability of myoblast cell proliferation and differentiation, making them excellent materials for the construction of scaffolds for cardiac regeneration [120].

Designing scaffolds that imitate the ECM through the inclusion of various peptide sequences is currently being studied. The arginine-glycine-aspartate (RGD) pattern was shown to increase cell adhesion to the matrix and the inducement of cardiomyocytes to arrange into cardiac muscle tissue [121].

In the realm of cardiac tissue engineering, the integration of natural biopolymer scaffolds and conductive nanomaterials has demonstrated significant potential. However, challenges persist in scaffold production, necessitating advancements in biocompatibility, nutrition transportation optimization, and the incorporation of features enhancing tissue growth, maturation, and functionality for therapeutic applications. In one of the recent studies, various scaffolds made of sodium alginate and Chi were constructed both with and without the inclusion of nanoparticles of metal and the effects of their construction on cardiomyocyte development were studied. Calcium gluconate added as a crosslinking agent, and hydrogel scaffolds were freeze dried. Furthermore, AuNp and a composite of gold plus nanoparticles with sodium alginate (AuNp+Alg) were used. The scaffolds were subjected to extensive physicochemical testing, including degradation, swelling, infrared spectroscopy and permeability. The findings show that the resultant scaffolds exhibit high porosity and hydrophilicity, as well as swelling percentages and permeability. Furthermore, the scaffolds promoted adhesion and the development of spheroids, as well as the production of cardiac markers such as troponin I, tropomyosin, and cardiac myosin. The inclusion of AuNp+Alg led in increased cardiac protein expression and cell proliferation, demonstrating its promising utility in cardiac tissue engineering [32].

In a study conducted in 2019, injectable hydrogels consisting of self-crosslinking gelatin and hyaluronic acid/gelatin were prepared for the purpose of controlling hemorrhage. These hydrogels exhibited good stability, low cytotoxicity, suitable bursting strength, and excellent hemostatic capabilities compared to commercial fibrin glue [122].

Another investigation focused on the development of a robustly adhesive hemostatic hydrogel for repairing arterial and cardiac hemorrhages. Following the ultraviolet irradiation of methacrylated HA, the hydrogel could rapidly form, adhere to, and seal bleeding arteries and heart walls. These repairs demonstrated the ability to withstand higher blood pressures than those encountered in most traditional clinical settings. Notably, the hydrogel could prevent hypertensive bleeding from a 4–5 mm incision wound in a pig carotid artery and a 6 mm penetrating hole in a pig heart, showcasing significant clinical advantages for wound sealants [123].

Wang and colleagues devised a one-step process for the controlled homopolymerization of hyperbranched PEG-diacrylate (HPEGDA) with reduced swelling and prolonged degradation time. Following UV curing, the resulting hydrogel exhibited effective adhesion to diverse biological tissues, with adhesion strengths ranging from approximately 40 kPa on porcine skin to around 60 kPa on bovine pericardium [124].

In another study, a biodegradable mussel-inspired adhesive polymer was synthesized, consisting of DOPA, polycaprolactone (PCL), and PEG. This copolymer exhibited adhesive strengths 10 times higher than commercial fibrin glue on commercial hernia repair biological meshes. Additionally, the lap shear and burst pressure performance of the adhesive polymer on bovine pericardium surpassed that of commercial fibrin glue [125].

Because of the covalent hydrazine connection which is easier to hydrolyze under physiological circumstances, alginate cross-linking utilizing the hydrazine-based method demonstrated appropriate physical and mechanical stability, biodegradability and cytocompatibility, thus laying the groundwork for the development of modular cross-linked gels that will improve the functioning and clinical relevance of cardiac tissue engineering [126].

Oxidized alginate (OA)-based hydrogels also known as alginate dialdehyde (ADA) can be produced by oxidizing sodium alginate, have received a lot of interest as biodegradable components for tissue engineering. Most earlier investigations have employed periodate as an oxidizing agent because it can oxidize both M and G subunits in the alginate structure. Sodium periodate can be used to oxidize the hydroxyl groups at

the C-2 and C-3 locations of the alginate chain. The carbon-carbon bond is cleaved during this oxidation process, resulting in the creation of two aldehyde functional groups on the monomeric unit's oxidized carbon [127]. When compared to native alginate, OA degrades faster and include more reactive groups. Furthermore, more research and development is needed for clinical translation studies and biodegradability advancements. Under physiological conditions, oxidized alginate has shown good biodegradability and is capable of being used for targeted medication and cell delivery. As an example, hydrogels made from oxidized alginate, PEG, and either gelatin or carboxymethyl Chi, have been developed. These substantial level of crosslinked hydrogels demonstrated the ability of MSCs to survive and proliferate, making them promising options for injectable self-crosslinking deployment in tissue engineering. Because of their biocompatibility and simplicity of modification, alginate-based biomaterials appear to have a promising therapeutic use [128].

The optimization procedure aimed to improve the mechanical and electrical conductivity of a recently developed in situ generating double-network hydrogel produced from biological macromolecules, namely OA and myocardial ECM and various amounts of 3-(2-aminoethyl amino) propyltrimethoxysilane (APTMS)-functionalized reduced graphene oxide (Amine-rGO) were incorporated into the system in order to enhance the electromechanical characteristics of the hydrogel. Cross-linking of partially OA with calcium ions facilitated a Schiff-base reaction with the amine groups of ECM and Amine-rGO. The resultant electroactive hydrogels exhibited semi-conductor electrical conductivity and a biodegradation profile that was appropriate for applications in cardiac tissue engineering [129].

2.5. Commonly Utilized Cells in Cardiac Tissue Engineering

2.5.1. Cardiac Fibroblast

A cardiac fibroblast is typically defined as a cell that generates connective tissue. In addition they are also known as "sentinel" cells because they can detect changes in mechanical, electrical, and chemical signals in the heart and create corresponding responses. Unlike the well-organized and regular collagen patterns found in connective tissue such as bone and tendon, the ECM of the heart is distinguished by its dense,

irregular arrangement of proteoglycans, collagens and glycoproteins. Cardiac fibroblasts, endothelial cells, myocytes and vascular smooth muscle cells comprise the permanent population of the heart. Vimentin, periostin, collagen types I, III, V, VI and fibronectin comprise the structural components of the heart generated by fibroblasts. While fibroblasts are widely recognized as the primary makers of these proteins, numerous other cell types within the heart are also able to producing these ECM constituents. Defining and analyzing fibroblasts is difficult because to the major difficulty of classifying these cells according to dynamically and stress-induced genes [130].

According to common knowledge, fibroblasts are the major cell population in the heart, albeit this may differ between species, particularly in mice. The main cell body of fibroblasts has a flat, spindle-shaped appearance, and it gives birth to numerous processes. A distinctive feature of fibroblasts apart from other permanent cell types in the heart, is their absence of a basement mebrane, however, all of the other permanent cell types possess a basement membrane. Cardiac fibroblasts are important for preserving normal heart function and in cardiac remodeling in response to pathological circumstances such as hypertension and (MI). These cells conduct a range of functions, which involves ECM formation and deposition, communicating with myocytes, signaling among fibroblasts, and contact with endothelial cells. These cellular connections alter electrophysiological parameters, secretory of both cytokines and growth factors, and contribute to development of blood vessel formation. While there is a wealth of knowledge regarding several of these processes, relatively little is known about fibroblasts and their function in angiogenesis during development or remodelling of the heart [131].

2.5.2. Cardiomyocytes

Kimes and Brandt (1976) established that the major clonal cell line produced from embryonic BD1X rat heart tissue is the source of the H9C2 subclonal lineage of embryonic rat cardiomyocytes. Because of the cell's physical similarities to immature embryonic cardiomyocytes, this cell line is commonly used in a variety of *in vitro* studies, especially in the field of cardiovascular research. However, these cells maintain essential components of the signaling pathway required for their development into

mature cardiac muscle cells. In particular, this cell line is used to examine cardiotoxicity associated with new substances, particularly anticancer medications. In addition, it provides a platform for delving into the mechanisms of myocyte impairment and assessing the harmful effects of chemicals under investigation on necrosis and apoptosis in cardiac myocytes. Cultivating embryonic H9C2 cardiomyocytes is a straightforward process, given their vigorous proliferation in *in vitro* conditions. However, the number of passages that H9C2 cardiomyocytes can go through is limited, in contrast to immortalized cell lines. H9C2 cells are an essential resource in cardiovascular research because of their unique properties and capacity for proliferation. They offer important insights into the reactions and behavior of cardiac muscle cells in various experimental conditions [132].

3. MATERIAL AND METHOD

3.1. Synthesis of Modified Polymers

Sodium alginate (W201502, Sigma Aldrich, St. Louis, Missouri, USA) and gelatin (Sigma/G1890-100G) were used with several modifications. The aim of these modifications, attained through the addition of particular functional groups, was to enable the produced hydrogels to exhibit conductive behavior, undergo curing upon exposure to ultraviolet (UV) light, and maintain high adhesive strength even in dynamic and aqueous environments.

3.1.1. Synthesis and Characterization of Oxidized Sodium Alginate (OSA) and Oxidized Methacrylated Alginate (OMA)

Oxidized sodium alginate (OSA) was produced by dissolving sodium alginate in distilled water (DDW) to 2% (w/v). Sodium periodate (311448, Honeywell, Charlotte, North Carolina, USA) was dissolved in DDW before adding dropwise to sodium alginate at 0.5 wt% in the reaction medium to initiate the oxidation reaction [133]. The reaction was continued for 24 hours at room temperature, in the dark, and with steady stirring. The reaction was stopped after 24 hours by adding 1:1 M ethylene glycol (324558, Sigma Aldrich, St. Louis, Missouri, USA) dropwise and stirring for another ten minutes. The reaction products were then transferred to a dialysis membrane (88244, Thermo Fisher Scientific, Waltham, Massachusetts, USA; MWCO: 3500 Da) and dialyzed against DDW for one week. Following dialysis, the products were frozen at -80°C overnight and then lyophilized. The lyophilized products were kept dry, at room temperature and in the dark.

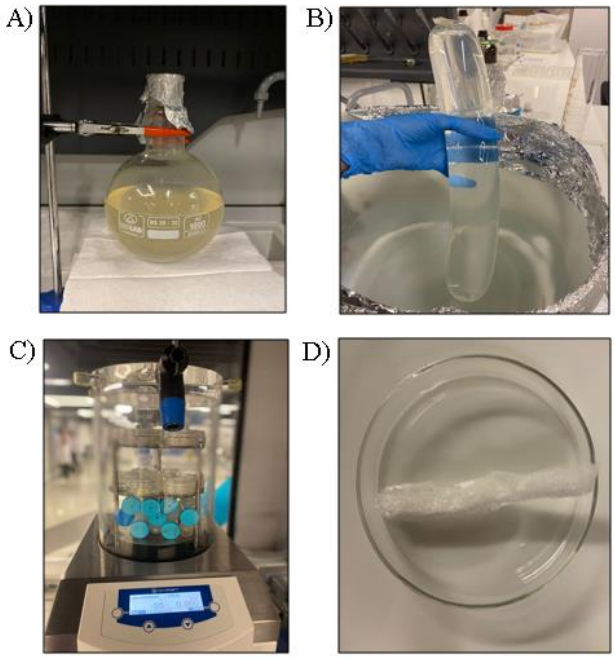

Figure 3.1: Synthesis steps of OSA: A) sodium alginate polymer dissolved in DDW for OSA synthesis, B) synthesis product taken on the dialysis membrane, C) samples being freeze-dried in a lyophilizer and D) synthesis of dried OSA.

In order to create oxidized methacrylated alginate (OMA), oxidized sodium alginate (OSA) was dissolved in phosphate-buffered saline (PBS; OxidizePBS404.100, Bioshop Canada Inc, Mainway, Burlington, Canada) to a concentration of 2% (w/v). A clear, white reaction medium was produced by adding dropwise amounts of metacrylic anhydride (276685, Sigma Aldrich, St. Louis, Missouri, USA) to the dissolved OSA until a ratio of 15 mL/g alginate was reached. The reaction was conducted for 72 hours at room temperature, in the absence of light, and with steady stirring. 10 M sodium hydroxide (NaOH; 106498, Merck Millipore, Burlington, Massachusetts, USA) solution was used to bring the pH of the reaction to 7. Following a 72-hour reaction period, the reaction products were transferred to a dialysis membrane (88244, Thermo Fisher Scientific, Waltham, Massachusetts, USA; MWCO: 3500 Da) and dialyzed for one week against DDW. After dialysis, the products passed through coarse filtration, were frozen at -80°C for an overnight period, and were finally lyophilized. To keep them dry, the lyophilized goods were kept at room temperature and in the dark.

Fourier-transform infrared spectroscopy (FTIR; FT/IR-4600, Jasco, Easton, USA) was used to characterize the OSA and OMA.

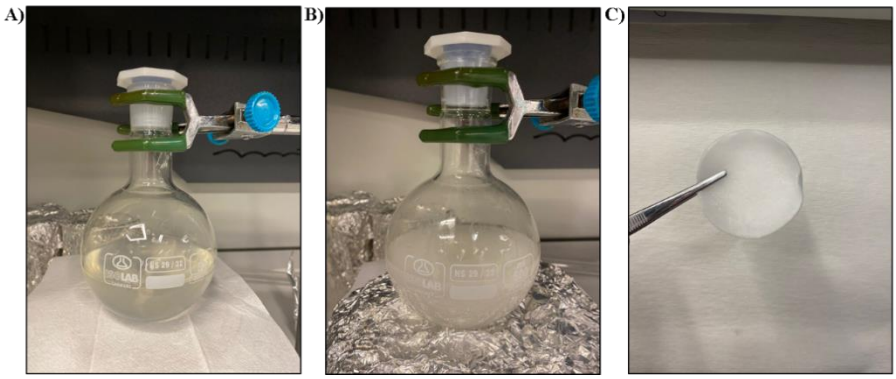

Figure 3.2: Synthesis steps of OMA: A) dissolution of OSA polymer with PBS, B) reaction medium after addition of methacrylic anhydride and C) synthesis of dried OMA.

3.1.2. Synthesis and Characterization of PPy Conjugated OMA (OMA-PPy)

The lyophilized OMA was firstly dissolved in DDW to 3% by weight to create OMA-PPy [134]. Dropwise additions of 0.1 M pyrrole (131709, Sigma Aldrich, St. Louis, Missouri, USA), prepared in 1 M HCl, were added to the OMA solution to make up 5% of its volume. For 30 minutes, the mixture was stirred at 90°C in the dark. The reaction was started after 30 minutes by adding a few drops of 0.2 M iron (III) chloride ($FeCl_3$; 157740, Sigma Aldrich, St. Louis, Missouri, USA), causing the solution to turn black. The reaction was then conducted in the dark at 90°C for a further 5 hours. The reaction product was put on a dialysis membrane (44311.02, SERVA Electrophoresis GmbH, Heidelberg, Germany; MWCO: 3500 Da) after 5 hours and dialyzed for 5 days against DDW. The products were lyophilized after being frozen at -80°C for an overnight period following dialysis. To keep them dry, the lyophilized products were kept at room temperature in the dark.

FTIR was used to characterize the produced product (OMA-PPy).

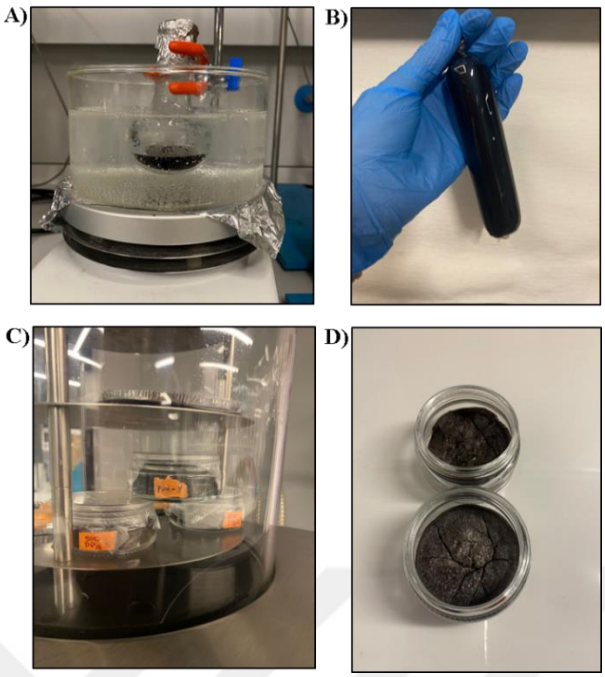

Figure 3.3: Synthesis steps of OMA-PPy: A) after the reaction started, the solution became black, B) the solution taken into the membrane for dialysis, C) image of samples being freeze-dried in a lyophilizer and D) synthesis of dried OMA-PPy.

3.1.3. Synthesis and Characterization of OMA-DOPA

OMA-DOPA was synthesized by combining DOPA and OMA in a Schiff-base reaction [135]. 10 mL of DDW were used to dissolve 1 mmol of OMA. Then, 0.2 mmol of DOPA (Sigma/H8502-25G) also in 10 mL of DDW, was added to the OMA solution, which was then let to incubate for a further hour at 37 °C. HCl was used to alter the pH of the solution, maintaining it at 5.0. Following the reaction, the final product was purified for three days against DDW at pH 5.0 using a dialysis membrane with a molecular weight cut-off of 12,000–14,000. The product was then freeze-dried. In accordance with the source article, the synthesis was conducted with minimal yet distinctive modifications.

UV-vis spectroscopy was used to quantify the DOPA concentration in OMA-DOPA. FTIR was used to characterize the OMA-DOPA.

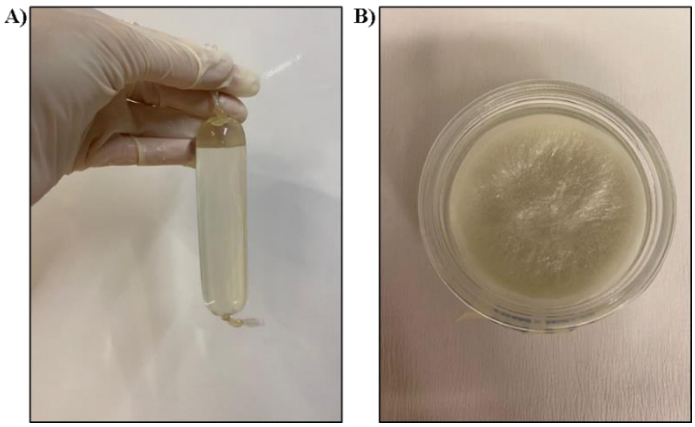

Figure 3.4: Several synthesis steps of OMA-DOPA: A) the solution taken into the membrane for dialysis and B) synthesis of dried OMA-DOPA.

3.1.4. Synthesis and Characterization of GelMA

10 grams of gelatin from porcine skin (Sigma/G1890-100G) were weighed and transferred into a 500 ml glass flask, to which 100 mL of PBS solution was added [136]. The mixture was set to 50 °C using a thermal tip in an oil bath and stirred at 250 rpm with a magnetic stirrer for 1 hour. Once the reaction reached homogeneity, 8 mL of methacrylic anhydride were added dropwise using a glass Pasteur pipette, one drop every 7 seconds. Upon completing this step, the entire reactor was sealed with aluminum foil. The temperature was maintained at 50°C and the mixture was stirred for an additional 2 hours at 250 rpm. After 2 hours, 100 mL of preheated PBS (prepared 30 minutes in advance at 50°C) was added to the mixture, and the reaction continued for another 10 minutes. The resulting reaction mixture was dialyzed in two separate dialysis membranes, totaling 5 L of DDW over 7 days with continuous stirring on a magnetic stirrer at 50°C, 250 rpm, using 12–14 kDa cutoff dialysis membranes from Sigma Aldrich. After 7 days, the mixture was poured into 200 mL of DDW and heated for 15 minutes in a 50°C water bath. Following heating, the liquid was filtered through regular filter paper using a funnel. The obtained liquid was transferred to glass containers, covered with Parafilm, punctured with a needle, and sealed. The containers were stored at -20 °C in a freezer for 2 days. The frozen product was lyophilized for 48 hours. After the lyophilization process was complete, the product was stored at room temperature.

FTIR was used to characterize the GelMA.

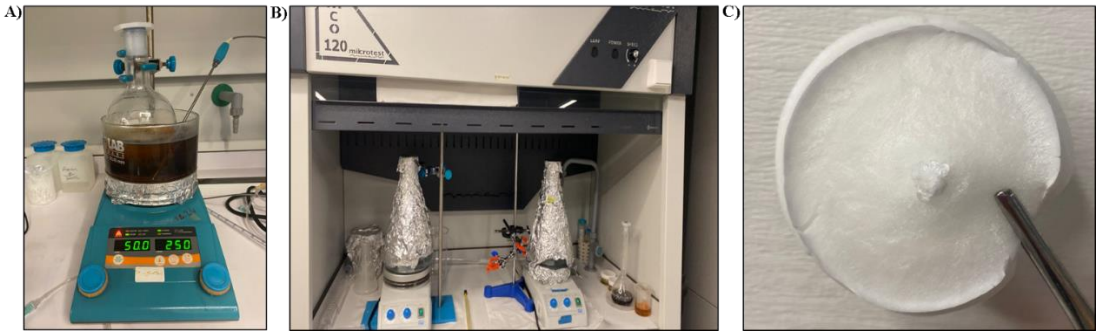

Figure 3.5: Synthesis steps of GelMA: A) mixture in an oil bath set at 50 °C using a thermal tip and stirred at 250 rpm, B) the final reaction mixture was dialyzed on two separate dialysis membranes with a total of 5 L of water for 7 days with continuous stirring on a magnetic stirrer at 50 °C and C) synthesis of dried GelMA.

3.1.5. Characterization of DOPA

The UV-vis spectrophotometer was used for the quantitative determination of the DOPA content in the OMA-DOPA polymer [135]. Readings were taken in OMA solution (1 mg/mL) in the presence of different amounts of Dopamine hydrochloride (0.02, 0.04, 0.06, 0.08, and 0.10 mg/mL), and standard curves were plotted. In the process of creating a calibration curve for the OMA-DOPA polymer, the OMA polymer solution serves as the blank, while the actual sample is denoted as OMA-DOPA. 24 mg of OMA polymer is weighed and dissolved in 12 mL of DDW, resulting in a concentration of 2 mg/mL. Concurrently, a stock solution of DOPA is prepared by dissolving 10 mg of DOPA in 50 mL of DDW, yielding a concentration of 0.2 mg/ml. Dilution process is carried out for each group, involving the addition of 2 ml of both DOPA samples and blank polymer (OMA) in a 1:1 ratio. Additionally, a DOPA sample without polymer at a concentration of 0.2 is diluted at a 1:1 ratio with DDW, where water serves as the blank for this specific sample. To obtain readings for the actual polymer, a solution of 2 mg OMA-DOPA in 2 mL DDW is prepared. The same procedure was employed for the quantitative determination of the DOPA content in the OMA-PPy-DOPA sample, with the only difference being that this time OMA-PPy served as the blank, while the main sample was OMA-PPy-DOPA. UV spectrophotometry, utilizing a quartz cuvette, is employed to read all samples within the range of 190-350 nm. The UV-vis absorbance at 280 nm wavelength of the OMA-DOPA solution (1 mg/mL) was recorded. The catechol content of the OMA-DOPA

polymer and OMA-PPy-DOPA samples was calculated using the standard curve. The, obtained results are then analyzed [137].

3.2. Preparation of Tissue Adhesives

Four different polymer groups were determined at the concentrations of 25% GelMA and 10% modified total Alginate (OMA, OMA-PPy and OMA-DOPA). There are 2 control groups, one of them is the GelMA control group and the other is the GelMA/OMA control group. The other two polymer groups have been constituted, with one group providing conductive properties (GelMA/OMA-PPy) and the other group providing both conductive and adhesive characteristics (GelMA/OMA-PPy/DOPA). Lithium phenyl-2,4,6-trimethylbenzoylphosphinate (LAP) (Sigma/900889-1G) was used as photoinitiator. Firstly, 2.5 mg/mL of LAP was thoroughly dissolved in PBS at room temperature in the dark. Subsequently, polymer mixtures, taken in the proportions given in Table 3.1, were weighed and placed into four different glass tubes. LAP, dissolved in PBS, was then added to each mixture, and the components were thoroughly mixed using a magnetic stirrer at room temperature in the dark. The resulting photo-crosslinked tissue adhesives were prepared by exposing them to UV light for 60 seconds in the presence of LAP photoinitiator (2.5 mg/mL). Certain sizes of Poly(dimethylsiloxane) (PDMS) molds were used in the necessary experiments by cross-linking with UV.

Table 3.1: GelMA, GelMA/OMA, GelMA/OMA-PPy and GelMA/OMA-PPy/DOPA tissue adhesives and their formulation contents.

Sample Codes	GelMA (mg/mL)	OMA (mg/mL)	OMA-PPy (mg/mL)	OMA-DOPA (mg/mL)	LAP (mg/mL)	Light exposure time (sec)
GelMA	250	-	-	-	2.5	60
GelMA/OMA	250	100	-	-	2.5	60
GelMA/OMA-PPy	250	50	50	-	2.5	60
GelMA/OMA-PPy/DOPA	250	-	50	50	2.5	60

3.3. Characterization of Tissue Adhesives

3.3.1. Structural Analysis

FTIR spectrum recorded in the range of 500-4000 cm^{-1} was used for chemical structure analysis of the prepared tissue adhesives.

3.3.2. Swelling Studies

The swelling capacities of hydrogel tissue adhesives were assessed through gravimetric measurements. To elaborate, hydrogels, cross-linked as previously outlined, underwent freeze-drying, initial weighing (W_i), and subsequent placement in eppendorf tubes containing 2 mL of PBS at pH 7.4 and 37°C.

After swelling for up to 48 hours, the hydrogels were weighed (W_f) following the removal of excess water from their surfaces. The equilibrium swelling ratio was then calculated using Equation 3.1.

$$\text{Equilibrium Swelling Ratio} = \frac{W_f - W_i}{W_i} \qquad (3.1)$$

In this context, "W_f" signifies the concluding weight following the swelling of hydrogel tissue scaffolds, and "W_i" represents their initial weight in a dry state. Each experimental group was executed with 5 repetitions [138].

3.3.3. Degradation Studies

The investigation into the *in vitro* hydrolytic degradation behaviours of hydrogel tissue adhesives was conducted in the presence of PBS (pH 7.4) with 0.02% sodium azide at 37°C for a maximum duration of 7 days [139]. Concisely, previously prepared cross-linked hydrogels were subjected to freeze-drying and initial weighing (W_i). The desiccated specimens were then introduced into eppendorf tubes, each containing 2 mL of PBS with 0.02% sodium azide at pH 7.4, and maintained at 37°C to ensure the integrity of the gels during measurements. After specific incubation periods (1, 3, and 7 days), PBS was removed, and the samples were subsequently freeze-dried and re-weighed (W_f). The remaining mass percentage was computed using Equation 3.2.

$$\text{Remaining Mass (\%)} = \frac{W_i - W_f}{W_i} \times 100 \quad (3.2)$$

In this context, "W_f" denotes the concluding weight following the incubation of hydrogel tissue scaffolds at 37°C for a specific period in a pH 7.4 PBS+sodium azide environment, and "W_i" represents their initial weight when dry. The experimentation for each group was carried out with 5 repetitions.

3.3.4. Compression Test

The compressive strength and strain at the point of rupture of hydrogel tissue adhesives were investigated through a compression test using a tissue analysis device (Stable Micro Systems, Godalming, United Kingdom). The prepared hydrogel tissue adhesives, as previously described, were uniformly shaped using a 5 mm diameter biopsy punch. The samples were placed on the device's base plate for measurement and subjected to static load conditions at a displacement rate of 1 mm/minute using a cylindrical compression probe [140].

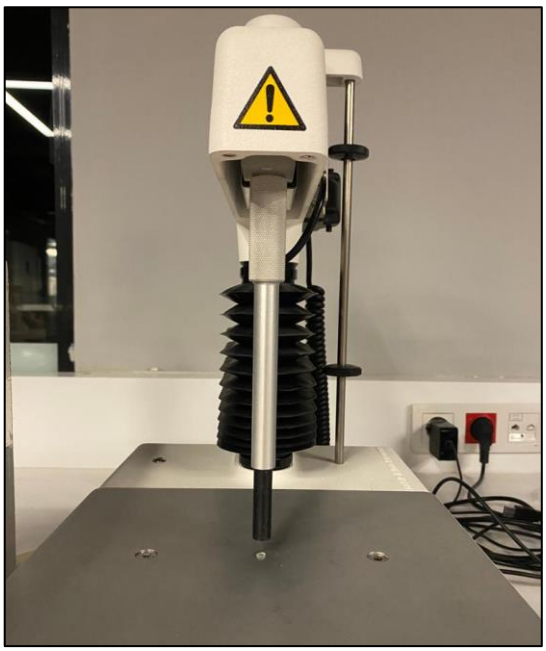

Figure 3.6: Compression testing system setup.

3.3.5. *In Vitro* Adhesion Tests

The adhesive capability of tissue adhesive is as important in medical applications as its other features because these characteristics can have an impact on the success of surgical procedures, patient comfort, and the healing process. The process of analyzing a material's ability to adhere to another surface, typically in a biological context, is known as bioadhesion analysis. This analysis is crucial in many areas, including pharmacology, biotechnology, and medicine. Analyses of different types can be used in bioadhesion studies, which seek to understand how materials stick to biological tissues or substrates [141].

3.3.5.1. *In vitro* Lap-shear Test

Lap-shear strength testing assesses a material’s capacity to withstand stresses applied in a plane where the shearing force acts to separate two substrates moving in opposite directions. The laboratory testing performed utilizes tensile probes to a texture analyzer (Stable Micro Systems, Godalming, United Kingdom) and is in the form of a single lap, with the base plate being held stationary. The slides, with the sample placed between them, are then pulled apart by the upward motion of the upper plate. Initially, the glass slides are bisected using a glass pencil, and subsequently, the slides are coated by immersion into a 10% gelatin solution prepared at 50°C. The coated slides are then positioned in a chalet and subsequently placed in an oven at 37°C for the purpose of drying. The hydrogel samples, as previously described, are carefully dispensed in 50 μL volumes within a designated 1 cm area positioned between two gelatin-coated slides. The two slides are then adhesively secured to each other at the location of the sample. Following this, they are cross-linked under UV light for a duration of 60 seconds. The samples, which had been cured between the slides, were positioned and securely clamped between the probes of the measurement device. Subsequently, they were subjected to a testing speed of 1.2 mm per minute [140].

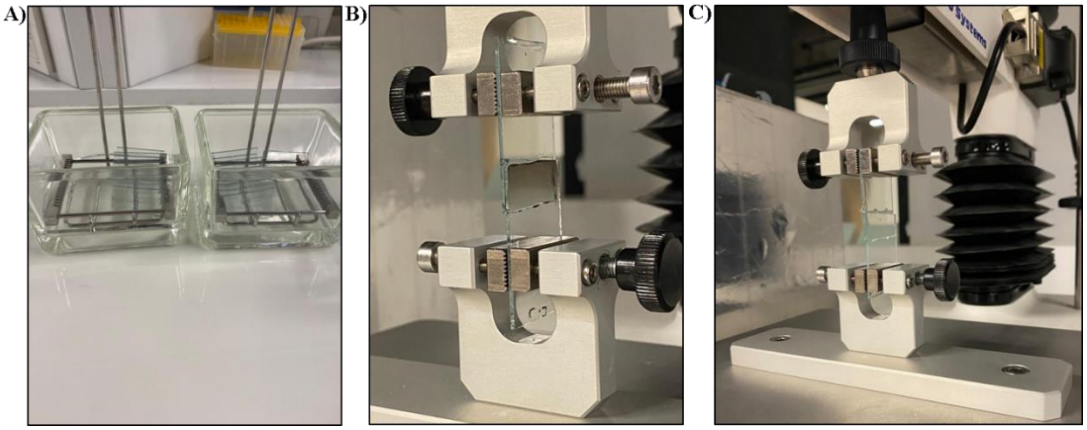

Figure 3.7: *In vitro* Lap-shear test setup: A) slides coated with a 10% gelatin solution are arranged in a chalet for the purpose of drying, B) before the experiment in the texture analyzer device, the post-curing appearance of the sample group containing DOPA between the slides, C) before the experiment in the texture analyzer device, the post-curing appearance of the sample group containing GelMA between the slides.

3.3.5.2 *In vitro* T-Peel Test

The T-peel test constitutes a standardized methodology employed for the assessment of the peel or bonding strength existing between two surfaces that are commonly joined by adhesives or bonded materials. The test specimen, frequently configured in the shape of a "T," undergoes exposure to a controlled force that induces the separation of the two bonded surfaces at a consistent angle. This testing protocol holds paramount significance in gauging the adhesion performance of materials, particularly within industries where the preservation of the integrity of bonded joints is of critical importance. The laboratory testing performed uses tensile probes aimed at a tissue analyzer (Stable Micro Systems, Godalming, United Kingdom) and is a single turn with the base plate held stationary. The slides with the sample placed between them are then separated from each other by the upward movement of the upper plate. Initially, within the scope of this experiment, collagen sheets are precisely cut to a width of up to 1 cm. Hydrogel samples are then meticulously dispensed in volumes of 50 μL over a specific area of 1 cm located between two collagen sheets, following the procedure outlined previously. Following adhesive bonding, the assets are exposed to UV for a period of 1 minute to cross-link.

The samples cured between the collagen sheets were placed in a T-shape between the probes of the measuring device and clamped securely. They were then subjected to a testing rate of 1.2 mm per minute [142].

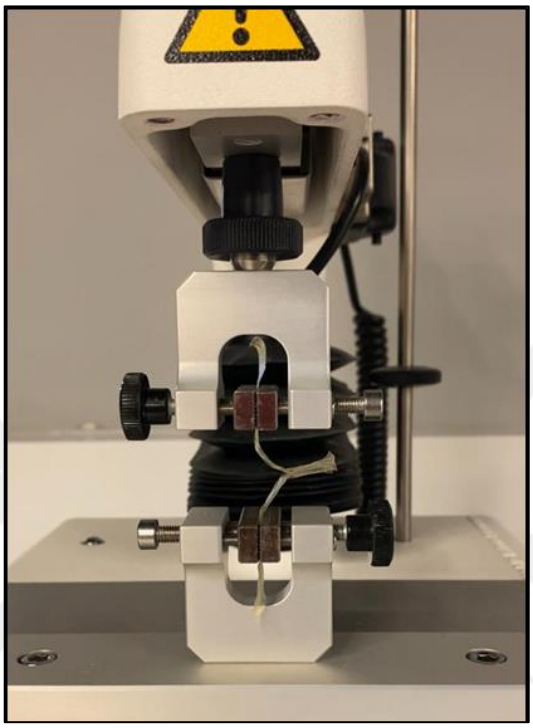

Figure 3.8: *In vitro* T-Peel test setup with collagen sheet.

3.3.6. *Ex Vivo* Adhesion Tests

3.3.6.1. *In vitro* Burst Pressure Test

In the burst pressure test, where the strength, adhesion, and cohesion of hydrogels are crucial, commercially available devitalized collagen sausage casings were cut and moistened, then placed on a specially designed test plate. The upper and lower plate layers, which include a 10 mm diameter hole, were compressed onto the collagen casing surface by tightening with a screw, and a 3 mm biopsy punch was used to create a hole at the exact center. To provide air pressure, the plates were connected to a peristaltic syringe pump (Harvard Apparatus, Standard PHD ULTRA^{TM} CP 4400) through tubes, and a pressure sensor was integrated into the system for pressure measurement. The hole created on the casing surface was sealed in situ with hydrogels prepared as previously described, and the gels were cross-linked under UV light for 60

seconds. Subsequently, air was sent into the system at a constant rate of 20 mm/min, and the maximum burst pressure values were recorded using SPARKvue® software (PASCO Scientific, Roseville, USA) [140].

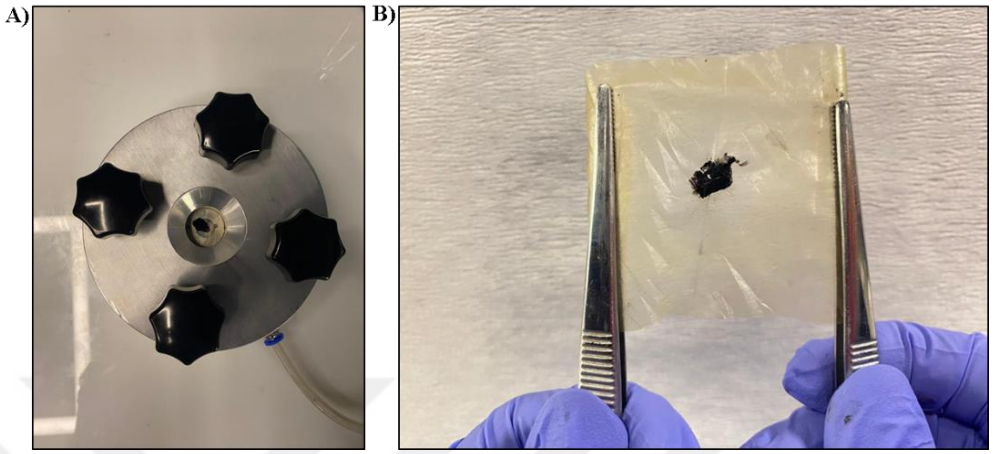

Figure 3.9: *In vitro* burst pressure test setup: A) the collagen casing compressed between specially designed plates for burst pressure, B) after air is introduced into the system, the collagen sheet explodes as a result of withstanding maximum pressure.

3.3.6.2 *Ex vivo* Burst Pressure Test

In the experiment conducted for *ex vivo* burst pressure, a heart taken from a slaughterhouse was used instead of a collagen sheet and its pericardial membrane, myocardial layer and artery were separated and used in the experiments, respectively. The remainder of the procedure was performed in an identical manner to the *in vitro* burst pressure. After the related tissue isolation, it was placed on a specially designed test plate. The upper and lower plate layers, which include a 10 mm diameter hole, were compressed onto the tissue surface by tightening with a screw, and a 2 mm biopsy punch was used to create a hole at the exact center. To provide air pressure, the plates were connected to a peristaltic syringe pump through tubes, and a pressure sensor was integrated into the system for pressure measurement. The hole created on the surface was sealed in situ with hydrogels prepared as previously described, and the gels were cross-linked under UV light for 60 seconds. Subsequently, air was sent into the system at a constant rate of 20 mm/min, and the maximum burst pressure values were recorded using SPARKvue® software (PASCO Scientific, Roseville, USA) [140].

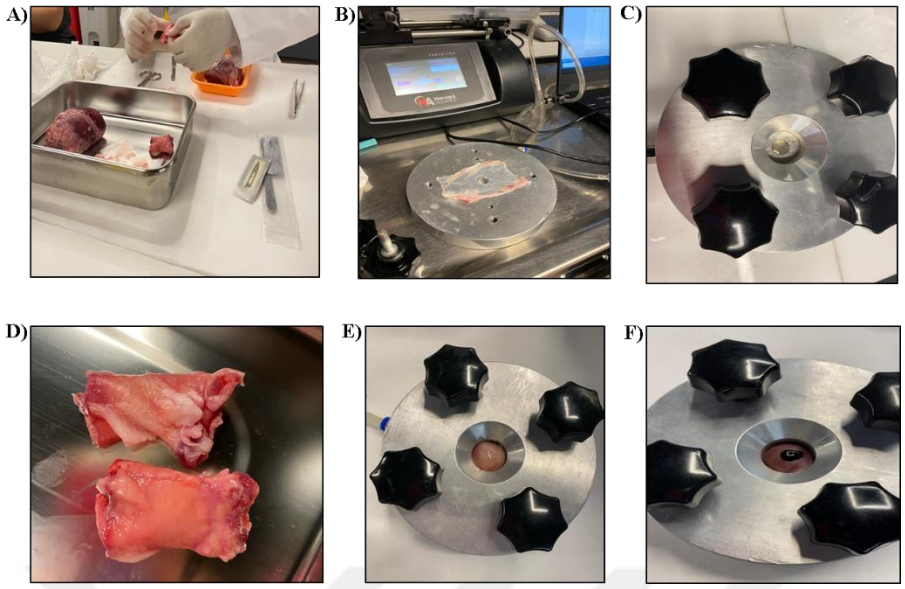

Figure 3.10: *Ex vivo* burst pressure test setup: A) the separation of the pericardium from the sheep's heart, B) setting up the experimental apparatus and placing pericardium on the plate, C) hydrogel placed on the pericardium which is compressed between specially designed plates for burst pressure testing, D) the separation of the artery from the sheep's heart, E) Hydrogel placed on the artery which is compressed between specially designed plates for burst pressure testing, F) hydrogel placed on the myocardium which is compressed between specially designed plates for burst pressure testing.

3.3.6.3 *Ex vivo* Myocardium Wound Closure Test

A laboratory or clinical process known as "wound closure testing" is used to assess a material's or substance's capacity to promote or aid a wound's closure and healing. The purpose of this test is often to assess the efficacy of tissue adhesives, wound dressings, and other wound care products. Initially, for the experiment, the glass slides were partitioned into two equal sections using a glass marker and a ruler. The sheep myocardium which was obtained from the slaughterhouse serving as our tissue samples for this experiment, was subsequently sliced into slender strips measuring 1×3 cm. Following that, the tissue sections were affixed onto the divided slides using EvoBond502 Super Strong Japanese Adhesive. Subsequently, the tissue at the center of the divided slides was meticulously incised and isolated from one another. Thereafter, 50 µL of the previously prepared hydrogel samples were meticulously dispensed onto the incised tissue and subsequently cross-linked using UV light for a duration of 60 seconds. This experiment was carried out by attaching miniature tensile probes to a texture analyzer (Stable Micro Systems, Godalming, United Kingdom). The samples, which had been cured on the tissue, were positioned and compressed between the

probes of the measurement device, and subsequently subjected to a testing speed of 10.2 mm per minute [143].

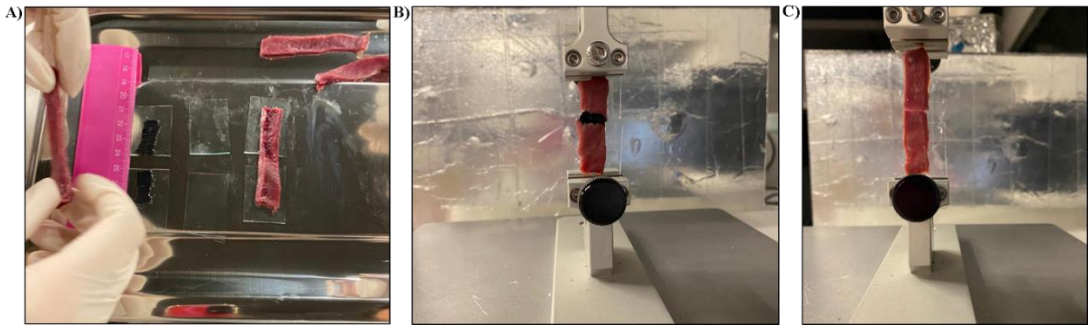

Figure 3.11: *Ex vivo* wound closure test setup: A) attaching tissue sections to separated slides using adhesive, B) before the experiment in the texture analyzer device, the post-curing appearance of the GelMA/OMA-PPy/DOPA hydrogel on the tissue, C) before the experiment in the texture analyzer device, the post-curing appearance of the GelMA hydrogel on the tissue.

3.3.7. Conductivity Test

The bulk conductivity of the specimens was assessed utilizing a multimeter (VC9808+digital multimeter) through a two-point probe technique [144]. Subsequently, the conductivity was computed using the provided Equation 3.3 and 3.4.

$$\rho = R\frac{A}{l} \quad (3.3)$$

$$\sigma = \frac{l}{\rho} \quad (3.4)$$

In this context, ρ represents resistivity ($1/\sigma$), R denotes resistance (Ω), A signifies the cross-sectional area of the specimen (cm^2), l represents the length of the specimen (cm), and σ corresponds to the conductivity (S cm^{-1}).

3.4. *In vitro* Cell Culture Studies

Within the scope of *in vitro* cell culture studies H9c2 cardiac myoblast cell line, at the 15th passage was used. The cells were supplied from Istanbul University Faculty of Pharmacy.

3.4.1. Preparation of Cell Culture Medium

For cell propagation, DMEM High Glucose (4.5 g/L) (Capricorn Scientific, Cat No: DMEM-HPA, supplemented with L-Glutamine and Sodium Pyruvate, sterile filtered) containing 10% Fetal Bovine Serum (FBS; Sigma, F9665, non USA), 1% penicillin-streptomycin-fungizone (PSF; 15240062, Thermo Fisher Scientific, Waltham, Massachusetts, USA), was employed.

3.4.2. Removal of Cells from Stock and Culturing

Cells were rapidly thawed in a 37°C water bath, and the entire content was transferred to a 15 mL centrifuge tube without delay. To prevent osmotic shock to the cells in the thawing solution, 9 mL of pre-warmed medium was gently added dropwise to the cells at 37°C. After gentle pipetting (1-2 times), the cells within the centrifuge tube were centrifuged at 200×g for 5 minutes. Following centrifugation, the supernatant was aspirated, and 1 mL of fresh medium was added to the cell pellet. The cells were resuspended and transferred to a T25 culture flask containing 4 mL of medium and then placed in a humidified incubator at 37°C and 5% CO_2.

3.4.3. Cell Culture Medium Replacement, Passaging and Cryopreservation

Over time, as cells proliferate, the constituents within the cell culture medium will be gradually consumed, leading to an accumulation of cellular debris. To maintain cell health, it is essential to perform medium changes. Typically, this is done every 2-3 days. Prior to using the complete medium, it is pre-warmed to 37°C in a water bath. For adherent cells, those that attach to the flask surface, the old medium is aspirated from the flask. If there is a substantial amount of cellular debris or dead cells in the culture, the flask can be rinsed with 1× PBS (2 mL for T25, 4 mL for T75, and 6 mL for T175 flasks). Following the rinse, PBS is aspirated, and if no rinse is performed, fresh medium is added directly to the flask (5 mL for T25, 10 mL for T75, and 20 mL for T175). The flask is then placed back in a 37°C, 5% CO_2 humidified incubator for further cultivation.

Passaging of adherent cells becomes necessary when they cover approximately 70-80% of the surface (reach confluence). Complete medium and Trypsin-EDTA

Solution C (0.05% Trypsin & 0.02% EDTA in DPBS, Mycoplasma Tested, (+) Phenol Red, 2143977, Biological Industries) are pre-warmed to 37°C before use. The old medium in the flask is aspirated. To remove dead cells, waste materials, Ca/Mg ions, and serum remnants from the environment, 2 mL of 1× Ca/Mg^{2+}-free PBS is added to a 25 cm² flask, allowing a gentle washing of the cell surfaces (4 mL for T75, and 6 mL for T175). Ca/Mg ions present in the environment partially inhibit trypsin activity, so rinsing with Ca/Mg^{2+}-free PBS allows trypsin to function more effectively. After PBS is aspirated and removed from the environment, 1 mL of trypsin-EDTA solution is used to facilitate the detachment of adherent cells from the flask surface. Cells are incubated at 37°C in a 5% CO_2 environment for 2-3 minutes (3 mL for T75, 7 mL for T175). The working activity of trypsin can vary depending on the brand/model and should be monitored during incubation. EDTA within the commercial trypsin-EDTA solution acts as a chelating agent, binding to any remaining Ca ions, thereby assisting trypsin. When cells begin to detach from the flask surface, a layer and particles sliding off the surface are observed. To ensure, when cells are seen lifting off the flask surface, to inhibit trypsin, an equal amount of complete medium is added (1:1). This prevents trypsin from causing damage to the cell membranes or membrane-bound protein structures after separating the cells from the surface. The complete medium contains bivalent cations and various protease inhibitors, mainly alpha-1-antitrypsin, which effectively inhibits trypsin. The cell suspension within the flask is transferred into a 15 mL Falcon tube, and after centrifugation at 1500 rpm for 5 minutes, the supernatant is aspirated. The resulting cell pellet is dissolved in 1 mL of medium, and the cell suspension is then transferred to 75 cm² flasks and placed in a 37°C, 5% CO_2 environment. At this stage, rather than transferring all the cells to a new flask, if needed, cell seeding can be performed for experimentation or a portion can be frozen for later use.

When cells reach an appropriate confluency, they should be cryopreserved for potential use in future experiments. Cells can be stored at low temperatures for months or even years in a cryopreservation solution containing a cryoprotectant. The cryopreservation solution consists of three main components: complete medium, FBS, and a cryoprotectant, typically DMSO (dimethyl sulfoxide). The ratios of these three components can vary from one laboratory to another. We typically use a composition of 60% FBS, 30% complete medium, and 10% DMSO. DMSO is a chemical that should be stored at room temperature in the dark, but due to its susceptibility to degradation,

the shelf life of the cryopreservation solution is not very long. It is recommended to prepare it fresh when needed. If the solution will be used again in the near future, it can be stored at -20°C for a short period. DMSO is a commonly used polar, aprotic organic solvent with the ability to penetrate cell membranes and displace water. It is added to the solution to reduce the formation of ice crystals during the freezing process, thereby preventing cell death. The concentration at which cells are cryopreserved can vary between cell types but typically falls within the range of $1x10^6 – 5x10^6$ cells/mL in the cryopreservation solution. Freezing cells at very low or very high densities can affect viability and should be avoided. During the freezing process, the same gentle pipetting steps, as described earlier for cell detachment, are followed, with the final step involving suspending the cells in the cryopreservation solution rather than fresh medium. The well-distributed cell suspension, ensured through gentle pipetting approximately 15-20 times, is then transferred to pre-labeled cryovials and promptly placed at -80 °C. Ideally, transferring the cryovials to liquid nitrogen for long-term preservation should be performed after overnight storage to ensure longer viability.

3.4.4. Sterilization of Polymers for Use in Cell Culture

In vitro cell culture studies should be conducted under aseptic conditions, using sterile materials and solutions. Therefore, it is imperative that the hydrogels to be used are also sterile. Given that methacrylate double bonds are susceptible to damage in the presence of light and UV, ethylene oxide gas was employed for the sterilization of polymers. The modified polymers were carefully weighed in the quantities required for cell culture, then packaged in PMSSteripack sterilization rolls and placed inside ethylene oxide sterilization device. The PBS solution containing the photoinitiator was sterilized by passing it through a 0.22 μm pore-sized polyethersulfone (PES) syringe filter and stored protected from light. Following this stage, all work was conducted under aseptic conditions, and the polymers were not exposed outside of the cabin. The hydrogels were prepared as previously described.

3.4.5 *In vitro* Cytotoxicity Test

To evaluate the biocompatibility of hydrogels, 250 mg of MTT (3-(4,5-Dimethylthiazol-2-yl)-2,5-Diphenyltetrazolium Bromide) powder is weighed and dissolved in 50 mL of PBS (5 mg/mL). Since MTT is light-sensitive, the falcon tube must be wrapped with foil. Due to the poor solubility of the dye, it is necessary to vortex for approximately 5 minutes to ensure that there are no particles left undissolved at the bottom. Again, in the dark and inside a biosafety cabinet, the solution is filtered through a 0.22 μm pore-sized PES syringe filter and aliquoted into 500 μL sterile tubes. The aliquots are stored at -20°C and removed when needed. The MTT assay is typically conducted using 96-well plates. Generally, 100 μL and $5x10^{-3}$ cells per well are suitable. For both the control and experimental groups, cell seeding is performed with a minimum of 5 technical replicates in each group. After cell seeding, the plate is placed in a 37°C incubator with 5% CO_2 overnight to allow the cells to adhere. Since an extract-based test is performed, which involves application with material release samples, the expected overnight incubation period for cell adherence is also considered for sample extraction. This process typically involves placing a certain amount of samples in a closed tube with medium for 24 hours at 37 °C. After 24 hours, the extract is diluted 1:1 with fresh medium. Since the samples are not sterile, the extracts are filtered through a 0.22 μm pore-sized syringe filter before use. After the overnight incubation and microscopic confirmation of cell adhesion, the cells are ready for treatment. If it is deemed appropriate to administer treatment, the old medium is aspirated from the wells, and medium containing the extract is added to the wells at 100 μL each. Even though normal medium is used in control wells, the conditions should be the same as those for treatment. This means that the old medium is removed from the control group wells, and fresh medium is added to the wells. The plate is then incubated for 24 hours at 37°C with 5% CO_2. Once the specified incubation period is completed, MTT can be added to the wells. At this stage, aliquots of the previously prepared MTT solution are used, and the work is carried out in the dark. Either directly add 10 μL of MTT solution to each well or prepare fresh medium containing MTT solution separately. The plate is then covered with foil and returned to the 37°C incubator with 5% CO_2. After 4 hours of incubation, the plate is removed from the incubator to dissolve the crystals. Before adding DMSO as a solvent to the wells, the medium containing MTT should be gently aspirated from the wells. After aspirating the old

medium, 100 μL of DMSO is added to each well. As soon as DMSO is added, the crystals will start to dissolve and give a purple color [145].

The darker the color, the more cells are implied. To ensure complete dissolution of the crystals, the plate can be shaken for approximately 5 minutes using a shaker. Then, absorbance is measured at 570 nm in the visible region using the BMG Labtech SPECTROstar Nano microplate reader.

3.5. Statistical Analysis

The analyses comparing two groups were performed using independent t-tests unless otherwise specified, utilizing GraphPad Prism 8.4.3 software (Dotmatics, Boston, USA). For analyses involving more than two groups, one-way analysis of variance was employed, followed by Tukey's multiple comparison test. The presented values represent the mean ± standard deviation (SD). P-values less than 0.05 were considered statistically significant.

4. RESULTS

4.1. Characterization of Modified Polymers

The sodium alginate polymer underwent oxidation using sodium periodate, and subsequently, it was methacrylated with methacrylic anhydride. Figure 4.1 displays the structure of the OSA polymer obtained following the oxidation of sodium alginate with sodium periodate.

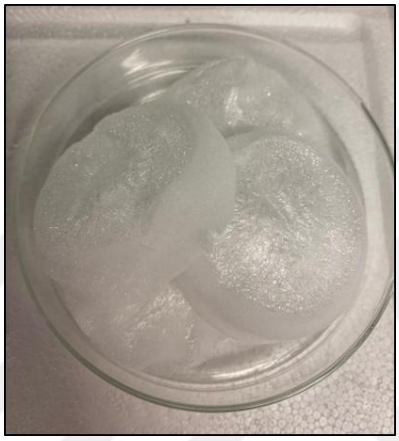

Figure 4.1: The structure of the lyophilized OSA polymer.

Figure 4.2 displays the structure of the OMA polymer obtained through methacrylation with methacrylic anhydride subsequent to the oxidation of Alginate.

Figure 4.2: The structure of the lyophilized OMA polymer.

Following the conjugation of OMA polymer with a 5% (w/w) pyrrole solution, the structure of the resulting OMA-PPy polymer is depicted in Figure 4.3.

Figure 4.3: The structure of the lyophilized OMA-PPy polymer.

The structure of OMA-DOPA, produced through the Schiff base reaction between dopamine and OMA, is depicted in Figure 4.4.

Figure 4.4: The structure of the lyophilized OMA-DOPA polymer.

Gelatin underwent methacrylation through the use of methacrylic anhydride. The structure of GelMA is depicted in Figure 4.5.

Figure 4.5: The structure of the lyophilized GelMA polymer.

4.1.1. FTIR Results

The chemical structures of sodium alginate, OSA, OMA, OMA-PPy OMA-DOPA, gelatin and GelMA polymers were assessed through FTIR spectroscopy in the range of 500-4000 cm^{-1}. The obtained FTIR spectra of the polymers are shown in Figure 4.6 and Figure 4.7.

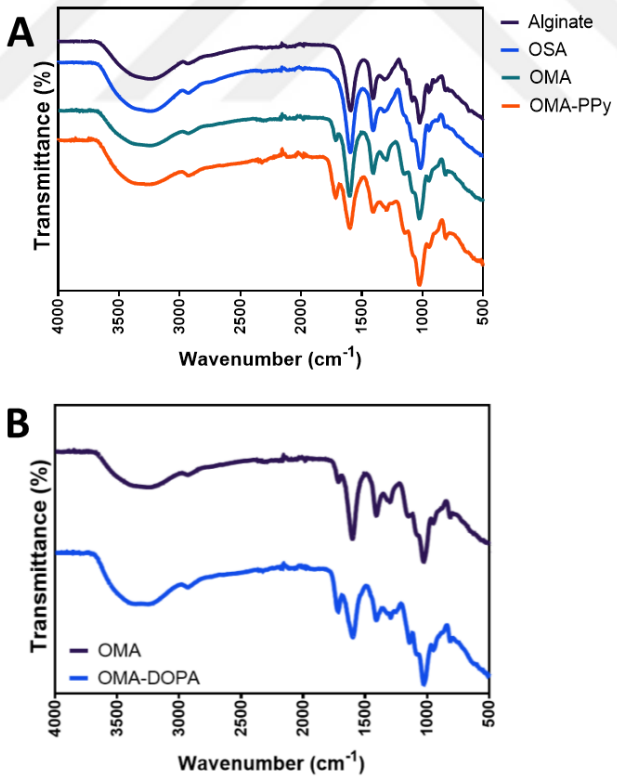

Figure 4.6: The FTIR spectra of (A) alginate, OSA, OMA, and OMA-PPy polymers, and (B) OMA and OMA-DOPA polymers.

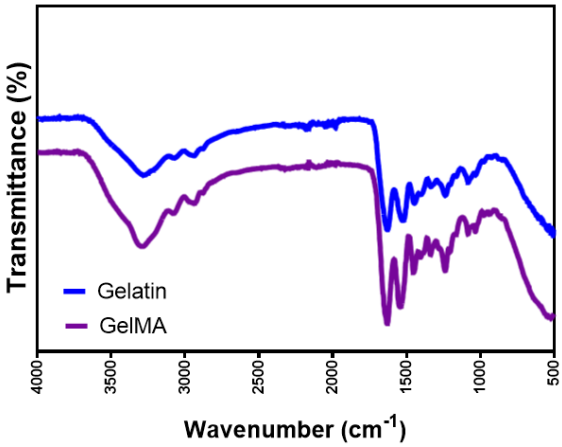

Figure 4.7: The FTIR spectra of Gelatin and GelMA polymers.

4.1.2. DOPA Quantification Using UV-Spectrophotometry

The graph in Figure 4.8 illustrates the wavelength-dependent absorbance curve of DOPA solutions at different concentrations for OMA-DOPA, along with the graph depicting the creation of a calibration curve using UV-Spectrophotometry for DOPA.

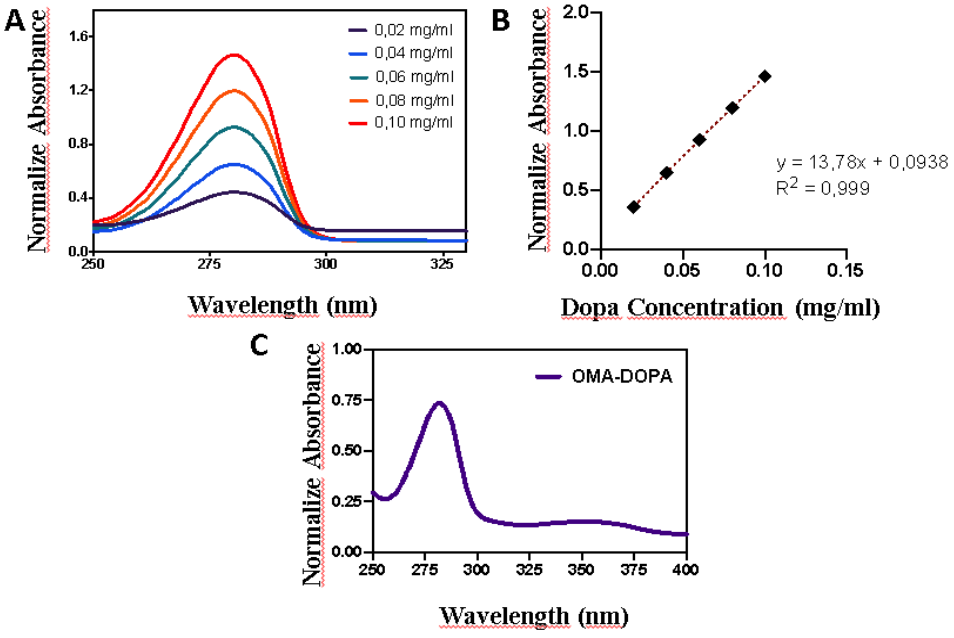

Figure 4.8: (A) UV-vis spectra of DOPA in the presence of OMA (1 mg/mL, (B) Standard curve of DOPA and (C) UV-vis spectrum of OMA-DOPA (1 mg/mL).

4.2. Characterization of Hydrogel Tissue Adhesives

4.2.1. FTIR Results

The chemical structures of the synthesized GelMA, GelMA/OMA, GelMA/OMA-PPy, and GelMA/OMA-PPy/DOPA hydrogels were evaluated through FTIR analysis conducted in the range of 500-4000 cm^{-1}. The FTIR spectra of the hydrogels are presented in Figure 4.9.

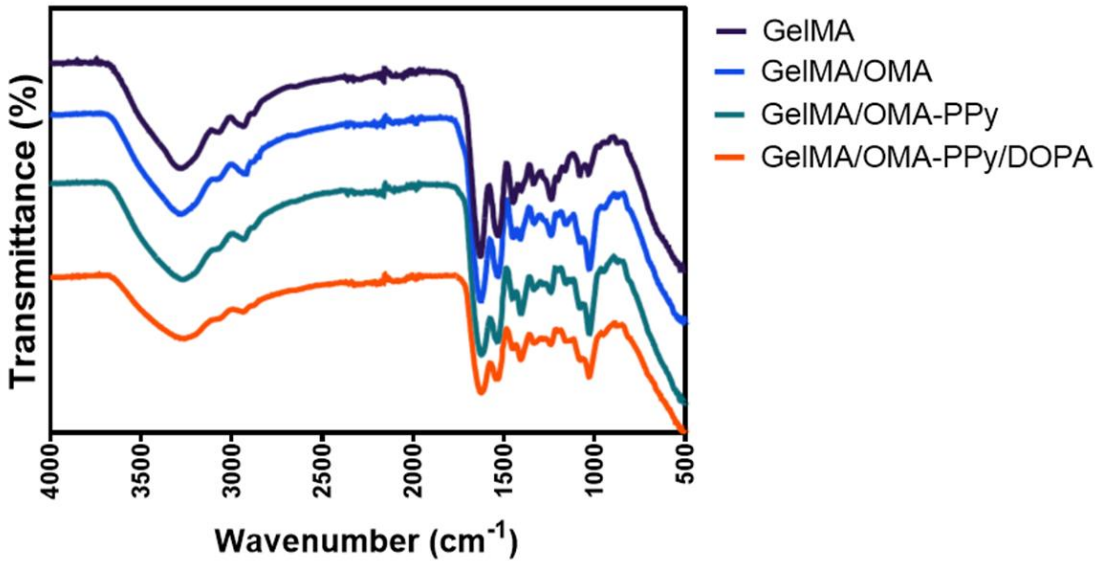

Figure 4.9: The FTIR spectra of GelMA, GelMA/OMA, GelMA/OMA-PPy, and GelMA/OMA-PPy/DOPA hydrogel tissue adhesives.

4.2.2 Swelling Analysis Results

The equilibrium swelling values of GelMA, GelMA/OMA, GelMA/OMA-PPy, and GelMA/OMA-PPy/DOPA hydrogel tissue adhesives at 24 hours are depicted in Figure 4.10. The equilibrium swelling ratios for GelMA, GelMA/OMA, GelMA/OMA-PPy, and GelMA/OMA-PPy/DOPA hydrogels were found to be 4.69 ± 0.11, 3.10 ± 0.018, 3.82 ± 0.35 and 3.60 ± 0.28 g/g, respectively.

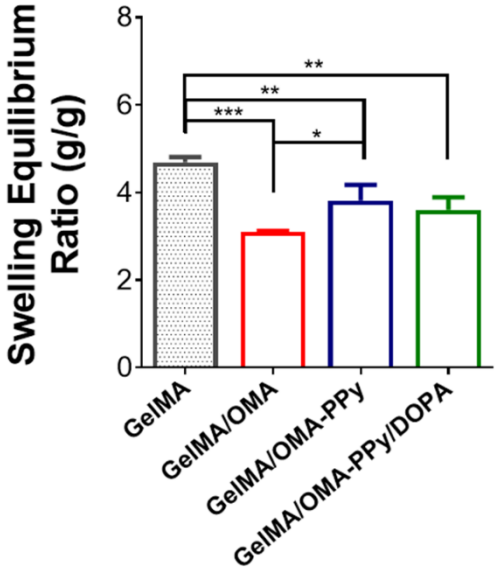

Figure 4.10: Equilibrium swelling ratios of GelMA, GelMA/OMA, GelMA/OMA-PPy, and GelMA/OMA-PPy/DOPA hydrogel tissue adhesives after 24 hours (ANOVA test analysis displays the data as mean ± SD, ns: P > 0.05, *: P ≤ 0.05, **: P ≤ 0.01, ***: P ≤ 0.001).

4.2.3 Degradation Analysis Results

The remaining mass percentages of GelMA, GelMA/OMA, GelMA/OMA-PPy, and GelMA/OMA-PPy/DOPA hydrogels obtained at specific time points (1st, 3rd, and 7th days) are presented in Figure 4.11. For GelMA, GelMA/OMA, GelMA/OMA-PPy, and GelMA/OMA-PPy/DOPA hydrogel tissue adhesives, the remaining mass (%) values on the first day were found to be 93.26 ± 2.25, 89.85 ± 0.28, 68.12 ± 5.9, and 62.49 ± 5.7, respectively. On the third day, the remaining mass (%) values for GelMA, GelMA/OMA, GelMA/OMA-PPy, and GelMA/OMA-PPy/DOPA hydrogel tissue adhesives were found to be 83.12 ± 2.60, 82.29 ± 2.0, 43.98 ± 8.33, and 42.22 ± 4.95, respectively. On the seventh day, the remaining mass (%) values for GelMA, GelMA/OMA, GelMA/OMA-PPy, and GelMA/OMA-PPy/DOPA hydrogel tissue adhesives were found to be 64.29 ± 9.51, 63.68 ± 2.77, 36.50 ± 5.75, and 33.52 ± 3.82, respectively.

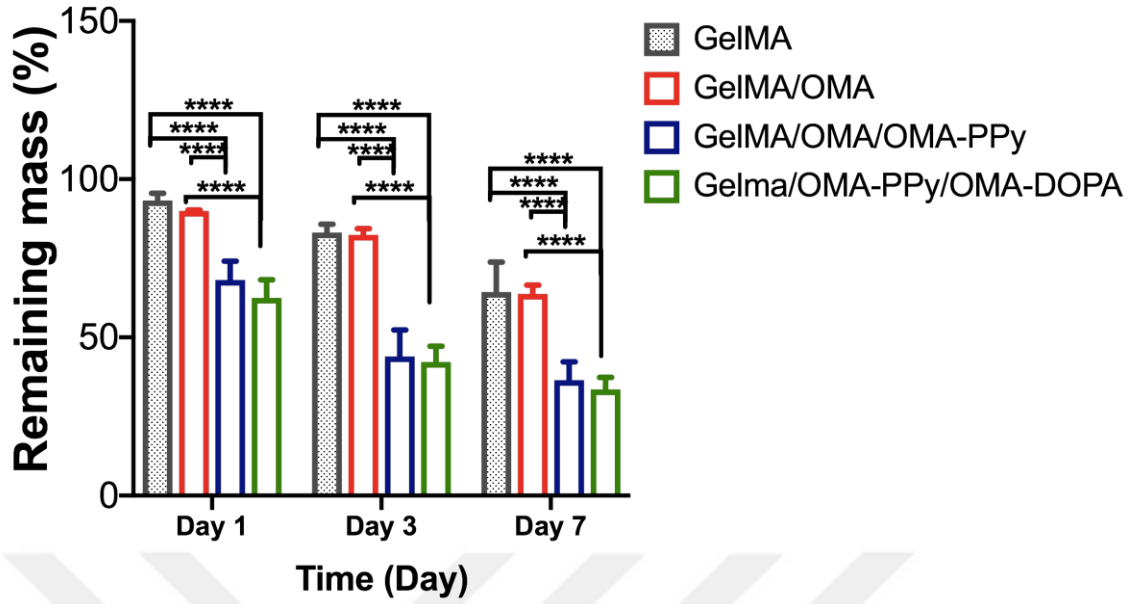

Figure 4.11: Degradation rates of GelMA, GelMA/OMA, GelMA/OMA-PPy, and GelMA/OMA-PPy/DOPA hydrogel tissue adhesives at 37°C in PBS (pH 7.4) with 0.02% sodium azide on days 1, 3, and 7 (ANOVA test analysis displays the data as mean ± SD, ns: P > 0.05, *: P ≤ 0.05, **: P ≤ 0.01, ***: P ≤ 0.001, , ****: P ≤ 0.0001).

4.2.4. Compression Test Results

The compression test results of GelMA, GelMA/OMA, GelMA/OMA-PPy, and GelMA/OMA-PPy/DOPA hydrogel tissue adhesives are presented in Figure 4.12. A column graph has been generated for each hydrogel sample for compression strength (kPa) and elongation at break (%) values, along with the creation of stress-strain curve graphs. For GelMA, GelMA/OMA, GelMA/OMA-PPy, and GelMA/OMA-PPy/DOPA hydrogels, the compression strength values (kPa) are 775.89 ± 123.45, 851.01 ± 88.80, 1033.05 ± 157.34, and 1007.35 ± 100.75, respectively. The elongation at break values (%) for GelMA, GelMA/OMA, GelMA/OMA-PPy, and GelMA/OMA-PPy/DOPA hydrogels are 104.92 ± 13.68, 61.28 ± 12.08, 84.67 ± 22.35, and 65.77 ± 22.96, respectively.

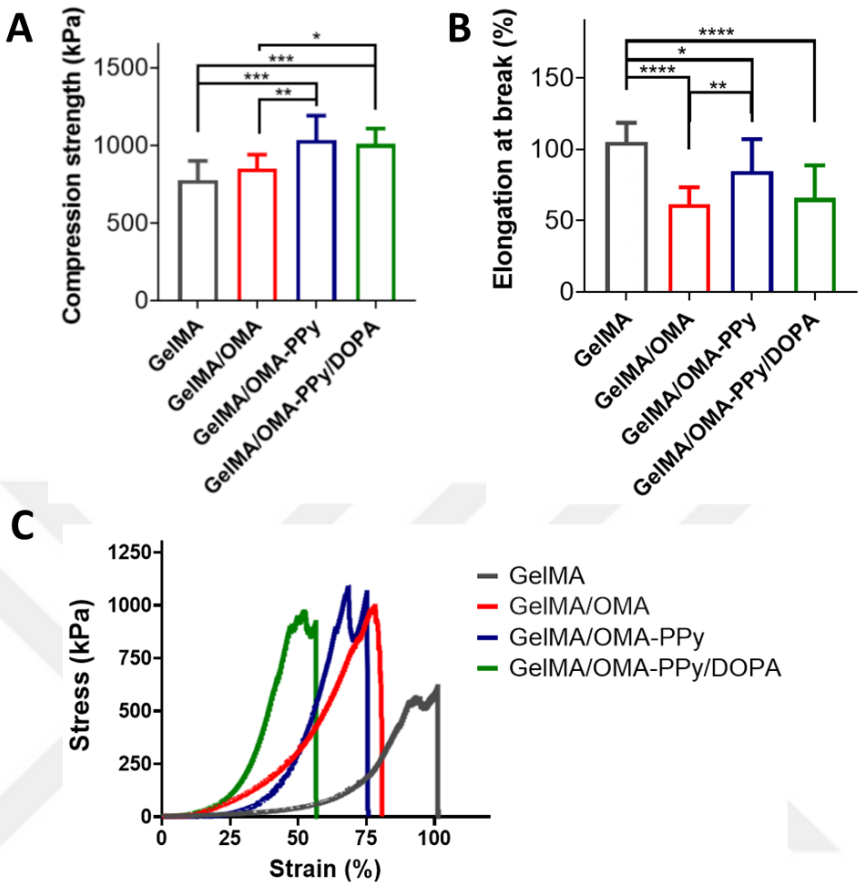

Figure 4.12: The compression test results of GelMA, GelMA/OMA, GelMA/OMA-PPy, and GelMA/OMA-PPy/DOPA hydrogel tissue adhesives: A) Compression strength (kPa), B) Elongation at break (%) and C) Stress-Strain curves (ANOVA test analysis displays the data as mean ± SD, ns: P > 0.05, *: P ≤ 0.05, **: P ≤ 0.01, ***: P ≤ 0.001).

4.2.5. *In Vitro* Adhesion Test Results

4.2.5.1 *In vitro* Lap Shear Test Results

The results of the lap shear test conducted with gelatin-coated microscope slide for GelMA, GelMA/OMA, GelMA/OMA-PPy, and GelMA/OMA-PPy/DOPA hydrogel tissue adhesives are depicted in Figure 4.13. The shear strength values for GelMA, GelMA/OMA, GelMA/OMA-PPy, and GelMA/OMA-PPy/DOPA hydrogel tissue adhesives are 17.35 ± 6.52, 28.86 ± 12.51, 24.43 ± 7.45, and 35.83 ± 10.62 kPa, respectively.

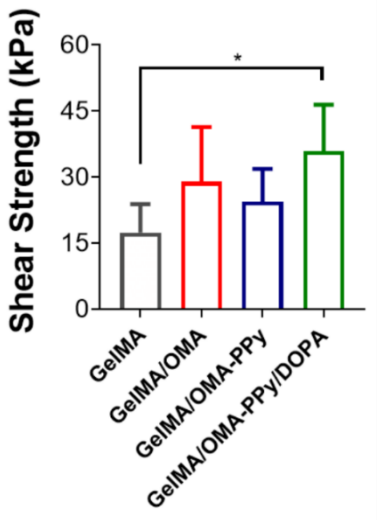

Figure 4.13: The lap shear test results of GelMA, GelMA/OMA, GelMA/OMA-PPy, and GelMA/OMA-PPy/DOPA hydrogel tissue adhesives. (ANOVA test analysis displays the data as mean ± SD, ns: P > 0.05, *: P ≤ 0.05, **: P ≤ 0.01, ***: P ≤ 0.001).

4.2.5.2. *In vitro* T-Peel Test Results

The results of the T-peel test conducted for GelMA, GelMA/OMA, GelMA/OMA-PPy, and GelMA/OMA-PPy/DOPA hydrogel tissue adhesives using a collagen sheets are illustrated in Figure 4.14. As a result of the T-peel test, the shear strength values for GelMA, GelMA/OMA, GelMA/OMA-PPy, and GelMA/OMA-PPy/DOPA hydrogel tissue adhesives are 112.5 ± 27.53, 212 ± 110.82, 57.85 ± 47.33, and 242.5 ± 143.38 kPa respectively. The adhesion energy values for GelMA, GelMA/OMA, GelMA/OMA-PPy, and GelMA/OMA-PPy/DOPA hydrogel tissue adhesives are 225 ± 55.07, 424 ± 221.65, 115.71 ± 94.66, and 485 ± 286.76 J/m^2, respectively.

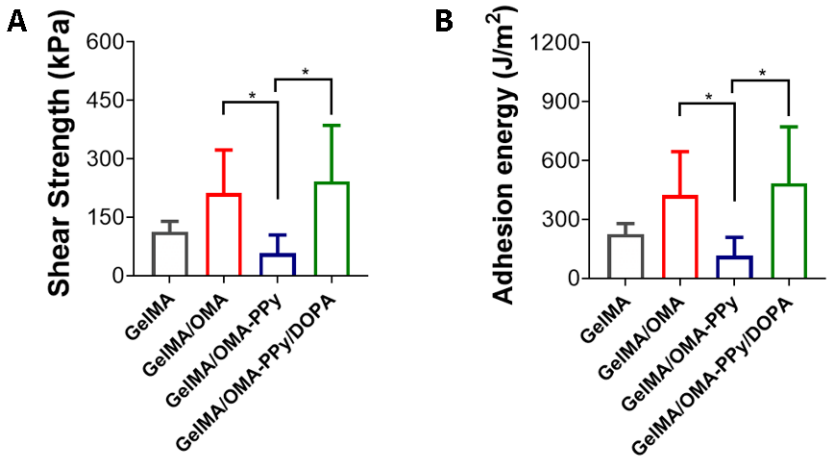

Figure 4.14:The t-peel test results of GelMA, GelMA/OMA, GelMA/OMA-PPy, and GelMA/OMA-PPy/DOPA hydrogel tissue adhesives: A) Shear strength (kPa) and B) Adhesion energy (J/m^2) (ANOVA test analysis displays the data as mean ± SD, ns: P > 0.05, *: P ≤ 0.05, **: P ≤ 0.01, ***: P ≤ 0.001).

4.2.5.3 *In vitro* Burst Pressure Test Results

The results of the *in vitro* burst pressure examination carried out using *in situ* UV curing on the collagen-coated surface are illustrated in Figure 4.15. As a result of the burst pressure test, the mmHg values for GelMA, GelMA/OMA, GelMA/OMA-PPy, and GelMA/OMA-PPy/DOPA hydrogel tissue adhesives are 150.39 ± 48.61, 192.23± 66.30, 162.02 ± 48.90, and 254.43 ± 24.98, respectively.

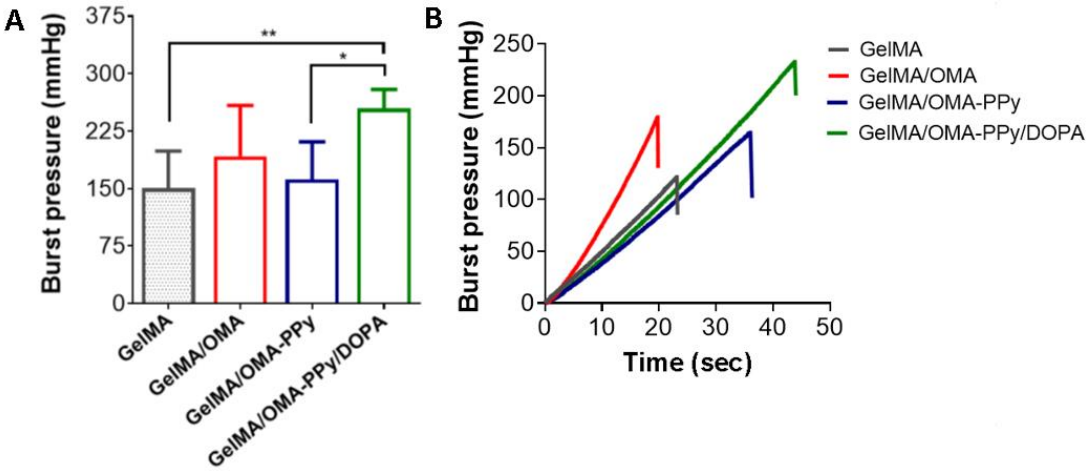

Figure 4.15: The *in vitro* burst pressure test results for GelMA, GelMA/OMA, GelMA/OMA-PPy, and GelMA/OMA-PPy/DOPA hydrogel tissue adhessives: A) Burst pressure values (mmHg) and B) Burst pressure curve (ANOVA test analysis displays the data as mean ± SD, ns: P > 0.05, *: P ≤ 0.05, **: P ≤ 0.01, ***: P ≤ 0.001).

4.2.6. *Ex Vivo* Adhesion Test Results

4.2.6.1. *Ex vivo* Burst Pressure Test Results

The findings from *ex vivo* burst pressure assessments conducted via *in situ* light curing on the pericardial membrane, myocardial layer, and artery, utilizing GelMA, GelMA/OMA, GelMA/OMA-PPy, and GelMA/OMA-PPy/DOPA hydrogel tissue adhesives, are sequentially presented in Figure 4.16, Figure 4.17, and Figure 4.18. In Figure 4.16, as a result of the burst pressure test performed on the pericardial membrane, the mmHg values of the hydrogels were found to be 123.12 ± 29.74, 242.43 ± 22.97, 130.51 ± 41.93 and 187.07 ± 11.67, respectively.

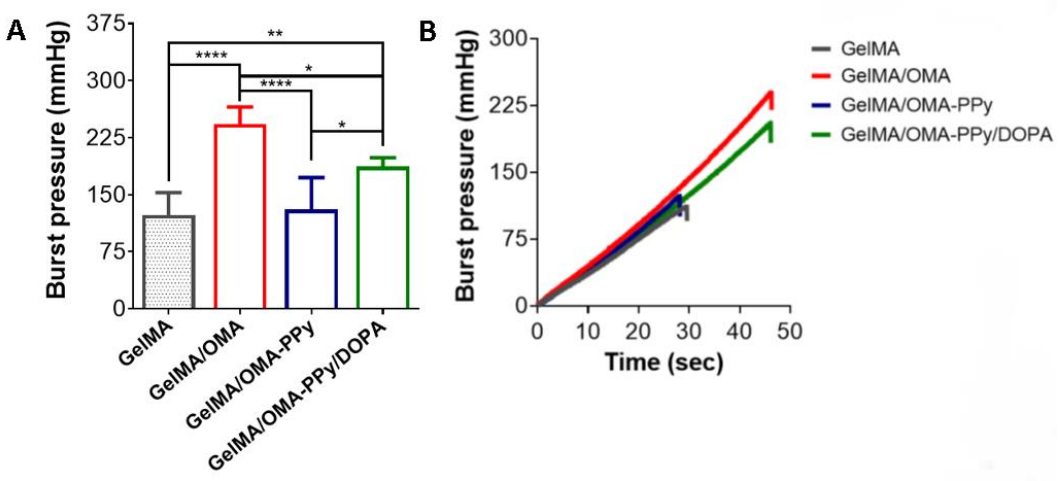

Figure 4.16: The *ex vivo* burst pressure test on the pericardial membrane for GelMA, GelMA/OMA, GelMA/OMA-PPy, and GelMA/OMA-PPy/DOPA hydrogel tissue adhesives: A) Burst pressure values (mmHg) and B) Burst pressure curves. (ANOVA test analysis displays the data as mean ± SD, ns: P > 0.05, *: P ≤ 0.05, **: P ≤ 0.01, ***: P ≤ 0.001).

In Figure 4.17, as a result of the burst pressure test performed on the myocardial layer, the mmHg values of the GelMA, GelMA/OMA, GelMA/OMA-PPy, and GelMA/OMA-PPy/DOPA hydrogel tissue adhesives were found to be 65.58 ± 29.19, 97.92 ± 16.41, 32.08 ± 8.98 and 191.03 ± 64.96, respectively.

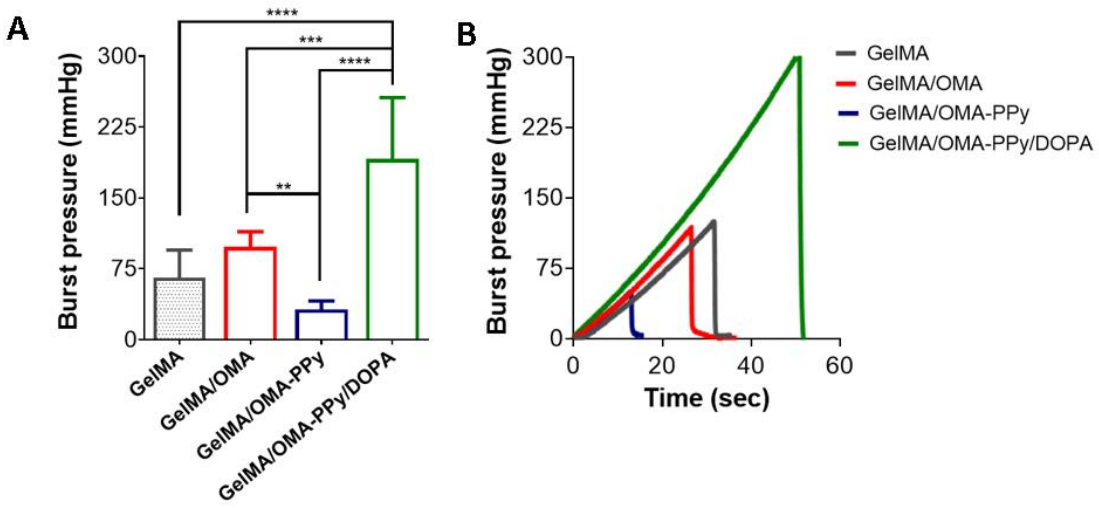

Figure 4.17: The *ex vivo* burst pressure test on the myocardial layer for GelMA, GelMA/OMA, GelMA/OMA-PPy, and GelMA/OMA-PPy/DOPA hydrogel tissue adhesives: A) Burst pressure values (mmHg) and B) Burst curves (ANOVA test analysis displays the data as mean ± SD, ns: P > 0.05, *: P ≤ 0.05, **: P ≤ 0.01, ***: P ≤ 0.001).

In Figure 4.18, as a result of the burst pressure test performed on the artery, the mmHg values of the GelMA, GelMA/OMA, GelMA/OMA-PPy, and GelMA/OMA-PPy/DOPA hydrogel tissue adhesives were found to be 94.2 ± 26.21, 120.22 ± 36.75, 49.21 ± 28.41 and 86.75 ± 33.08, respectively.

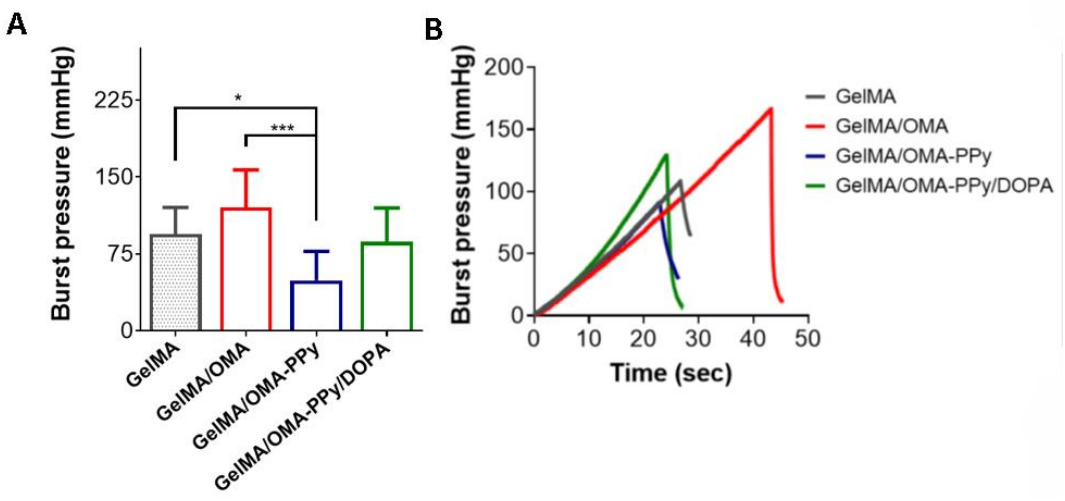

Figure 4.18: The *ex vivo* burst pressure test on the artery for GelMA,GelMA/OMA, GelMA/OMA-PPy, and GelMA/OMA-PPy/DOPA hydrogel tissue adhesives: A) Burst pressure values (mmHg) and B) Burst pressure curves (ANOVA test analysis displays the data as mean ± SD, ns: P > 0.05, *: P ≤ 0.05, **: P ≤ 0.01, ***: P ≤ 0.001).

4.2.6.2. *Ex vivo* Wound Closure Test Results

The results of the *ex vivo* wound closure experiment conducted on the sheep myocardium obtained from the abattoir are presented in Figure 4.19. As a result of the wound closure test, mean values for the GelMA, GelMA/OMA, GelMA/OMA-PPy, and GelMA/OMA-PPy/DOPA hydrogel tissue adhesives are 0.20 ± 0.07, 0.61± 0.19, 0.28 ± 0.09, and 0.37 ± 0.09 MPa, respectively.

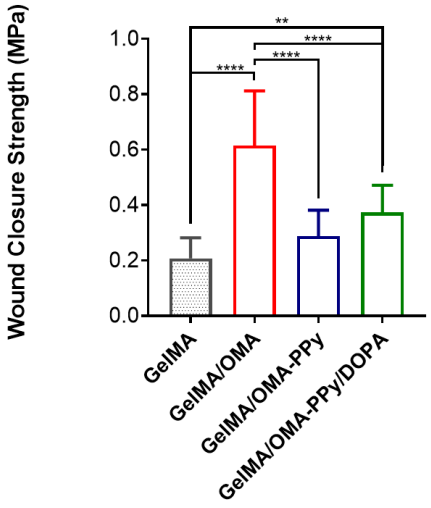

Figure 4.19: The *ex vivo* wound closure test results of GelMA, GelMA/OMA, GelMA/OMA-PPy, and GelMA/OMA-PPy/DOPA hydrogel tissue adhesives (ANOVA test analysis displays the data as mean ± SD, ns: P > 0.05, *: P ≤ 0.05, **: P ≤ 0.01, ***: P ≤ 0.001).

4.2.7. Conductivity Test Results

The conductivity test results of the prepared hydrogel molds of GelMA, GelMA/OMA, GelMA/OMA-PPy, and GelMA/OMA-PPy/DOPA are shown in Figure 4.20. As a result of the conductivity test, mean values for the GelMA, GelMA/OMA, GelMA/OMA-PPy, and GelMA/OMA-PPy/DOPA hydrogel tissue adhesives are 3.48, 3.42667, 3.75 and 3.76333 (S/cm), respectively.

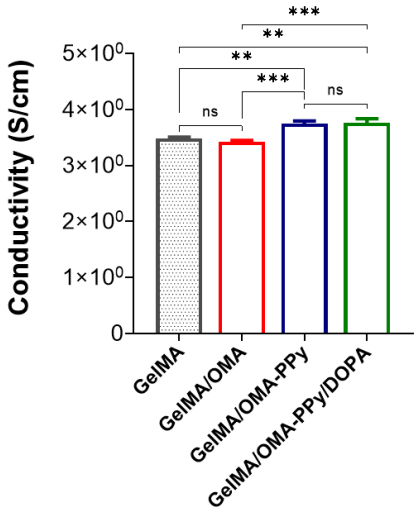

Figure 4.20: The conductivity test results (S/cm) of GelMA, GelMA/OMA, GelMA/OMA-PPy, and GelMA/OMA-PPy/DOPA hydrogel tissue adhesives (ANOVA test analysis displays the data as mean ± SD, ns: P > 0.05, *: P ≤ 0.05, **: P ≤ 0.01, ***: P ≤ 0.001, , ****: P ≤ 0.0001).

4.2.8. *In vitro* Cytotoxicity Test Results

The viability of H9C2 cells was assessed through the MTT assay to evaluate the cytotoxic effects of GelMA, GelMA/OMA, GelMA/OMA-PPy, and GelMA/OMA-PPy/DOPA hydrogel tissue adhesives. The cell viability percentages is presented in Figure 4.21. Cell viability percentages for the negative control group were 100 ± 15,39, while for GelMA, GelMA/OMA, GelMA/OMA-PPy, and GelMA/OMA-PPy/DOPA hydrogel tissue adhesives, they are 89.61 ± 16.72, 92.19 ± 13.25, 85.96 ± 6.90, and 80.17 ± 6.92, respectively.

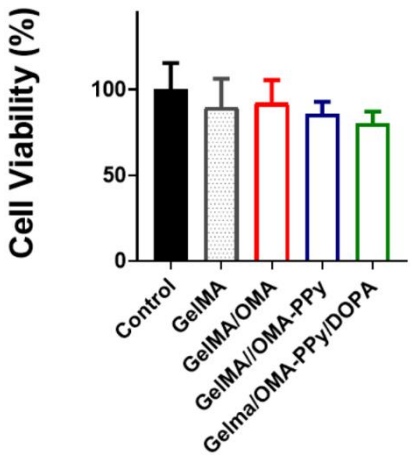

Figure 4.21: H9C2 cell viability (%) determined by the MTT test on GelMA, GelMA/OMA, GelMA/OMA-PPy and GelMA/OMA-PPy/DOPA tissue adhesives (ANOVA test analysis displays the data as mean ± SD, ns: P > 0.05, *: P ≤ 0.05, **: P ≤ 0.01, ***: P ≤ 0.001).

5. DISCUSSION

5.1. Synthesis and Characterization of OSA, OMA, OMA-PPy, and OMA-DOPA Polymers

The oxidation reaction occurs at the -OH groups of the uronate residues at C-2 and C-3 positions in sodium alginate. The carbon-carbon bond is disrupted through the oxidation process of vicinal -OH groups located at the C-2 and C-3 positions of sodium alginate using sodium periodate. This transformation results in the creation of two aldehyde groups within each oxidized monomeric unit, leading to a polysaccharide chain that is more flexible and incorporates two reactive functional groups [146]. It is understood that this process reduces the molecular weight, swelling degree, elastic modulus, rheological properties, and cross-linking efficiency with calcium ions of sodium alginate [147]. The degradation rate of the structural units of OSA in the *in vivo* environment increases compared to unmodified alginate [148]. The increased degradation rate can stem from both enzymatic and hydrolytic breakdown, as well as a decrease in the polymer's molecular weight. Given the significance of biological breakdown properties for biomedical applications, the degradation rate of the alginate backbone can be controlled by oxidizing uronate -OH groups to dialdehyde groups. As the degree of oxidation increases, the storage modulus of hydrogels significantly decreases. Additionally, the aldehyde groups introduced to the polymer can form imine and hydrogen bonds with the amino groups present in living tissues, imparting adhesive properties to the material [149].

The synthesis of OMA was carried out based on protocols recommended in the literature. Throughout the synthesis of OMA, various factors including the rate of methacrylic anhydride addition, the speed at which the reaction is stirred, the duration of the reaction, the temperature maintained during the reaction, pH, and all other conditions play a role in affecting both dispersion and the quality of the resulting product. All these variables collectively contribute to shaping the methacrylation degree of the ultimate product and influencing the characteristics of hydrogels derived from it. In this thesis study, 15 mL of methacrylic anhydride was employed per gram of OSA. The metacrylation reaction, conducted through methacrylic anhydride, involves the displacement of secondary alcohol groups in the OSA structure with methacrylate groups, resulting in the formation of OMA [150]. In order to enhance the efficiency of

the methacrylation reaction, systematic pH monitoring was conducted, and it was adjusted to a pH of 7. Special attention was given to ensuring that the pH environment was not excessively high to induce ester hydrolysis. In addition, alginate is methacrylated to introduce a methacrylate functional group, allowing it to undergo free radical polymerization in the presence a photoinitiator under low-intensity light exosure, thereby forming covalent bonds within itself. In this study, LAP was chosen as the photoinitiator. The overall cell viability using LAP was found to be significantly higher than that using Irgacure 2959 [151].

The swelling and degradation outcomes of modified sodium alginate cured with LAP photoinitiator can be influenced by various factors. These factors include the concentration of the photoinitiator, light exposure time and the characteristics of the initial structure of sodium alginate. Initiator toxicity grows with increasing concentration of the initiator as well as with increasing light exposure time [152].

PPy polymers exhibit outstanding electrical conductivity, primarily owing to the presence of conjugated double bonds. Due to being a conjugated polymer, PPy possesses a conjugation system that allows electrons to move freely. This enables the polymer to absorb light at specific wavelengths, resulting in its acquisition of a black color [153]. The PPy polymer is approaching the oxygen regions in alginate. The conductivity is associated with the incorporation of doped electron donors or electron acceptors. Pyrrole polymerization can be conducted through either chemical oxidation or electrochemical methods. In this thesis study, the polymerization of pyrrole is achieved through chemical oxidation mediated by $FeCl_3$ and during this process, a polymer known as polypyrrole is formed. Initially, during chemical oxidation, an electron is released from the pyrrole ring, resulting in the formation of a radical cation. Subsequently, the two radical cations generated are coupled, followed by the deprotonation of two hydrogen atoms, resulting in the production of bipyrrole. This process is iteratively repeated to generate polymer chains. Furthermore, the radical cation can engage in a chain-growth polymerization mechanism by reacting with the pyrrole ring. It is anticipated that both mechanisms occur concurrently [154].

Pyrrole polymerization is commonly carried out in acidic environments, facilitating the oxidation of the pyrrole ring and supporting polymer formation. A frequently used acidic agent could be an oxidative agent such as $FeCl_3$. In such an

environment, pH significantly affects the efficiency and yield of polymerization. Both pH value and temperature are crucial factors influencing the efficiency of this polymerization reaction. Generally, the reaction rate tends to increase with higher temperatures; however, the choice of temperature can vary depending on the reactants, catalysts, and specific applications. In our system, the reaction was conducted at a temperature of 90 °C.

Moreover, to improve the material's adhesive properties, even in aqueous environments, OMA was subjected to a reaction with dopamine hydrochloride to produce OMA-DOPA. DOPA undergoes oxidation to a quinone form and exhibits robust reactivity with biomacromolecules, as well as both organic and inorganic materials through Schiff-base reactions. This characteristic of DOPA has been utilized to enhance the tissue adhesion of oxidized and methacrylated alginate, which forms Schiff-bases.

In the literature, the Schiff-base reaction between the aldehyde groups of OSA and the amine groups of tissue proteins forms a rigid mechanical barrier for hemorrhage control. However, over time, a decrease in the adhesive properties of OSA adhesive and its detachment from the wound tissue have been observed. To address this issue, mussel-inspired DOPA was conjugated into OSA, and its physical properties were compared with OSA adhesive. The elasticity (storage modulus, G') of DOPA-OSA adhesive was lower than that of OSA adhesive, indicating better applicability at the bleeding site. Additionally, the tissue adhesion force of Dopa-OSA adhesive was significantly higher than that of OSA adhesive. Moreover, demonstrated a substantial increase in the elongation (stickiness) of Dopa-OSA adhesive after the incorporation of DOPA into the hydrogel system [155]. Therefore, in our study, DOPA was incorporated into the OMA polymer instead of OSA, aiming to increase tissue adhesion force, as achieved in this study.

5.1.1. FTIR Results

The FTIR analysis results of sodium alginate and modified polymers (OSA, OMA and OMA-PPy) are presented in Figure 4.6A. In the structure of all polymers, bands corresponding to the stretching of -OH and -CH groups are observed in the

regions of 3700-3000 cm^{-1} and 2980-2850 cm^{-1}, respectively, which are common to all polysaccharides [156]. The peak observed at 1735 cm^{-1} in the OSA polymer indicates the presence of aldehyde groups in the oxidized sample [157]. However, many researchers have reported that aldehyde peaks are generally not observed in the FTIR spectrum of dry samples due to hemiacetal formation [127]. In the OSA sample, the intensity of the symmetric C-O-C (cyclic ether) stretching at 1081 and 814 cm^{-1} has also decreased, confirming the cleavage of chains [157]. The presence of -COO ester bonds in the OMA sample is confirmed by the newly formed band at 1715 cm^{-1} [158]. The FTIR spectrum of the OMA-PPy sample shows a band at 1550 cm^{-1}, indicating the stretching of C=C (pyrrole ring) [159]. Additionally, a decrease in the intensity of several peaks in the spectrum is observed. The low intensity of characteristic pyrrole peaks is thought to be due to the low pyrrole ratio.

The FTIR analysis results of the OMA-DOPA polymer are presented in Figure 4.6.B. In the OMA-DOPA polymer, the presence of alginate in the structure is indicated by a broad band at 3250 cm^{-1}, showing the presence of hydroxyl groups. Characteristic carboxylate vibration modes are observed at 1596 cm^{-1} as an antisymmetric stretch and at 1406 cm^{-1} as a symmetric stretch. The peaks observed at 1638 cm^{-1} in the OMA and OMA-PPy polymers indicate the presence of aldehyde groups (resulting from the oxidation of alginate) [157]. The decrease in the intensities of these peaks in the OMA-DOPA polymer indicates that DOPA is successfully bound to the polymer chain through a Schiff-base reaction (between the aldehyde groups in the structure of OMA and the amine groups in the structure of DOPA). Additionally, vibrations of the DOPA ring are observed with an increase in the intensities of peaks at 1360-1257 cm^{-1}, corresponding to the CO stretching vibration of the phenol group.

5.2. Synthesis and Characterization of GelMA

Gelatin was methacrylated with metacrylic anhydride to obtain GelMA. GelMA hydrogels have found extensive use in diverse biomedical applications owing to their favorable biological properties and adjustable physical attributes. GelMA hydrogels exhibit characteristics closely resembling those of the native ECM attributed to the inclusion of peptide motifs responsive to cell attachment and matrix metalloproteinases. These motifs facilitate cell proliferation and spreading within GelMA-based scaffolds.

GelMA is also versatile in terms of processing; upon exposure to light irradiation, it undergoes covalently crosslinking in the presence of a photoinitiator, to create hydrogels with adjustable mechanical properties. Recent studies have showcased the effectiveness of GelMA-based hydrogels across various tissue engineering applications, encompassing the development of bone, cartilage, cardiac, and vascular tissues, among others [160]. Hence, to harness the advantageous effects of GelMA, it has been included in the compositions when preparing hydrogels.

5.2.1. FTIR Results

The structural characterizations of Gelatin and GelMA were conducted through FTIR analysis. FTIR analyses were performed using the Jasco FT/IR-4600 model ATR unit in the range of 4000-500 cm^{-1}. The FTIR spectrum of the GelMA polymers obtained from the modification reaction of gelatin with methacrylic anhydride is presented in Figure 4.7.

The peaks observed at 1630 cm^{-1} (amide I), 1540 cm^{-1} (amide II), and 1450 cm−1 (amide III) in GelMA correspond to the stretching vibration of the –C=O bond, bending vibration of the N-H bond, and in-plane bending vibration of the C-N and N-H bonds, respectively [161]. It is noteworthy that there is an increase in the intensities of the amide peaks after methacrylation. These results indicate the successful completion of the methacrylation reaction. Additionally, the peaks at 3260 cm-1 and 2915 cm-1 in the spectra originate from the stretching vibrations of O-H and C-H, respectively [162].

5.3. DOPA Quantification Results

The quantification of the DOPA content in the OMA-DOPA polymer was carried out using a UV-vis spectrophotometer. Readings were taken in the presence of different concentrations of Dopamine hydrochloride (0.02, 0.04, 0.06, 0.08, and 0.10 mg/mL) in OMA solution (Figure 4.8A-B) at a concentration of 1 mg/mL, and standard curves were constructed. The UV-vis absorbances at 280 nm wavelength for the OMA-DOPA solution (1 mg/mL) were recorded. The catechol content of OMA-DOPA and OMA-PPy-DOPA samples was calculated using standard curves [137]. As seen in Figure 4.8C, the absorbance of the OMA-DOPA sample (1 mg/mL) at 280 nm was

measured as 0.728. Substituting this value into the calibration curve and performing the necessary calculations revealed that there were $3x10^{-6}$ mol DOPA per gram of OMA-DOPA ($3x10^{-6}$ mol DOPA/g OMA-DOPA).

5.4. Characterization of Hydrogel Tissue Adhesives

5.4.1 FTIR Results

The hydrogels, GelMA, GelMA/OMA, GelMA/OMA-PPy, and GelMA/OMA-PPy/DOPA, prepared as described in Table 3.1, were cross-linked in PDMS molds under UV light for 1 minute. After freezing at -80 °C for one day and lyophilizing, the FTIR spectra of the samples were generated and examined (Figure 4.9). The GelMA spectrum exhibits the characteristic peaks of the gelatin polymer. The typical absorption band around 3346 cm^{-1} is associated with the stretching vibrations of O-H and N-H. The peaks within the range of 2800–3100 cm^{-1} are assigned to the stretching vibration of C-H groups. The structural framework of gelatin is linked to the absorption bands at 1651 cm^{-1} (C=O stretching, amide I), 1544 cm^{-1} (N-H bending coupled to C-H stretching, amide II), and 1253 cm^{-1} (C-N stretching and N-H bending, amide III). It is worth noting that the typical peak around 1640 cm^{-1} in the GelMA spectrum, corresponding to the C=C stretching of the methacrylate groups, is closely positioned to the amide I C=O stretching peak. As a result, it becomes challenging to detect and confirm its disappearance after crosslinking. Confirmation of the success of the cross-linking reaction would be evident in this characteristic region. However, this was achieved through the observation of an increase or emergence of typical peaks in the region of 2800–3100 cm^{-1}, which can be attributed to the stretching of C-H bonds in CH_2 and tertiary CH groups formed during the crosslinking reaction [163].

5.4.2 Swelling Analysis Results

The swelling behavior of hydrogels is a crucial factor that impacts solute diffusion and mechanical properties. This characteristic is influenced by structural properties such as the interaction with the solvent, crosslinking density, and hydrophilicity. Swelling studies showed that equilibrium swelling was achieved after immersing the hydrogel composites in PBS for 24 hours (Figure 4.10). According to the

literature, the swelling degree of the hydrogel exhibits an inverse relationship with the gel concentration due to the increase in polymer network density as the gel concentration rises [164]. According to additional information in the literature, higher degrees of methacrylation are associated with a higher compressive modulus, slower swelling kinetics, and smaller pore sizes [150]. Therefore, it is reasonable to expect a reduction in the equilibrium swelling ratio when GelMA polymer is combined with OMA to obtain GelMA/OMA hydrogel. PPy is a hydrophobic polymer with limited ability to form hydrogen bonds. Therefore, it was anticipated that the GelMA/OMA-PPy hydrogel would exhibit more hydrophobic characteristics compared to the GelMA/OMA hydrogel, leading to a decrease in water retention capacity. However, contrary to expectations, an increase in the equilibrium swelling ratio was observed instead. The reason for this could be that while a decrease in the concentration of OMA in the GelMA/OMA-PPy hydrogel would typically lead to more swelling behavior, the addition of pyrrole to the structure, which is expected to reduce swelling due to its hydrophobic nature, might have been less effective. This might be attributed to the relatively low concentration of pyrrole used in the structure, leading to a less pronounced effect than anticipated. DOPA conjugation typically contributes to the formation of hydrogen bonds, thereby enhancing the hydrophilic properties of the hydrogel. Consequently, the incorporation of DOPA might lead to an anticipated increase in the swelling behavior of the hydrogel. However, the extent of this effect could vary, depending on dopa's integration into the molecular structure and the other components of the hydrogel matrix. Therefore, the relatively low concentration of DOPA in the OMA-DOPA structure might not have significantly influenced the high swelling ratio observed, as it could be influenced by a multitude of factors in the matrix composition.

5.4.3. Degradation Analysis Results

The degradation behavior of hydrogels is of great significance for the treatment process. The implanted scaffolds need to remain in the environment for a certain period during the treatment and gradually degrade over time, allowing the host tissue to take over as the healing process continues. This ensures compatibility with tissue kinetics. While hydrolytic degradation may not fully represent the degradation in the body or

cellular environment, it provides some understanding of the hydrogel's strength. Throughout the conducted experiments, it is essential for hydrogels to maintain their functionality without undergoing degradation. Using conductive polymers poses a limitation due to their inherent resistance to *in vivo* degradation, potentially leading to chronic inflammation. Additionally, their fragility and lack of mechanical manipulability and processability make standalone application challenging. Consequently, research efforts have predominantly concentrated on incorporating biological and physical modifications to create composite conductive polymers. Achieving biocompatibility and biodegradability in conductive polymers is commonly realized by modifying them with appropriate natural biodegradable polymers like alginate [159]. As depicted in Figure 4.11, the degradation behavior of hydrogel groups was observed over a period of 7 days in the conducted hydrolytic degradation test. The sodium azide wasused in degradation tests, in conjunction with PBS buffer. The addition of OMA to GelMA did not have a significant impact on the degradation behavior. On the other hand, the addition of PPy increased degradation, while the addition of DOPA did not have a meaningful effect. When observing the trends in the degradation behavior of hydrogels on the 1st, 3rd, and 7th days, they remained consistent. The findings indicated a progressive increase in hydrogel degradation over distinct time intervals (1, 3, and 7 days). This controlled degradation is a crucial aspect in tissue engineering and may be associated with the crosslinkers employed in scaffold fabrication.

5.4.4. Compression Test Results

A critical aspect in the design of a tissue adhesive is to ensure that its mechanical properties align with those of the underlying tissue. While current adhesive designs primarily prioritize biocompatibility and adhesive strength, the potential consequences of mechanical mismatch are frequently neglected. The fundamental metric for assessing the mechanical properties of a material is its elastic modulus or stiffness, indicating the material's ability to resist deformation under applied stress. The unit deformation or strain occurring when a material is subjected to compressive force provides information about its elastic behavior. In the case of biological tissues, elastic modulus values vary from tens of pascals to hundreds of kilopascals. Elastic modulus value is approximately

20 kPA for the heart [1]. The cardiovascular system presents one of the most challenging environments for tissue adhesives due to its dynamically mechanical nature and the frequent presence of blood, which can compromise the reactive groups of adhesives. Adhesives intended for these tissues must endure elevated pulsatile pressures, particularly in the aorta (~120 mmHg), and withstand myocardial strains ranging from 10% to 20% [1]. Additionally, they must maintain their mechanical properties over time without impeding tissue function. The cyclic strain and mechanical pressure experienced by cardiovascular tissues emphasize the significance of the adhesive's fatigue resistance. The results presented in Figure 4.12 were obtained from the compression test applied in this study. The compressive force used to measure the stress under compression of the material significantly increased with the addition of PPy. This effect was also maintained with the addition of DOPA. The addition of PPy has again increased elongation at break (%) compared to the GelMA/OMA control group. Although elongation at break (%) decreases with the addition of DOPA, it is still higher than the GelMA/OMA control group. In the literature, the volume modulus values of the myocardium indicate low values, suggesting minimal changes observed during the diastolic phase, such as 28 kPa and 160 kPa. However, higher values are required for analyses during the systolic phase, such as 380 kPa, 600 kPa, and 25 MPa [165]. These elevated figures reflect the tissue's compressibility due to systolic intra and extra-vascular blood displacements. This also indicates that the obtained experimental results hold promise for cardiac tissue adhesive.

5.2.5. *In Vitro* Adhesion Test Results

The primary goal of hydrogel tissue adhesives is to establish strong and durable bonds between both two tissues and tissue and scaffold, promoting integration. In this study, *in vitro* adhesion tests were conducted to anticipate the interactions of the designed hydrogels, aiming for their use as cardiac tissue adhesives.

5.2.5.1. *In vitro* Lap Shear Test Results

In Figure 4.13, glass coated with gelatin was employed as the substrate to measure adhesion strength. Comparing the adhesive behaviors of hydrogel groups with

each other through Lap-shear tests, it was observed that the group containing DOPA exhibited the highest adhesive properties. Based on the information in the literature, DOPA has been identified as a crucial element in the interfacial adhesion and curing processes of adhesive plaque proteins. The versatile chemical nature of DOPA molecules allows them to adhere to various surfaces, whether organic or inorganic, through the formation of reversible non-covalent and irreversible covalent bonds. DOPA can create robust hydrogen bonds through its dihydroxy functionality, enhancing its adherence to tissue surfaces, particularly mucosal tissues. Catechol-containing polymers exhibit enhanced cohesion attributed to the benzene ring within catechol. This benzene ring is capable of engaging in π-π interactions with other aromatic rings, contributing to increased cohesive properties. Furthermore, the benzene ring can establish interactions with positively charged ions through cation-π interactions, recognized as highly stable non-covalent interactions in aqueous environments. This characteristic enables these polymers to adhere to positively charged surfaces and substrates containing abundant cationic functional groups. Moreover, catechol has the capability to create strong and reversible connections with metal ions like Cu^{+2} and Zn^{+2}, along with interfacial bonds established with metal oxide surfaces [166].

Considering these informations, DOPA may have reacted with the active gelatin groups coated on the glasses, effectively bonding the two glasses together. Therefore, the adhesion strength of the hydrogels is primarily contingent on the quantity of DOPA.

5.2.5.2. *In vitro* T-peel Test Results

The T-peel test is commonly employed to assess the adhesive properties of a material. In this test, material samples are typically adhered to a substrate, and then a tensile force is applied to measure the adhesive strength of the material. Collagen is a protein commonly found in biological tissues. Therefore, conducting T-peel tests with a collagen sheets aims to simulate adhesive tests performed under conditions more akin to biological tissues. Studies investigating the robust adhesion of mussel plaque structures have demonstrated the critical role of the amino acid DOPA in underwater adhesion. According to the T-peel results presented in Figure 4.14, it is observed that the shear strength and adhesion energy values of the developed GelMA/OMA-PPy hydrogel are lower compared to the GelMA and GelMA/OMA control groups. However, with the

influence of DOPA, the GelMA/OMA-PPy/DOPA hydrogel exhibits higher adhesion performance compared to other hydrogel groups. Examining the conducted research, numerous adhesive hydrogels based on DOPA have been developed, exhibiting moderate adhesion (interfacial toughness less than 100 J/m^2) [167-169]. T-peel results of the developed GelMA/OMA-PPy/DOPA hydrogel indicate high adhesion performance compared to the literature.

5.2.5.3. *In vitro* Burst Pressure Test Results

This biomacromolecule-based matrix hydrogel, capable of rapid gel formation after exposure to UV light, has been considered to have the ability to adhere and seal arteries and cardiac walls based on experiments conducted on collagen. The observed data in Figure 4.15 these repairs can withstand blood pressure up to approximately 254 mmHg, significantly higher than blood pressures commonly found in clinical settings (systolic BP 60–160 mm Hg) [170]. Most importantly, the hydrogel can stop high-pressure bleeding from 3 mm diameter penetration holes. The burst pressure of GelMA/OMA-PPy/DOPA hydrogel on the collagen casing was significantly higher than the normal systolic blood pressure (120 mm Hg), making it a promising sealant for cardiac applications.

5.2.6. *Ex Vivo* Adhesion Test Results

5.2.6.1. *Ex vivo* Burst Pressure Test Results

The promising results observed in the burst pressure experiments on the collagen sheets *in vitro* led to the transition to *ex vivo* experiments. The burst pressure experiments were sequentially conducted, as shown in Figures 4.16, 4.17, and 4.18, not only on the pericardial and myocardial layers of the heart but also on the artery. According to the burst pressure test results observed in Figures 4.16, 4.17, and 4.18, the addition of PPy significantly reduced the adhesive property of the hydrogel. This is believed to be attributed to the PPy approaching the polymer matrix from all oxygen regions and partially blocking adhesive end groups like aldehydes [134]. The experiments conducted on the pericardium and myocardium with the developed GelMA/OMA-PPy/DOPA hydrogel yielded higher results compared to the heart artery.

However, similar to the experiments on the collagen sheet, the burst pressure on the pericardium, and myocardium significantly higher than the normal systolic blood pressure (120 mm Hg). This demonstrates the hydrogel's promising potential as a cardiac sealant.

5.2.6.2. *Ex vivo* Wound Closure Test Results

Many wound closure bioadhesives face challenges related to inadequate sealing effectiveness, particularly when applied to stretchable organs. Adhesives employed for wound closure need to possess flexibility to conform to dynamic wounds, thereby minimizing discomfort. To better replicate how the hydrogel adheres to damaged tissues, an experiment focusing on wound closure has been devised. The research suggests that the wound closure test could serve as an optimal assessment technique for anticipating the effectiveness of a wound-sealing adhesive when exposed to tensile or stretching forces [143]. In the experiment conducted on the sheep myocardium, the myocardium was divided, and four different hydrogel groups were sequentially applied and cured with UV light before undergoing testing. In Figure 4.19, while the GelMA/OMA hydrogel exhibited the highest adhesion, the incorporation of PPy into the structure resulted in a decrease in this outcome. As mentioned earlier, this phenomenon may stem from the PPy approaching the polymer matrix from all oxygen regions and partially obstructing adhesive end groups such as aldehydes [134]. However, as anticipated, the adhesion increased with the addition of DOPA because, DOPA found in mussels is the crucial functional group that has been shown to play a significant role in the mechanism of wet adhesion [54].

5.2.7. Conductivity Test Results

The conductivity properties altered by the incorporation of PPy conductive polymer into hydrogel structures have been investigated. Electrical conductivity achieved through conductive polymers is dependent on the conjugated π system, characterized by overlapping π orbitals along the polymer chain (π-π stacking). At the molecular level, the presence of aromatic rings allows for varying single and double bond patterns, facilitating charge transfer. In conductive polymers, aromatic stacking

rings or the conjugated π system enable charge transfer either along the chains (intrachain transfer) or between conductive polymer chains within the hydrogel (interchain transfer). During the polymerization of PPy, delocalized electrons emerge, capable of freely moving along the chain and carrying energy. These electrons are responsible for the electrical conductivity properties of the polymer [134]. The addition of PPy to the structure, as observed in Figure 4.20, enhances the material's conductivity, as expected. More current passed through the system with the incorporation of PPy, and the conductivity of the materials can be adjusted by varying the PPy concentration.

5.2.8. *In vitro* Cytotoxicity Test Results

The MTT cytotoxicity assay is a colorimetric test designed to quantify the population of viable cells exhibiting active enzymes. This involves the conversion of a yellow tetrazolium salt into an insoluble purple formazan. The intensity of the purple hue is directly correlated with the metabolically active living cells and is evaluated through colorimetric analysis. In Figure 4.21, the cytotoxic effects of GelMA, GelMA/OMA, GelMA/OMA-PPy, and GelMA/OMA-PPy/DOPA hydrogel groups were investigated on the H9C2 rat cardiomyocyte cell line, alongside the control group. The viability of cells in wells where no treatment was applied, representing the control group with only cells and medium, was 100%. In comparison, the GelMA group exhibited a cell viability of 89%, GelMA/OMA group showed 92%, GelMA/OMA-PPy group displayed 85%, and GelMA/OMA-PPy/DOPA group demonstrated 80% cell viability. In cell culture experiments, cell viability percentages exceeding 80% are classified as non-cytotoxic, those ranging from 80% to 60% are considered weakly cytotoxic, percentages from 60% to 40% are categorized as moderately cytotoxic, and values below 40% indicate strong cytotoxicity.This indicates that the majority of cells are healthy and metabolically active [171].

6. CONCLUSION, RECOMMENDATIONS AND CONTRIBUTION TO SOCIETY

In this thesis study, sodium alginate and gelatin polymers were initially modified to introduce various end groups to the polymers. The synthesized OMA polymer gained the ability to form dynamic covalent bonds with amines and undergo UV-crosslinking with methacrylate groups, owing to the introduced aldehyde groups. Additionally, the OMA-PPy polymer, incorporating PPy, exhibited electroconductive properties. Furthermore, for enhanced adhesive characteristics, especially in aqueous environments, OMA was reacted with Dopamine Hydrochloride to yield OMA-DOPA. The successful synthesis of modified polymers was confirmed through the FTIR analysis. Gelatin was also methacrylated using methacrylic anhydride to produce GelMA polymer, which is versatile for processing and can be covalently crosslinked upon light exposure in the presence of a photoinitiator, creating hydrogels with adjustable mechanical properties. Consequently, GelMA has been incorporated into the compositions during the hydrogel preparation to leverage its beneficial effects.

The tissue adhesives were prepared by exposing them to light for 60 seconds in the presence of LAP photoinitiator (2.5 mg/mL). The structural analyses of the GelMA, GelMA/OMA, GelMA/OMA-PPy, and GelMA/OMA-PPy/DOPA tissue adhesives were conducted using FTIR. Subsequently, their swelling and degradation behaviors were monitored. The inclusion of PPy led to a substantial increase in the compressive force applied to assess the material's stress under compression. This effect was consistently observed even with the introduction of DOPA. The addition of PPy and DOPA has been observed to enhance the elasticity of the material compared to the GelMA/OMA control group. Consequently, an increase in the mechanical strength and elasticity of the hydrogels has been noted. The obtained values are consistent with and higher than those reported in the literature. In order to foresee the interactions of the formulated hydrogels intended for use as tissue adhesives, various bioadhesion tests including *in vitro* lap shear, *in vitro* t-peel, *in vitro* burst pressure, and *ex vivo* burst pressure, as well as *ex vivo* wound closure tests, were carried out. In general, across all tests, the introduction of PPy markedly diminished the adhesive characteristics of the hydrogel. This is thought to be due to PPy infiltrating the polymer matrix from various oxygen regions and partially obstructing adhesive end groups, such as aldehydes.

Nevertheless, it has been concluded that the primary developed hydrogel, GelMA/OMA-PPy/DOPA, enhanced adhesive properties despite this. Nevertheless, akin to the trials conducted on the collagen sheet, the burst pressure observed in the pericardium and myocardium significantly exceeds the typical systolic blood pressure level (120 mm Hg). This underscores the hydrogel's encouraging potential as an effective hemostatic sealant. Furthermore, in the cell culture experiments, MTT testing has been employed to assess the hydrogels' biocompatibility with cells and their cytotoxic effects. The H9C2 rat cardiomyocyte cell line was used to examine the GelMA, GelMA/OMA, GelMA/OMA-PPy, and GelMA/OMA-PPy/DOPA hydrogel groups. The results indicate that the hydrogel is also biocompatible. In conclusion, based on all findings, it is evident that the produced hydrogels have broad potential applications in various fields, particularly in cardiac engineering, and could find extensive use in clinical settings.

There is a significant need in the clinical setting for materials that are multifunctional, conductive, and capable of adhering to wet surfaces. The use of such materials is believed to facilitate the smoother and faster execution of cardiovascular operations, especially in complex scenarios. This, in turn, may lead to a reduction in the duration of surgical procedures, support in wound healing, and ultimately enhance the quality of life for patients. Further testing should be conducted on the recently developed hydrogel product, and its effectiveness should be examined in more detail. Since this thesis work also reflects a part of the TUSEB project in which I am involved, even though experiments for the master's thesis have been conducted up to this point, additional experiments will be continued as part of the ongoing project. In this context, in addition to experiments such as hemostatic effect experiments, conductivity experiments, and cell culture, it is planned to conduct *in vivo* experiments in the future within the scope of the project.

REFERENCES (APA FORMAT)

[1] Nam, S., & Mooney, D. (2021). Polymeric tissue adhesives. Chemical Reviews, 121(18), 11336-11384. https://doi.org/10.1021/acs.chemrev.0c00798

[2] Taboada, G. M., Yang, K., Pereira, M. J., Liu, S. S., Hu, Y., Karp, J. M., ... & Lee, Y. (2020). Overcoming the translational barriers of tissue adhesives. Nature Reviews Materials, 5(4), 310-329. https://doi.org/10.1038/s41578-019-0171-7

[3] Ge, L., & Chen, S. (2020). Recent advances in tissue adhesives for clinical medicine. Polymers, 12(4), 939. https://doi.org/10.3390/polym12040939

[4] Bré, L. P., Zheng, Y., Pêgo, A. P., & Wang, W. (2013). Taking tissue adhesives to the future: from traditional synthetic to new biomimetic approaches. Biomaterials science, 1(3), 239-253. doi: 10.1039/C2BM00121G

[5] Mehdizadeh, M., & Yang, J. (2013). Design strategies and applications of tissue bioadhesives. Macromolecular bioscience, 13(3), 271-288. https://doi.org/10.1002/mabi.201200332

[6] Olympia, R. P., O'Neill, R., & Silvis, M. (2017). Urgent care medicine secrets. Elsevier Health Sciences.

[7] Deng, T., Gao, D., Song, X., Zhou, Z., Zhou, L., Tao, M., ... & Wu, M. (2023). A natural biological adhesive from snail mucus for wound repair. Nature Communications, 14(1), 396. https://doi.org/10.1038/s41467-023-35907-4

[8] Duarte, A. P., Coelho, J. F., Bordado, J. C., Cidade, M. T., & Gil, M. H. (2012). Surgical adhesives: Systematic review of the main types and development forecast. Progress in Polymer Science, 37(8), 1031-1050.

[9] Bitton, R., Josef, E., Shimshelashvili, I., Shapira, K., Seliktar, D., & Bianco-Peled, H. (2009). Phloroglucinol-based biomimetic adhesives for medical applications. Acta biomaterialia, 5(5), 1582-1587. https://doi.org/10.1016/j.actbio.2008.10.004

[10] Martinowitz, U., & Spotnitz, W. D. (1997). Fibrin tissue adhesives. Thrombosis and haemostasis, 78(07), 661-666. doi: 10.1055/s-0038-1657608

[11] Horowitz, B., & Busch, M. (2008). Estimating the pathogen safety of manufactured human plasma products: application to fibrin sealants and to thrombin. Transfusion, 48(8), 1739-1753. https://doi.org/10.1111/j.1537-2995.2008.01717.x

[12] Spotnitz, W. D., Falstrom, J. K., & Rodeheaver, G. T. (1997). The role of sutures and fibrin sealant in wound healing. Surgical Clinics, 77(3), 651-669. doi:https://doi.org/10.1016/S0039-6109(05)70573-9

[13] Spotnitz, W. D. (2001). Commercial fibrin sealants in surgical care. *The American journal of surgery*, *182*(2), S8-S14. https://doi.org/10.1016/S0002-9610(01)00771-1

[14] Sekine, T., Nakamura, T., Shimizu, Y., Ueda, H., Matsumoto, K., Takimoto, Y., & Kiyotani, T. (2001). A new type of surgical adhesive made from porcine collagen and polyglutamic acid. Journal of Biomedical Materials Research: An Official Journal of

The Society for Biomaterials and The Japanese Society for Biomaterials, 54(2), 305-310. https://doi.org/10.1002/1097-4636(200102)54:2<305::AID-JBM18>3.0.CO;2-B

[15] Rathi, S., Saka, R., Domb, A. J., & Khan, W. (2019). Protein-based bioadhesives and bioglues. Polymers for Advanced Technologies, 30(2), 217-234. https://doi.org/10.1002/pat.4465

[16] Bal-Ozturk, A., Cecen, B., Avci-Adali, M., Topkaya, S. N., Alarcin, E., Yasayan, G., ... & Hassan, S. (2021). Tissue adhesives: From research to clinical translation. *Nano Today*, *36*, 101049. https://doi.org/10.1016/j.nantod.2020.101049

[17] Raja, S. T. K., Thiruselvi, T., Aravindhan, R., Mandal, A. B., & Gnanamani, A. (2015). In vitro and in vivo assessments of a 3-(3, 4-dihydroxyphenyl)-2-propenoic acid bioconjugated gelatin-based injectable hydrogel for biomedical applications. Journal of Materials Chemistry B, 3(7), 1230-1244. https://doi.org/10.1039/C4TB01196A

[18] Liu, Y., Ng, S. C., Yu, J., & Tsai, W. B. (2019). Modification and crosslinking of gelatin-based biomaterials as tissue adhesives. Colloids and Surfaces B: Biointerfaces, 174, 316-323. https://doi.org/10.1016/j.colsurfb.2018.10.077

[19] Xing, Y., Qing, X., Xia, H., Hao, S., Zhu, H., He, Y., ... & Gu, Z. (2021). Injectable hydrogel based on modified gelatin and sodium alginate for soft-tissue adhesive. Frontiers in Chemistry, 656. https://doi.org/10.3389/fchem.2021.744099

[20] Roberts, A. D., Finnigan, W., Kelly, P. P., Faulkner, M., Breitling, R., Takano, E., ... & Hay, S. (2020). Non-covalent protein-based adhesives for transparent substrates—bovine serum albumin vs. recombinant spider silk. Materials Today Bio, 7, 100068. https://doi.org/10.1016/j.mtbio.2020.100068

[21] Zhu, W., Peck, Y., Iqbal, J., & Wang, D. A. (2017). A novel DOPA-albumin based tissue adhesive for internal medical applications. Biomaterials, 147, 99-115. https://doi.org/10.1016/j.biomaterials.2017.09.016

[22] Li, D., Chen, J., Wang, X., Zhang, M., Li, C., & Zhou, J. (2020). Recent advances on synthetic and polysaccharide adhesives for biological hemostatic applications. Frontiers in Bioengineering and Biotechnology, 8, 926. https://doi.org/10.3389/fbioe.2020.00926

[23] He, X. Y., Sun, A., Li, T., Qian, Y. J., Qian, H., Ling, Y. F., ... & Qian, Z. (2020). Mussel-inspired antimicrobial gelatin/chitosan tissue adhesive rapidly activated in situ by H2O2/ascorbic acid for infected wound closure. Carbohydrate polymers, 247, 116692. https://doi.org/10.1016/j.carbpol.2020.116692

[24] Du, X., Liu, Y., Yan, H., Rafique, M., Li, S., Shan, X., ... & Wang, L. (2020). Anti-infective and pro-coagulant chitosan-based hydrogel tissue adhesive for sutureless wound closure. Biomacromolecules, 21(3), 1243-1253. https://doi.org/10.1021/acs.biomac.9b01707

[25] Lee, K. Y., & Mooney, D. J. (2012). Alginate: properties and biomedical applications. Progress in polymer science, 37(1), 106-126. https://doi.org/10.1016/j.progpolymsci.2011.06.003

[26] Kazi, G. A., & Yamamoto, O. (2019). Effectiveness of the sodium alginate as surgical sealant materials. Wound Medicine, 24(1), 18-23. https://doi.org/10.1016/j.wndm.2019.02.001

[27] Abka-Khajouei, R., Tounsi, L., Shahabi, N., Patel, A. K., Abdelkafi, S., & Michaud, P. (2022). Structures, properties and applications of alginates. Marine Drugs, 20(6), 364. https://doi.org/10.3390/md20060364

[28] Xia, L., Huang, H., Fan, Z., Hu, D., Zhang, D., Khan, A. S., ... & Pan, L. (2019). Hierarchical macro-/meso-/microporous oxygen-doped carbon derived from sodium alginate: A cost-effective biomass material for binder-free supercapacitors. Materials & Design, 182, 108048. https://doi.org/10.1016/j.matdes.2019.108048

[29] Abourehab, M. A., Rajendran, R. R., Singh, A., Pramanik, S., Shrivastav, P., Ansari, M. J., ... & Deepak, A. (2022). Alginate as a promising biopolymer in drug delivery and wound healing: A review of the state-of-the-art. International Journal of Molecular Sciences, 23(16), 9035. https://doi.org/10.3390/ijms23169035

[30] Frent, O. D., Vicas, L. G., Duteanu, N., Morgovan, C. M., Jurca, T., Pallag, A., ... & Marian, E. (2022). Sodium alginate—Natural microencapsulation material of polymeric microparticles. International Journal of Molecular Sciences, 23(20), 12108. https://doi.org/10.3390/ijms232012108

[31] Aderibigbe, B. A., & Buyana, B. (2018). Alginate in wound dressings. Pharmaceutics, 10(2), 42. https://doi.org/10.3390/pharmaceutics10020042

[32] Beltran-Vargas, N. E., Peña-Mercado, E., Sánchez-Gómez, C., Garcia-Lorenzana, M., Ruiz, J. C., Arroyo-Maya, I., ... & Campos-Terán, J. (2022). Sodium alginate/chitosan scaffolds for cardiac tissue engineering: The influence of its three-dimensional material preparation and the use of gold nanoparticles. Polymers, 14(16), 3233. https://doi.org/10.3390/polym14163233

[33] Wang, T., Zhang, F., Zhao, R., Wang, C., Hu, K., Sun, Y., ... & Nie, L. (2020). Polyvinyl alcohol/sodium alginate hydrogels incorporated with silver nanoclusters via green tea extract for antibacterial applications. Designed monomers and polymers, 23(1), 118-133. https://doi.org/10.1080/15685551.2020.1804183

[34] Bai, Z., Dan, W., Yu, G., Wang, Y., Chen, Y., Huang, Y., ... & Dan, N. (2018). Tough and tissue-adhesive polyacrylamide/collagen hydrogel with dopamine-grafted oxidized sodium alginate as crosslinker for cutaneous wound healing. RSC advances, 8(73), 42123-42132. DOI: 10.1039/C8RA07697A

[35] Suneetha, M., Rao, K. M., & Han, S. S. (2019). Mussel-inspired cell/tissue-adhesive, hemostatic hydrogels for tissue engineering applications. ACS omega, 4(7), 12647-12656. https://doi.org/10.1021/acsomega.9b01302

[36] Charron, P. N., Fenn, S. L., Poniz, A., & Floreani, R. (2016). Mechanical properties and failure analysis of visible light crosslinked alginate-based tissue sealants. Journal of the mechanical behavior of biomedical materials, 59, 314-321. https://doi.org/10.1016/j.jmbbm.2016.02.003

[37] Kim, J., Lee, C., & Ryu, J. H. (2020). Adhesive catechol-conjugated hyaluronic acid for biomedical applications: A mini review. Applied Sciences, 11(1), 21. https://doi.org/10.3390/app11010021

[38] Zhou, D., Li, S., Pei, M., Yang, H., Gu, S., Tao, Y., ... & Xiao, P. (2020). Dopamine-modified hyaluronic acid hydrogel adhesives with fast-forming and high tissue adhesion. ACS applied materials & interfaces, 12(16), 18225-18234. https://doi.org/10.1021/acsami.9b22120

[39] Zhang, X., Jiang, Y., Han, L., & Lu, X. (2021). Biodegradable polymer hydrogel-based tissue adhesives: A review. Biosurface and Biotribology, 7(4), 163-179. https://doi.org/10.1049/bsb2.12016

[40] Lu, S., Zhang, X., Tang, Z., Xiao, H., Zhang, M., Liu, K., ... & Wu, H. (2021). Mussel-inspired blue-light-activated cellulose-based adhesive hydrogel with fast gelation, rapid haemostasis and antibacterial property for wound healing. Chemical Engineering Journal, 417, 129329. https://doi.org/10.1016/j.cej.2021.129329

[41] Suneetha, M., Moo, O. S., Choi, S. M., Zo, S., Rao, K. M., & Han, S. S. (2021). Tissue-adhesive, stretchable, and self-healable hydrogels based on carboxymethyl cellulose-dopamine/PEDOT: PSS via mussel-inspired chemistry for bioelectronic applications. Chemical Engineering Journal, 426, 130847. https://doi.org/10.1016/j.cej.2021.130847

[42] Kwon, H. J., & Han, Y. (2016). Chondroitin sulfate-based biomaterials for tissue engineering. Turkish Journal of Biology, 40(2), 290-299.doi: 10.3906/biy-1507-16

[43] Jiang, X., Liu, J., Liu, Q., Lu, Z., Zheng, L., Zhao, J., & Zhang, X. (2018). Therapy for cartilage defects: functional ectopic cartilage constructed by cartilage-simulating collagen, chondroitin sulfate and hyaluronic acid (CCH) hybrid hydrogel with allogeneic chondrocytes. Biomaterials science, 6(6), 1616-1626. https://doi.org/10.1039/C8BM00354H

[44] Shin, J., Kang, E. H., Choi, S., Jeon, E. J., Cho, J. H., Kang, D., ... & Cho, S. W. (2021). Tissue-adhesive chondroitin sulfate hydrogel for cartilage reconstruction. ACS Biomaterials Science & Engineering, 7(9), 4230-4243. https://doi.org/10.1021/acsbiomaterials.0c01414

[45] Koivisto, L. (2022). ADHESION MECHANISMS OF NATURAL SYNTEHTIC TISSUE ADHESIVE HYDROGELS.

[46] Yang, W., Kang, X., Gao, X., Zhuang, Y., Fan, C., Shen, H., ... & Dai, J. (2023). Biomimetic Natural Biopolymer-Based Wet-Tissue Adhesive for Tough Adhesion, Seamless Sealed, Emergency/Nonpressing Hemostasis, and Promoted Wound Healing. Advanced Functional Materials, 33(6), 2211340. https://doi.org/10.1002/adfm.202211340

[47] Cui, C., & Liu, W. (2021). Recent advances in wet adhesives: Adhesion mechanism, design principle and applications. Progress in Polymer Science, 116, 101388. https://doi.org/10.1016/j.progpolymsci.2021.101388

[48] Waite, J. H., Andersen, N. H., Jewhurst, S., & Sun, C. (2005). Mussel adhesion: finding the tricks worth mimicking. The journal of adhesion, 81(3-4), 297-317. https://doi.org/10.1080/00218460590944602

[49] Lee, B. P., Messersmith, P. B., Israelachvili, J. N., & Waite, J. H. (2011). Mussel-inspired adhesives and coatings. Annual review of materials research, 41, 99-132. https://doi.org/10.1146/annurev-matsci-062910-100429

[50] Floriolli, R. Y., von Langen, J., & Waite, J. H. (2000). Marine surfaces and the expression of specific byssal adhesive protein variants in Mytilus. Marine Biotechnology, 2, 352-363. https://doi.org/10.1007/s101269900032

[51] Priemel, T., Degtyar, E., Dean, M. N., & Harrington, M. J. (2017). Rapid self-assembly of complex biomolecular architectures during mussel byssus biofabrication. Nature communications, 8(1), 14539. https://doi.org/10.1038/ncomms14539

[52] Guo, Q., Chen, J., Wang, J., Zeng, H., & Yu, J. (2020). Recent progress in synthesis and application of mussel-inspired adhesives. Nanoscale, 12(3), 1307-1324. https://doi.org/10.1039/C9NR09780E

[53] Han, L., Lu, X., Liu, K., Wang, K., Fang, L., Weng, L. T., ... & Li, Z. (2017). Mussel-inspired adhesive and tough hydrogel based on nanoclay confined dopamine polymerization. ACS nano, 11(3), 2561-2574. https://doi.org/10.1021/acsnano.6b05318

[54] Nicklisch, S. C., & Waite, J. H. (2012). Mini-review: The role of redox in Dopa-mediated marine adhesion. Biofouling, 28(8), 865-877. https://doi.org/10.1080/08927014.2012.719023

[55] Wang, C. S., & Stewart, R. J. (2013). Multipart copolyelectrolyte adhesive of the sandcastle worm, Phragmatopoma californica (Fewkes): catechol oxidase catalyzed curing through peptidyl-DOPA. Biomacromolecules, 14(5), 1607-1617. https://doi.org/10.1021/bm400251k

[56]Choi, Y. C., Choi, J. S., Jung, Y. J., & Cho, Y. W. (2014). Human gelatin tissue-adhesive hydrogels prepared by enzyme-mediated biosynthesis of DOPA and Fe 3+ ion crosslinking. Journal of Materials Chemistry B, 2(2), 201-209. https://doi.org/10.1039/C3TB20696C

[57] Zhu, W. (2018). Novel dopa-functionalized bioadhesives for internal medical applications (Doctoral dissertation). DOI:10.32657/10220/46630

[58] Pal, K., Banthia, A. K., & Majumdar, D. K. (2009). Polymeric hydrogels: characterization and biomedical applications. Designed monomers and polymers, 12(3), 197-220. https://doi.org/10.1163/156855509X436030

[59] Mandal, A., Clegg, J. R., Anselmo, A. C., & Mitragotri, S. (2020). Hydrogels in the clinic. Bioengineering & translational medicine, 5(2), e10158. https://doi.org/10.1002/btm2.10158

[60] Xu, F., Dawson, C., Lamb, M., Mueller, E., Stefanek, E., Akbari, M., & Hoare, T. (2022). Hydrogels for tissue engineering: Addressing key design needs toward clinical

translation. Frontiers in Bioengineering and Biotechnology, 10, 849831. https://doi.org/10.3389/fbioe.2022.849831

[61] Ma, S., Yu, B., Pei, X., & Zhou, F. (2016). Structural hydrogels. Polymer, 98, 516-535. https://doi.org/10.1016/j.polymer.2016.06.053

[62] Parhi, R. (2017). Cross-linked hydrogel for pharmaceutical applications: A review. Advanced pharmaceutical bulletin, 7(4), 515-530. doi: 10.15171/apb.2017.064

[63] Hu, W., Wang, Z., Xiao, Y., Zhang, S., & Wang, J. (2019). Advances in crosslinking strategies of biomedical hydrogels. Biomaterials science, 7(3), 843-855.

DOI: 10.1039/C8BM01246F

[64] Wu, Y., Chen, Y. X., Yan, J., Quinn, D., Dong, P., Sawyer, S. W., & Soman, P. (2016). Fabrication of conductive gelatin methacrylate–polyaniline hydrogels. Acta biomaterialia, 33, 122-130. https://doi.org/10.1016/j.actbio.2016.01.036

[65] Kaur, G., Adhikari, R., Cass, P., Bown, M., & Gunatillake, P. (2015). Electrically conductive polymers and composites for biomedical applications. Rsc Advances, 5(47), 37553-37567. DOI: 10.1039/C5RA01851J

[66] Xu, J., Tsai, Y. L., & Hsu, S. H. (2020). Design strategies of conductive hydrogel for biomedical applications. Molecules, 25(22), 5296. https://doi.org/10.3390/molecules25225296

[67] Li, L., Wang, Y., Pan, L., Shi, Y., Cheng, W., Shi, Y., & Yu, G. (2015). A nanostructured conductive hydrogels-based biosensor platform for human metabolite detection. Nano letters, 15(2), 1146-1151. https://doi.org/10.1021/nl504217p

[68] Indermun, S., Choonara, Y. E., Kumar, P., du Toit, L. C., Modi, G., Luttge, R., & Pillay, V. (2014). An interfacially plasticized electro-responsive hydrogel for transdermal electro-activated and modulated (TEAM) drug delivery. International journal of pharmaceutics, 462(1-2), 52-65. https://doi.org/10.1016/j.ijpharm.2013.11.014

[69] Baei, P., Jalili-Firoozinezhad, S., Rajabi-Zeleti, S., Tafazzoli-Shadpour, M., Baharvand, H., & Aghdami, N. (2016). Electrically conductive gold nanoparticle-chitosan thermosensitive hydrogels for cardiac tissue engineering. Materials Science and Engineering: C, 63, 131-141. https://doi.org/10.1016/j.msec.2016.02.056

[70] Yang, S., Jang, L., Kim, S., Yang, J., Yang, K., Cho, S. W., & Lee, J. Y. (2016). Polypyrrole/alginate hybrid hydrogels: electrically conductive and soft biomaterials for human mesenchymal stem cell culture and potential neural tissue engineering applications. Macromolecular Bioscience, 16(11), 1653-1661. https://doi.org/10.1002/mabi.201600148

[71] Raus, R. A., Nawawi, W. M. F. W., & Nasaruddin, R. R. (2021). Alginate and alginate composites for biomedical applications. *Asian Journal of Pharmaceutical Sciences*, *16*(3), 280-306. https://doi.org/10.1016/j.ajps.2020.10.001

[72] Grzeszczuk, M. (2018). Polymer Electrodes: Preparation, Properties, and Applications. DOI:10.1016/B978-0-12-409547-2.11676-2

[73] Benseddik, E., Makhlouki, M., Bernede, J. C., Lefrant, S., & Proń, A. (1995). XPS studies of environmental stability of polypyrrole-poly (vinyl alcohol) composites. Synthetic Metals, 72(3), 237-242. https://doi.org/10.1016/0379-6779(95)03285-1

[74] Deshmukh, K., Ahamed, M. B., Deshmukh, R. R., Pasha, S. K., Bhagat, P. R., & Chidambaram, K. (2017). Biopolymer composites with high dielectric performance: interface engineering. In Biopolymer composites in electronics (pp. 27-128). Elsevier. https://doi.org/10.1016/B978-0-12-809261-3.00003-6

[75] Harlin, A., & Ferenets, M. (2006). Introduction to conductive materials. In Intelligent textiles and clothing. Woodhed Puhlishing in Textiles (pp. 217-237). https://doi.org/10.1533/9781845691622.3.217

[76] Cetiner, S., Kalaoglu, F., Karakas, H., & Sarac, A. S. (2010). Electrospun nanofibers of polypyrrole-poly (acrylonitrile-co-vinyl acetate). Textile research journal, 80(17), 1784-1792. https://doi.org/10.1177/0040517510365953

[77] Torrent-Guasp, F., Kocica, M. J., Corno, A. F., Komeda, M., Carreras-Costa, F., Flotats, A., ... & Wen, H. (2005). Towards new understanding of the heart structure and function. European journal of cardio-thoracic surgery, 27(2), 191-201.https://doi.org/10.1016/j.ejcts.2004.11.026

[78] Klein, I., & Danzi, S. (2007). Thyroid disease and the heart. Circulation, 116(15), 1725-1735. https://doi.org/10.1161/CIRCULATIONAHA.106.678326

[79] Fukuta, H., & Little, W. C. (2008). The cardiac cycle and the physiologic basis of left ventricular contraction, ejection, relaxation, and filling. Heart failure clinics, 4(1), 1-11. https://doi.org/10.1016/j.hfc.2007.10.004

[80] Nibhoria, S., Jhajj, K. K., Nibhoria, V. K., Sandhu, S. K., Bamra, N. S., & Padda, P. (2013). A case study-Role of heart autopsy in evaluating the cause of death. Indian journal of forensic medicine & Toxicology, 7(1), 72.

[81] Rodriguez, E. R., & Tan, C. D. (2017). Structure and anatomy of the human pericardium. Progress in cardiovascular diseases, 59(4), 327-340. https://doi.org/10.1016/j.pcad.2016.12.010

[82] Whitaker, R. H. (2010). Anatomy of the heart. Medicine, 38(7), 333-335.

https://doi.org/10.1016/j.mpmed.2010.04.005

[83] Anderson, R. H., Spicer, D. E., Brown, N. A., & Mohun, T. J. (2014). The development of septation in the four-chambered heart. The Anatomical Record, 297(8), 1414-1429. https://doi.org/10.1002/ar.22949

[84] Naeije, R. (2013). Physiology of the pulmonary circulation and the right heart. Current hypertension reports, 15(6), 623-631. https://doi.org/10.1007/s11906-013-0396-6

[85] Piersanti, R. (2022). Mathematical and numerical modeling of cardiac fiber generation and electromechanical function: towards a realistic simulation of the whole heart. DOI:10.13140/RG.2.2.32187.08485

[86] Mahadevan, V. (2018). Anatomy of the heart. Surgery (Oxford), 36(2), 43-47. (https://doi.org/10.1016/j.mpsur.2017.11.010) .

[87] Kroeker, C. G. (2018). Cardiovascular system: anatomy and physiology. Cardiovascular Mechanics, 2(5), 1.

[88] Tortora, G. J., & Derrickson, B. H. (2018). Principles of anatomy and physiology. John Wiley & Sons.

[89] Padala, S. K., Cabrera, J. A., & Ellenbogen, K. A. (2021). Anatomy of the cardiac conduction system. Pacing and Clinical Electrophysiology, 44(1), 15-25. https://doi.org/10.1111/pace.14107

[90] Kerckhoffs, R. C. P., Bovendeerd, P. H. M., Prinzen, F. W., Smits, K., & Arts, T. (2003). Intra-and interventricular asynchrony of electromechanics in the ventricularly paced heart. Journal of Engineering Mathematics, 47, 201-216. https://doi.org/10.1023/B:ENGI.0000007972.73874.da

[91] Sperelakis, N. I. C. H. O. L. A. S., Sunagawa, M. A. S. A. N. O. R. I., & Nakamura, M. A. R. I. K. O. (2001). Electrogenesis of the resting potential. In Heart physiology and pathophysiology (pp. 175-198). Academic Press San Diego.

[92] Heshmatzad, K., Naderi, N., Maleki, M., Abbasi, S., Ghasemi, S., Ashrafi, N., ... & Kalayinia, S. (2023). Role of non-coding variants in cardiovascular disease. Journal of Cellular and Molecular Medicine. https://doi.org/10.1111/jcmm.17762

[93] Cetin, Y., Sahin, M. G., & Kok, F. N. (2021). Application potential of three-dimensional silk fibroin scaffold using mesenchymal stem cells for cardiac regeneration. Journal of Biomaterials Applications, 36(4), 740-753. https://doi.org/10.1177/08853282211018529

[94] Carrier, R. L., Papadaki, M., Rupnick, M., Schoen, F. J., Bursac, N., Langer, R., ... & Vunjak-Novakovic, G. (1999). Cardiac tissue engineering: cell seeding, cultivation parameters, and tissue construct characterization. Biotechnology and bioengineering, 64(5), 580-589. https://doi.org/10.1002/(SICI)1097-0290(19990905)64:5<580::AID-BIT8>3.0.CO;2-X

[95] Erdal, Y., Seçkin, U. D., Kılıç, K. D., & Erbaş, O. (2017). Kardiyovasküler doku mühendisliği: Yaklaşımlar ve klinik öncesi uygulamalar. İstanbul Bilim Üniversitesi Florence Nightingale Transplantasyon Dergisi, 2(2), 74-78.

[96] Adel, I. M., ElMeligy, M. F., & Elkasabgy, N. A. (2022). Conventional and recent trends of scaffolds fabrication: a superior mode for tissue engineering. Pharmaceutics, 14(2), 306. https://doi.org/10.3390/pharmaceutics14020306

[97] Bitar, K. N., & Zakhem, E. (2014). Design strategies of biodegradable scaffolds for tissue regeneration. Biomedical engineering and computational biology, 6, BECB-S10961. https://doi.org/10.4137/BECB.S10961

[98] Mousaei Ghasroldasht, M., Seok, J., Park, H. S., Liakath Ali, F. B., & Al-Hendy, A. (2022). Stem cell therapy: from idea to clinical practice. International journal of molecular sciences, 23(5), 2850. https://doi.org/10.3390/ijms23052850

[99] Madonna, R., Van Laake, L. W., Botker, H. E., Davidson, S. M., De Caterina, R., Engel, F. B., ... & Sluijter, J. P. G. (2019). ESC Working Group on Cellular Biology of the Heart: Tissue Engineering and Cell-Based Therapies for Cardiac Repair in Ischemic Heart Disease and Heart Failure. Cardiovascular Research, 115(3), 488-500. DOI:10.1093/cvr/cvz010

[100] Severs, N. J. (2000). The cardiac muscle cell. Bioessays, 22(2), 188-199. https://doi.org/10.1002/(SICI)1521-1878(200002)22:2<188::AID-BIES10>3.0.CO;2-T

[101] Vunjak-Novakovic, G., Tandon, N., Godier, A., Maidhof, R., Marsano, A., Martens, T. P., & Radisic, M. (2010). Challenges in cardiac tissue engineering. Tissue Engineering Part B: Reviews, 16(2), 169-187. https://doi.org/10.1089/ten.teb.2009.0352

[102] Tenreiro, M. F., Louro, A. F., Alves, P. M., & Serra, M. (2021). Next generation of heart regenerative therapies: Progress and promise of cardiac tissue engineering. NPJ Regenerative Medicine, 6(1), 30. https://doi.org/10.1038/s41536-021-00140-4

[103] Zhang, J., Wilson, G. F., Soerens, A. G., Koonce, C. H., Yu, J., Palecek, S. P., ... & Kamp, T. J. (2009). Functional cardiomyocytes derived from human induced pluripotent stem cells. Circulation research, 104(4), e30-e41. https://doi.org/10.1161/CIRCRESAHA.108.192237

[104] Lakshmanan, R., Kumaraswamy, P., Krishnan, U. M., & Sethuraman, S. (2016). Engineering a growth factor embedded nanofiber matrix niche to promote vascularization for functional cardiac regeneration. Biomaterials, 97, 176-195. https://doi.org/10.1016/j.biomaterials.2016.02.033

[105] Stoppel, W. L., Kaplan, D. L., & Black III, L. D. (2016). Electrical and mechanical stimulation of cardiac cells and tissue constructs. Advanced drug delivery reviews, 96, 135-155. https://doi.org/10.1016/j.addr.2015.07.009

[106] Mancuso, A., Barone, A., Cristiano, M. C., Cianflone, E., Fresta, M., & Paolino, D. (2020). Cardiac stem cell-loaded delivery systems: A new challenge for myocardial tissue regeneration. International Journal of Molecular Sciences, 21(20), 7701. https://doi.org/10.3390/ijms21207701

[107] McMahan, S., Taylor, A., Copeland, K. M., Pan, Z., Liao, J., & Hong, Y. (2020). Current advances in biodegradable synthetic polymer based cardiac patches. Journal of Biomedical Materials Research Part A, 108(4), 972-983. https://doi.org/10.1002/jbm.a.36874

[108] Sharma, D., Ferguson, M., Kamp, T. J., & Zhao, F. (2019). Constructing biomimetic cardiac tissues: a review of scaffold materials for engineering cardiac patches. Emergent materials, 2, 181-191. https://doi.org/10.1007/s42247-019-00046-4

[109] Mohammadi Nasr, S., Rabiee, N., Hajebi, S., Ahmadi, S., Fatahi, Y., Hosseini, M., ... & Webster, T. J. (2020). Biodegradable nanopolymers in cardiac tissue engineering: From concept towards nanomedicine. International Journal of Nanomedicine, 4205-4224. doi: 10.2147/IJN.S245936

[110] Reis, L. A., Chiu, L. L., Feric, N., Fu, L., & Radisic, M. (2016). Biomaterials in myocardial tissue engineering. Journal of tissue engineering and regenerative medicine, 10(1), 11-28. https://doi.org/10.1002/term.1944

[111] Spearman, B. S., Hodge, A. J., Porter, J. L., Hardy, J. G., Davis, Z. D., Xu, T., ... & Lipke, E. A. (2015). Conductive interpenetrating networks of polypyrrole and polycaprolactone encourage electrophysiological development of cardiac cells. Acta biomaterialia, 28, 109-120. https://doi.org/10.1016/j.actbio.2015.09.025

[112] Liu, Y., Xu, Y., Wang, Z., Wen, D., Zhang, W., Schmull, S., ... & Xue, S. (2016). Electrospun nanofibrous sheets of collagen/elastin/polycaprolactone improve cardiac repair after myocardial infarction. American journal of translational research, 8(4), 1678.

[113] Sant, S., Hwang, C. M., Lee, S. H., & Khademhosseini, A. (2011). Hybrid PGS–PCL microfibrous scaffolds with improved mechanical and biological properties. Journal of tissue engineering and regenerative medicine, 5(4), 283-291. https://doi.org/10.1002/term.313

[114] Marsano, A., Maidhof, R., Luo, J., Fujikara, K., Konofagou, E. E., Banfi, A., & Vunjak-Novakovic, G. (2013). The effect of controlled expression of VEGF by transduced myoblasts in a cardiac patch on vascularization in a mouse model of myocardial infarction. Biomaterials, 34(2), 393-401. https://doi.org/10.1016/j.biomaterials.2012.09.038

[115] Zhou, Q., Zhou, J. Y., Zheng, Z., Zhang, H., & Hu, S. S. (2010). A novel vascularized patch enhances cell survival and modifies ventricular remodeling in a rat myocardial infarction model. The Journal of Thoracic and Cardiovascular Surgery, 140(6), 1388-1396. https://doi.org/10.1016/j.jtcvs.2010.02.036

[116] Morais, J. M., Papadimitrakopoulos, F., & Burgess, D. J. (2010). Biomaterials/tissue interactions: possible solutions to overcome foreign body response. The AAPS journal, 12, 188-196. https://doi.org/10.1208/s12248-010-9175-3

[117] Majid, Q. A., Fricker, A. T., Gregory, D. A., Davidenko, N., Hernandez Cruz, O., Jabbour, R. J., ... & Roy, I. (2020). Natural biomaterials for cardiac tissue engineering: a highly biocompatible solution. Frontiers in cardiovascular medicine, 192. https://doi.org/10.3389/fcvm.2020.554597

[118] Sun, J., & Tan, H. (2013). Alginate-based biomaterials for regenerative medicine applications. Materials, 6(4), 1285-1309. https://doi.org/10.3390/ma6041285

[119] Rioux, Y., Fradette, J., Maciel, Y., Bégin-Drolet, A., & Ruel, J. (2022). Biofabrication of sodium alginate hydrogel scaffolds for heart valve tissue engineering. International Journal of Molecular Sciences, 23(15), 8567. https://doi.org/10.3390/ijms23158567

[120] Rosellini, E., Cristallini, C., Barbani, N., Vozzi, G., & Giusti, P. (2009). Preparation and characterization of alginate/gelatin blend films for cardiac tissue engineering. Journal of Biomedical Materials Research Part A: An Official Journal of The Society for Biomaterials, The Japanese Society for Biomaterials, and The Australian Society for Biomaterials and the Korean Society for Biomaterials, 91(2), 447-453. https://doi.org/10.1002/jbm.a.32216

[121] Schussler, O., Coirault, C., Louis-Tisserand, M., Al-Chare, W., Oliviero, P., Menard, C., ... & Lecarpentier, Y. (2009). Use of arginine–glycine–aspartic acid adhesion peptides coupled with a new collagen scaffold to engineer a myocardium-like tissue graft. Nature Reviews Cardiology, 6(3), 240-249. https://doi.org/10.1038/ncpcardio1451

[122] Luo, J. W., Liu, C., Wu, J. H., Lin, L. X., Fan, H. M., Zhao, D. H., ... & Sun, Y. L. (2019). In situ injectable hyaluronic acid/gelatin hydrogel for hemorrhage control. Materials Science and Engineering: C, 98, 628-634. https://doi.org/10.1016/j.msec.2019.01.034

[123] Hong, Y., Zhou, F., Hua, Y., Zhang, X., Ni, C., Pan, D., ... & Ouyang, H. (2019). A strongly adhesive hemostatic hydrogel for the repair of arterial and heart bleeds. Nature communications, 10(1), 2060. https://doi.org/10.1038/s41467-019-10004-7

[124] Zhang, H., Zhao, T., Duffy, P., Dong, Y., Annaidh, A. N., O'Cearbhaill, E., & Wang, W. (2015). Hydrolytically degradable hyperbranched PEG-polyester adhesive with low swelling and robust mechanical properties. Advanced healthcare materials, 4(15), 2260-2268. https://doi.org/10.1002/adhm.201500406

[125] Bhagat, V., & Becker, M. L. (2017). Degradable adhesives for surgery and tissue engineering. Biomacromolecules, 18(10), 3009-3039. https://doi.org/10.1021/acs.biomac.7b00969

[126] Dahlmann, J., Krause, A., Möller, L., Kensah, G., Möwes, M., Diekmann, A., ... & Dräger, G. (2013). Fully defined in situ cross-linkable alginate and hyaluronic acid hydrogels for myocardial tissue engineering. Biomaterials, 34(4), 940-951. https://doi.org/10.1016/j.biomaterials.2012.10.008

[127] Reakasame, S., & Boccaccini, A. R. (2018). Oxidized alginate-based hydrogels for tissue engineering applications: a review. Biomacromolecules, 19(1), 3-21. https://doi.org/10.1021/acs.biomac.7b01331

[128] Farshidfar, N., Iravani, S., & Varma, R. S. (2023). Alginate-Based Biomaterials in Tissue Engineering and Regenerative Medicine. Marine Drugs, 21(3), 189. https://doi.org/10.3390/md21030189

[129] Mousavi, A., Mashayekhan, S., Baheiraei, N., & Pourjavadi, A. (2021). Biohybrid oxidized alginate/myocardial extracellular matrix injectable hydrogels with improved electromechanical properties for cardiac tissue engineering. International Journal of Biological Macromolecules, 180, 692-708. https://doi.org/10.1016/j.ijbiomac.2021.03.097

[130] Ivey, M. J., & Tallquist, M. D. (2016). Defining the cardiac fibroblast. Circulation Journal, 80(11), 2269-2276. doi: 10.1253/circj.CJ-16-1003

[131] Souders, C. A., Bowers, S. L., & Baudino, T. A. (2009). Cardiac fibroblast: the renaissance cell. Circulation research, 105(12), 1164-1176. doi:10.1161/CIRCRESAHA.109.209809

[132] Witek, P., Korga, A., Burdan, F., Ostrowska, M., Nosowska, B., Iwan, M., & Dudka, J. (2016). The effect of a number of H9C2 rat cardiomyocytes passage on repeatability of cytotoxicity study results. Cytotechnology, 68, 2407-2415. https://doi.org/10.1007/s10616-016-9957-2

[133] Jeon, O., Alt, D. S., Ahmed, S. M., & Alsberg, E. (2012). The effect of oxidation on the degradation of photocrosslinkable alginate hydrogels. Biomaterials, 33(13), 3503-3514. https://doi.org/10.1016/j.biomaterials.2012.01.041

[134] Torkay, G. (2023). Conductive, self-healing, injectable hydrogel tissue scaffolds for use in neural tissue engineering (Master's thesis). [Istinye University], [Istanbul, Turkey].

[135] Song, C. K., Kim, M. K., Lee, J., Davaa, E., Baskaran, R., & Yang, S. G. (2019). Dopa-empowered Schiff base forming alginate hydrogel glue for rapid hemostatic control. Macromolecular Research, 27(2), 119-125. DOI 10.1007/s13233-019-7026-3

[136] Nichol, J. W., Koshy, S. T., Bae, H., Hwang, C. M., Yamanlar, S., & Khademhosseini, A. (2010). Cell-laden microengineered gelatin methacrylate hydrogels. Biomaterials, 31(21), 5536-5544. https://doi.org/10.1016/j.biomaterials.2010.03.064

[137]Kale, R. N., & Bajaj, A. N. (2010). Ultraviolet spectrophotometric method for determination of gelatin crosslinking in the presence of amino groups. Journal of Young Pharmacists, 2(1), 90-94. https://doi.org/10.4103/0975-1483.62223

[138] Bal-Öztürk, A., Torkay, G., İdil, N., Özkahraman, B., & Özbaş, Z. (2023). Gellan gum/guar gum films incorporated with honey as potential wound dressings. Polymer Bulletin, 1-18. https://doi.org/10.1007/s00289-023-04763-z

[139] Murdock, M. H., Chang, J. T., Luketich, S. K., Pedersen, D., Hussey, G. S., D'Amore, A., & Badylak, S. F. (2019). Cytocompatibility and mechanical properties of surgical sealants for cardiovascular applications. The Journal of thoracic and cardiovascular surgery, 157(1), 176-183. https://doi.org/10.1016/j.jtcvs.2018.08.043

[140]Tutar, R., Yüce-Erarslan, E., İzbudak, B., & Bal-Öztürk, A. (2022). Photocurable silk fibroin-based tissue sealants with enhanced adhesive properties for the treatment of

corneal perforations. Journal of Materials Chemistry B, 10(15), 2912-2925. https://doi.org/10.1039/D1TB02502C

[141] Zheng, K., Gu, Q., Zhou, D., Zhou, M., & Zhang, L. (2022). Recent progress in surgical adhesives for biomedical applications. Smart Materials in Medicine, 3, 41-65. https://doi.org/10.1016/j.smaim.2021.11.004

[142] Bartlett, M. D., Case, S. W., Kinloch, A. J., & Dillard, D. A. (2023). Peel tests for quantifying adhesion and toughness: A review. Progress in Materials Science, 101086. https://doi.org/10.1016/j.pmatsci.2023.101086

[143] Huang, H., Xu, R., Ni, P., Zhang, Z., Sun, C., He, H., ... & Liu, H. (2022). Water-driven noninvasively detachable wet tissue adhesives for wound closure. Materials Today Bio, 16, 100369. https://doi.org/10.1016/j.mtbio.2022.100369

[144] Javadi, M., Gu, Q., Naficy, S., Farajikhah, S., Crook, J. M., Wallace, G. G., ... & Moulton, S. E. (2018). Conductive tough hydrogel for bioapplications. Macromolecular bioscience, 18(2), 1700270. https://doi.org/10.1002/mabi.201700270

[145] Bal-Öztürk, A., Torkay, G., Alarçin, E., Özbaş, Z., & Özkahraman, B. (2022). The effect of thiol functional groups on bovine serum albumin/chitosan buccal mucoadhesive patches. Journal of Drug Delivery Science and Technology, 74, 103493. https://doi.org/10.1016/j.jddst.2022.103493

[146] Rosiak, P., Latanska, I., Paul, P., Sujka, W., & Kolesinska, B. (2021). Modification of alginates to modulate their physic-chemical properties and obtain biomaterials with different functional properties. Molecules, 26(23), 7264. doi: 10.3390/molecules26237264

[147] Gomez, C. G., Rinaudo, M., & Villar, M. A. (2007). Oxidation of sodium alginate and characterization of the oxidized derivatives. Carbohydrate Polymers, 67(3), 296-304. https://doi.org/10.1016/j.carbpol.2006.05.025

[148] Wang, Y., Wang, X., Liu, X., Niu, C., Yu, G., Hou, Y., ... & Shi, J. (2023). Fabrication, characterization and potential application of biodegradable polydopamine-modified scaffolds based on natural macromolecules. International Journal of Biological Macromolecules, 253, 126596. https://doi.org/10.1016/j.ijbiomac.2023.126596

[149] Ren, H., Zhang, Z., Chen, X., & He, C. (2023). Stimuli-responsive Hydrogel Adhesives for Wound Closure and Tissue Regeneration. Macromolecular Bioscience, 2300379. https://doi.org/10.1002/mabi.202300379

[150] Hasany, M., Talebian, S., Sadat, S., Ranjbar, N., Mehrali, M., Wallace, G. G., & Mehrali, M. (2021). Synthesis, properties, and biomedical applications of alginate methacrylate (ALMA)-based hydrogels: Current advances and challenges. Applied Materials Today, 24, 101150. https://doi.org/10.1016/j.apmt.2021.101150

[151] Xu, H., Casillas, J., Krishnamoorthy, S., & Xu, C. (2020). Effects of Irgacure 2959 and lithium phenyl-2, 4, 6-trimethylbenzoylphosphinate on cell viability, physical properties, and microstructure in 3D bioprinting of vascular-like constructs. Biomedical Materials, 15(5), 055021. doi: 10.1088/1748-605X/ab954e.

[152] Tomal, W., & Ortyl, J. (2020). Water-soluble photoinitiators in biomedical applications. Polymers, 12(5), 1073. https://doi.org/10.3390/polym12051073

[153] Yin, J., Liu, Q., Zhou, J., Zhang, L., Zhang, Q., Rao, R., ... & Jiao, T. (2020). Self-assembled functional components-doped conductive polypyrrole composite hydrogels with enhanced electrochemical performances. RSC advances, 10(18), 10546-10551. DOI: 10.1039/D0RA00102C

[154] Nada, A. A., Eckstein Andicsová, A., & Mosnáček, J. (2022). Irreversible and self-healing electrically conductive hydrogels made of bio-based polymers. International Journal of Molecular Sciences, 23(2), 842. https://doi.org/10.3390/ijms23020842

[155] Song, C. K., Kim, M. K., Lee, J., Davaa, E., Baskaran, R., & Yang, S. G. (2019). Dopa-empowered Schiff base forming alginate hydrogel glue for rapid hemostatic control. Macromolecular Research, 27(2), 119-125. DOI 10.1007/s13233-019-7026-3

[156] Gómez-Ordóñez, E., & Rupérez, P. (2011). FTIR-ATR spectroscopy as a tool for polysaccharide identification in edible brown and red seaweeds. Food hydrocolloids, 25(6), 1514-1520. https://doi.org/10.1016/j.foodhyd.2011.02.009

[157] Emami, Z., Ehsani, M., Zandi, M., & Foudazi, R. (2018). Controlling alginate oxidation conditions for making alginate-gelatin hydrogels. Carbohydrate polymers, 198, 509-517. https://doi.org/10.1016/j.carbpol.2018.06.080

[158] Araiza-Verduzco, F., Rodríguez-Velázquez, E., Cruz, H., Rivero, I. A., Acosta-Martínez, D. R., Pina-Luis, G., & Alatorre-Meda, M. (2020). Photocrosslinked alginate-methacrylate hydrogels with modulable mechanical properties: Effect of the molecular conformation and electron density of the methacrylate reactive group. Materials, 13(3), 534.https://doi.org/10.3390/ma13030534

[159] Manzari-Tavakoli, A., Tarasi, R., Sedghi, R., Moghimi, A., & Niknejad, H. (2020). Fabrication of nanochitosan incorporated polypyrrole/alginate conducting scaffold for neural tissue engineering. Scientific reports, 10(1), 22012. https://doi.org/10.1038/s41598-020-78650-2

[160] Yue, K., Trujillo-de Santiago, G., Alvarez, M. M., Tamayol, A., Annabi, N., & Khademhosseini, A. (2015). Synthesis, properties, and biomedical applications of gelatin methacryloyl (GelMA) hydrogels. Biomaterials, 73, 254-271. https://doi.org/10.1016/j.biomaterials.2015.08.045

[161] Mamaghani, K. R., Naghib, S. M., Zahedi, A., & Mozafari, M. (2018). Synthesis and microstructural characterization of GelMa/PEGDA hybrid hydrogel containing graphene oxide for biomedical purposes. Materials Today: Proceedings, 5(7), 15635-15644. https://doi.org/10.1016/j.matpr.2018.04.173

[162] Usal, T. D., Yucel, D., & Hasirci, V. (2019). A novel GelMA-pHEMA hydrogel nerve guide for the treatment of peripheral nerve damages. International journal of biological macromolecules, 121, 699-706. https://doi.org/10.1016/j.ijbiomac.2018.10.060

[163] Fonseca, D. F., Costa, P. C., Almeida, I. F., Dias-Pereira, P., Correia-Sá, I., Bastos, V., ... & Freire, C. S. (2020). Swellable gelatin methacryloyl microneedles for extraction of interstitial skin fluid toward minimally invasive monitoring of urea. Macromolecular Bioscience, 20(10), 2000195. https://doi.org/10.1002/mabi.202000195

[164] Yoon, H. J., Shin, S. R., Cha, J. M., Lee, S. H., Kim, J. H., Do, J. T., ... & Bae, H. (2016). Cold water fish gelatin methacryloyl hydrogel for tissue engineering application. PloS one, 11(10), e0163902. ttps://doi.org/10.1371/journal.pone.0163902

[165] Hassaballah, A. I., Hassan, M. A., Mardi, A. N., & Hamdi, M. (2013). An inverse finite element method for determining the tissue compressibility of human left ventricular wall during the cardiac cycle. PloS one, 8(12), e82703. https://doi.org/10.1371/journal.pone.0082703

[166] Pandey, N., Soto-Garcia, L. F., Liao, J., Zimmern, P., Nguyen, K. T., & Hong, Y. (2020). Mussel-inspired bioadhesives in healthcare: design parameters, current trends, and future perspectives. Biomaterials science, 8(5), 1240-1255.https://doi.org/10.1039/C9BM01848D

[167] Zhang, T., Yuk, H., Lin, S., Parada, G. A., & Zhao, X. (2017). Tough and tunable adhesion of hydrogels: experiments and models. Acta Mechanica Sinica, 33, 543-554. https://doi.org/10.1007/s10409-017-0661-z

[168] Kim, B. J., Oh, D. X., Kim, S., Seo, J. H., Hwang, D. S., Masic, A., ... & Cha, H. J. (2014). Mussel-mimetic protein-based adhesive hydrogel. Biomacromolecules, 15(5), 1579-1585. https://doi.org/10.1021/bm4017308

[169] Brubaker, C. E., & Messersmith, P. B. (2011). Enzymatically degradable mussel-inspired adhesive hydrogel. Biomacromolecules, 12(12), 4326-4334. https://doi.org/10.1021/bm201261d

[170] Hong, Y., Zhou, F., Hua, Y., Zhang, X., Ni, C., Pan, D., ... & Ouyang, H. (2019). A strongly adhesive hemostatic hydrogel for the repair of arterial and heart bleeds. Nature communications, 10(1), 2060. https://doi.org/10.1038/s41467-019-10004-7

[171] Ruiz, A., Lucherelli, M. A., Murera, D., Lamon, D., Ménard-Moyon, C., & Bianco, A. (2020). Toxicological evaluation of highly water dispersible few-layer graphene in vivo. Carbon, 170, 347-360. https://doi.org/10.1016/j.carbon.2020.08.023

APPENDIX 1: PLAGIARISM REPORT

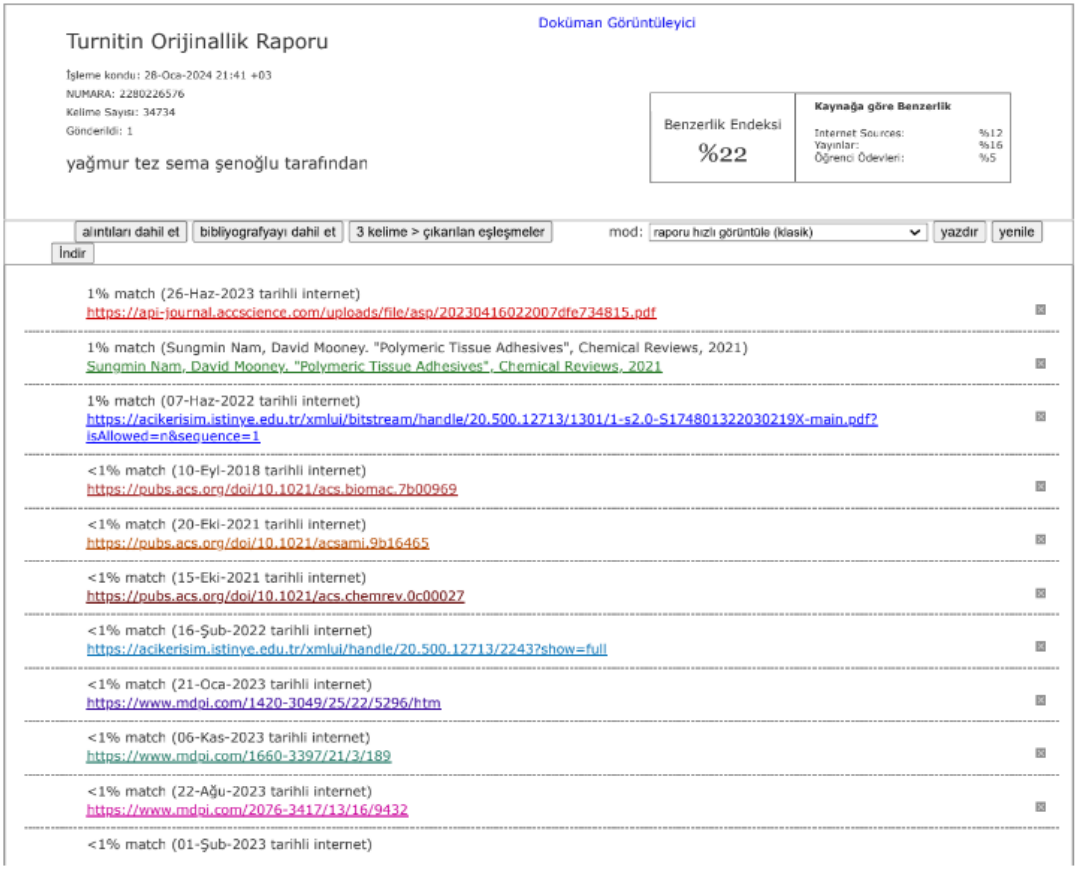

Doküman Görüntüleyici

Turnitin Orijinallik Raporu

İşleme konu: 28-Oca-2024 21:41 +03
NUMARA: 2280226576
Kelime Sayısı: 34734
Gönderildi: 1

yağmur tez sema şenoğlu tarafından

Benzerlik Endeksi	Kaynağa göre Benzerlik	
%22	Internet Sources:	%12
	Yayınlar:	%16
	Öğrenci Ödevleri:	%5

alıntıları dahil et | bibliyografyayı dahil et | 3 kelime > çıkarılan eşleşmeler | mod: raporu hızlı görüntüle (klasik) | yazdır | yenile | İndir

1% match (26-Haz-2023 tarihli internet)
https://api-journal.accscience.com/uploads/file/asp/20230416022007dfe734815.pdf

1% match (Sungmin Nam, David Mooney. "Polymeric Tissue Adhesives", Chemical Reviews, 2021)
Sungmin Nam, David Mooney. "Polymeric Tissue Adhesives", Chemical Reviews, 2021

1% match (07-Haz-2022 tarihli internet)
https://acikerisim.istinye.edu.tr/xmlui/bitstream/handle/20.500.12713/1301/1-s2.0-S174801322030219X-main.pdf?isAllowed=n&sequence=1

<1% match (10-Eyl-2018 tarihli internet)
https://pubs.acs.org/doi/10.1021/acs.biomac.7b00969

<1% match (20-Eki-2021 tarihli internet)
https://pubs.acs.org/doi/10.1021/acsami.9b16465

<1% match (15-Eki-2021 tarihli internet)
https://pubs.acs.org/doi/10.1021/acs.chemrev.0c00027

<1% match (16-Şub-2022 tarihli internet)
https://acikerisim.istinye.edu.tr/xmlui/handle/20.500.12713/2243?show=full

<1% match (21-Oca-2023 tarihli internet)
https://www.mdpi.com/1420-3049/25/22/5296/htm

<1% match (06-Kas-2023 tarihli internet)
https://www.mdpi.com/1660-3397/21/3/189

<1% match (22-Ağu-2023 tarihli internet)
https://www.mdpi.com/2076-3417/13/16/9432

<1% match (01-Şub-2023 tarihli internet)